Doctoral Thesis

THE ROLE OF MEIS TRANSCRIPTION FACTORS IN CARDIOMYOCYTES

Noelia Muñoz Martín

Programa de Doctorado de Biociencias Moleculares
Universidad Autónoma de Madrid

July 2019
Madrid

DEPARTAMENTO DE BIOLOGÍA MOLECULAR
FACULTAD DE CIENCIAS

NOELIA MUÑOZ MARTÍN

Licenciada en Biología

Director: Miguel Torres Sánchez

Centro Nacional de Investigaciones Cardiovasculares

Julio, 2019

This work was performed in Miguel Torres' laboratory in the Cell and Developmental Biology Area at the Centro Nacional de Investigaciones Cardiovasculares Carlos III (CNIC) in Madrid.

The CNIC is supported by the Ministerio de Ciencia, Innovación y Universidades (MCNU) and the Pro CNIC Foundation, and is a Severo Ochoa Center of Excellence (SEV-2015-0505).

This study was funded by grants RD12/0019/0005 and RD16/0011/0019 (TerCel, RETICS); S2010-BMD-2315 (Comunidad de Madrid); BFU2012-31086 (MINECO); BFU2015-71519 (MEIC) and ref. 17CVD04 (Leudcq Foundation Transatlantic Networks).

Noelia Muñoz Martín was recipient of a fellowship from "La Caixa-Severo Ochoa 2014" and EMBO-Short Term 2018.

TABLE OF CONTENTS

LIST OF ABBREVIATIONS

AP	Action Potential
ARVC	Arrhythmogenic Right Ventricular Cardiomyopathy
AVC	Atrio-Ventricular Canal
AVN	Atrio-Venticular Node
BB	Bundle Brunch
BPM	Beats per minute
CC	Cardiac Crescent
CCS	Cardiac Conduction System
CHD	Congenital Heart Defect
CICR	Calcium Induced Calcium Release
CM	Cardiomyocyte
CNC	Cardiac Neural Crest
dKO	double Knockout
ECG	Electrocardiogram
EF	Ejection Fraction
FHF	First Heart Field
HB	Hiss Bundle
HT	Heart Tube
ID	Intercalated Disc
idKO	inducible double Knockout
IVS	Interventricular septum
LA	Left atrium
LAX	Long axis
LV	Left Ventricle
LVPW	Left ventricular posterior wall
OFT	Outflow Tract
PF	Purkinje Fiber
RA	Right atrium
RV	Right ventricle
SAN	Sinoatrial Node
SAX	Short axis
SHF	Second Heart Field
SR	Sarcoplasmic Reticulum
TF	Transcription Factor
Tx	Tamoxifen
VCS	Ventricular Conduction System
VOCC	L-type Voltage-operated Calcium Channel
WGA	Wheat germ agglutinin
WT	Wild type

SUMMARY

The heart is the pump that irrigates the body to satisfy the nutrient and oxygen demands essential for keeping the organism alive. Understanding how the heart is formed and how its homeostasis is maintained in adulthood, is of great interest and can provide new insights on the etiology of cardiovascular diseases. In this doctoral thesis we studied the role of Meis1 and Meis2 transcription factors as possible regulators of cardiac development and homeostasis.

We developed two mouse models for the conditional simultaneous deletion of *Meis1* and *Meis2* in cardiomyocytes either during development or during adulthood. Analysis of Meis1 and Meis2 double deletion in the developing heart revealed cardiac malformations and perinatal death, together with impaired electrical impulse propagation through the ventricles. Adult mice with Meis1 and Meis2 loss of function in cardiomyocytes presented mild cardiac hypertrophy, polyploidization of mononucleated cardiomyocytes and impaired electrical impulse conduction through ventricular myocardium.

The transcriptomic analysis of the mutants suggests that Meis1 and Meis2 transcription factors regulate calcium and sodium currents and GAP junction communication in developing and adult cardiomyocytes, which is in accordance with the electrical phenotypes observed. Moreover, the set of genes sensitive to *Meis1* and *Meis2* deletion shows significant coincidence with those altered in mouse models of arrhythmogenic right ventricular cardiomyopathy, suggesting a role for these transcription factors in the pathogenesis of this disease.

RESUMEN

El corazón es la bomba que alimenta el sistema circulatorio para satisfacer las necesidades de nutrientes y oxígeno del cuerpo. Entender cómo se regula el desarrollo del corazón y su homeostasis durante la vida adulta es de vital importancia para comprender la etiología de muchas enfermedades cardiovasculares. En esta tesis doctoral, estudiamos el papel de los factores de transcripción Meis1 y Meis2 como posibles reguladores de estos procesos.

Hemos generado dos modelos de ratón para el estudio de la función de Meis1 y Meis2 en cardiomiocitos bien durante el desarrollo o durante la edad adulta. Tras la pérdida de función de Meis1 y Meis2 en cardiomiocitos durante el desarrollo, encontramos que los fetos mueren al nacer, presentando alteraciones morfológicas y defectos en la propagación del impulso eléctrico, necesario para el mantenimiento del ritmo de latido. Por otro lado, la deleción de estos factores en los cardiomiocitos del corazón adulto no es letal, pero conlleva la aparición de fibrosis, poliploidización de los cardiomiocitos mononucleados y cierta respuesta hipertrófica. Además, de forma similar a los observado en la deleción embrionaria, encontramos un empeoramiento de la conducción eléctrica con alargamiento del segmento QRS en el electrocardiograma.

El análisis del transcriptoma de los mutantes indica que Meis1 y Meis2 podrían estar regulando las corrientes de sodio y calcio y la formación de uniones GAP, lo que correlaciona con las alteraciones encontradas en la propagación del impulso eléctrico del corazón en ambos modelos. Además, el conjunto de genes alterados por la falta de función de Meis presenta coincidencias significativas con el grupo de genes que se altera en un modelo de ratón de la enfermedad ARVC ("*Arrhythmogenic Right Ventricular Cardiomyopathy*"), sugiriendo que Meis1 y Meis2 podrían estar implicados en la patogénesis de esta cardiomiopatía.

INTRODUCTION

The heart is a powerful pump that impulses the blood to irrigate all body organs. The mechanical action of the heart is provided by the cardiac muscle, which contracts during systole to pump the blood. After contraction, the muscle is dilated during diastole, creating negative pressure to get the blood back into the heart and pump it again. The adult mammalian heart is composed by two atria and two ventricles feeding two parallel circuits: the systemic circulation and the pulmonary circulation (FIG. 1). Atria and ventricles communicate through the atrioventricular valves. When the deoxygenated blood (blue in FIG. 1) from the systemic circulation enters the right atrium, there is an increase in pressure that leads to the opening of the tricuspid valve and the subsequent filling of the right ventricle. Then, the blood goes through the pulmonary valve to the lungs, gets oxygenated and comes back to the heart trough the left atrium, where the same process is repeated (pink in FIG. 1). In this case, the atrioventricular valve is called mitral or bicuspid and the oxygenated blood leaves the ventricle through the aortic valve.

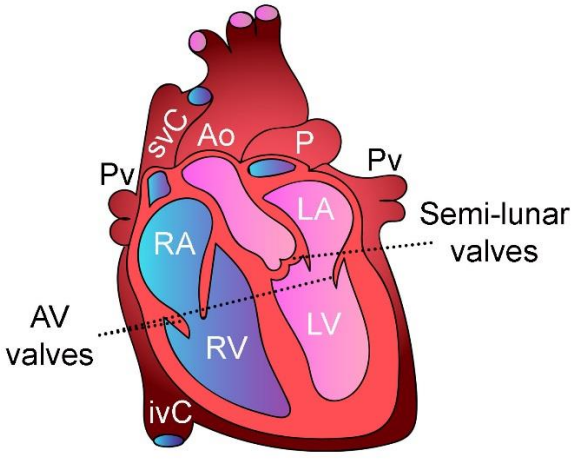

Figure 1. Anatomy of the mammalian adult heart. Blue and pink colors represent deoxygenated and oxygenated blood respectively. RA, right atrium, RV, right ventricle, LA, left atrium, LV, left ventricle, Ao, aorta, P, pulmonary artery, svC and ivC, superior and inferior vena cava, Pv, pulmonary veins.

This process is essential for life, because it supplies a constant flow of nutrients and oxygen to all cells in the body. Thus, the heart is the first functional organ during embryonic development and any alteration of cardiac formation can lead to embryonic lethality or congenital heart defects (CHD). Currently, 30% of human pregnancies that do not come to term present cardiac malformations (Bruneau, 2008) and 3% of born

humans present some kind of CHD (Fahed et al., 2013; Parker et al., 2010). These percentages reflect how important the proper regulation of heart development is, in order to produce a functional organ throughout lifespan.

Heart development

Mouse gestation spans 19 days, which implies that developmental processes occur very rapidly. The mammalian heart starts to be formed very early in development as the first cardiac progenitors arise at E6.5 from the pluripotent cells of the epiblast. These epiblast-derived cells migrate anteriorly from the primitive streak and form the cardiac mesoderm at both sides of the ventral midline (Lawson et al., 1991; Tam & Behringer, 1997). This pool of cells expresses Mesp1 (Mesoderm Posterior 1) which is a key regulator for cardiac specification (Saga et al., 1999; Saga et al., 2000). One day later, Mesp1+ cells migrate anteriorly and fuse medially, forming the cardiac crescent (CC) (FIG. 2). At this stage, many transcription factors necessary for cardiogenesis are activated: *Gata4, Nkx2.5, Mef2c, Hand1/2 and Tbx5* (Martin-Puig *et al*, 2008; Bondue & Blanpain, 2010). The CC is a peristaltic pump located under the growing head folds (Ivanovitch *et al*, 2017). It is composed of an inner layer of endocardium and an outer layer of myocardium (Vincent & Buckingham, 2010). The progenitors that give rise to the CC are known as First Heart Field (FHF) (Kelly, 2012; Später et al., 2013).

As the CC grows, cells move to form a transversal hemi-tube which later adopts a more spherical shape and is still dorsally dorsally open (Ivanovitch *et al*, 2017). The endoderm serves as a transient dorsal wall and the hemi-tube is progressively closed giving rise to the primitive heart tube (Kelly *et al*, 2014; Evans *et al*, 2010). The primitive HT has the same two layers as the CC, but venous and arterial poles are now present. The future left ventricle and part of the atria arise from the primitive HT (Zaffran *et al*, 2004). There is another pool of cardiac progenitors which remains undifferentiated and starts differentiation after the linear HT is formed. This pool is called Second Heart Field (SHF). Fgf10 and Isl1 are some of the factors characteristic of this region. The SHF is located dorso-medially to the CC in the region of the splanchnic mesoderm and progenitors are incorporated into the HT trough the venous and arterial poles,

contributing to HT elongation (Kelly *et al*, 2001; Mjaatvedt *et al*, 2001; Waldo *et al*, 2001; Cai *et al*, 2003). SHF progenitors will form the right ventricle, the outflow tract and part of the atria (Zaffran *et al*, 2004). As the HT elongates, it undergoes rightward looping and chambers start to be specified (E8.5) (FIG. 2). Outflow tract (OFT) and forming right and left ventricles can be already identified at this point. The connection between atria and ventricles is made by the atrioventricular canal. At E10.5 outflow and inflow tracts align with the ventricles reaching their definitive location (Watanabe & Buckingham, 2010).

Later on, the developing heart initiates an expansion process by proliferation at specific regions of the outer curvature of the heart tube, which generates the chambers, according to the ballooning model (Christoffels *et al*, 2000). Between E9.5 and E14.5 there is not only growth but also complete chamber specification and morphogenesis. After looping, CMs continue dividing and some of the newly formed CMs will protrude towards the endocardium. This protruding CMs slow their proliferative rate and form the trabeculae, which are transient ridge-like structures that protrude towards the lumen of the chambers. The initial layer of myocardium is now called compact layer and will continue proliferating and increasing in thickness (Blausen *et al*, 1990; Sedmera *et al*, 2000, 2003; Staudt *et al*, 2014). At E14.5 all chambers are established and further proliferation and maturation will occur until the first postnatal days (FIG. 2). The increase in compact layer thickness is accompanied by the development of the coronary system that serves to irrigate the myocardium, which satisfies the high metabolic rate of cardiomyocytes. Ventricular chamber maturation involves trabecular remodeling and compaction. During compaction, the trabecules become thicker and coalesce until the spaces between them form capillaries (Wessels & Sedmera, 2003). By the end of gestation, right and left ventricles are completely separated by the septum. However, the atrial septum does not close until around postnatal day 7 (P7) (Cole-Jeffrey *et al*, 2012).

The FHF and SHF are the main sources of progenitors during cardiogenesis, but there are other pools of progenitor which are essential for heart formation (Vincent & Buckingham, 2010).

The epicardium is the outer-most layer of the heart and it derives from the proepicardium. The proepicardium is a pool of cells that derive from the coelomic epithelium located in the dorsal pericardial wall. PE cells expressed different markers, among which, Tbx18 and Wt1 are the best established. From E9.5 to approximately E14.5, cells detach from the PE and cover the heart progressively by migration and proliferation, (FIG. 2) (Viragh & Challice, 1981) (Wu *et al*, 2010).

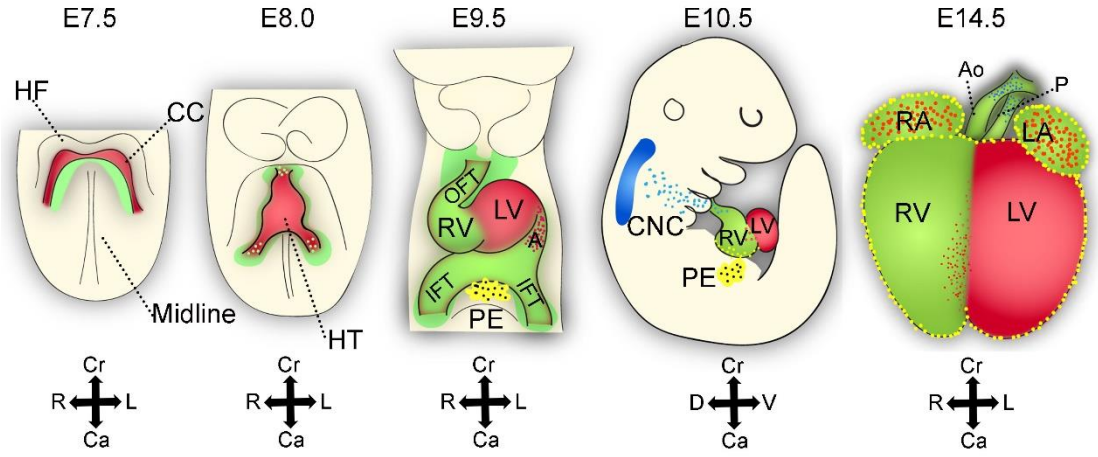

Figure 2. Embryonic heart development in mouse. Schematic representation of key phases in murine cardiac development. From left to right, cardiac crescent (CC) at E7.5 with first heart field (FHF, in red) and second heart field progenitors (SHF, in green). The heart tube (HT) is formed (E8.0) and elongates as SHF progenitors incorporate to the tube through the arterial and venous poles (E9.5). Between E8.0 and E9.5,the heart loops and chambers are specified. The right ventricle (RV), outflow tract (OFT) and inflow tract (IFT) are represented in green as SHF derivatives, while left ventricle (LV) and part of the atria (A) are in red, as FHF derivatives. The proepicardium (PE) is represented in yellow. Cardiac neural crest cells (CNC) are incorporated into the OFT region. The last draw represent an E14.5 embryonic heart with the 4 chambers and great vessels, aorta and pulmonary arteries (Ao;P) differentiated. Cartoon adapted from Stéphane D. Vincent and Margaret E. Buckingham, 2010.

Moreover, epicardial cells undergo epithelial-mesenchymal transition to invade the myocardium and there differentiate into fibroblasts, vascular smooth muscle cells and part of the vascular endothelial cells (Wessels & Pérez-Pomares, 2004). It has been proposed they might also contribute to CMs but this is still a debate and remains to be elucidated (Krainock *et al*, 2016).

Another source of progenitors is the **cardiac neural crest (CNC)**. This progenitor population arises from the dorsal neural tube and migrates towards the heart around mid-gestation (FIG. 2) (Lee *et al*, 1995; Jiang *et al*, 2000; Brown & Baldwin, 2006). It has been shown that CNC cells contribute to the smooth muscle cells from the arterial

pole of the heart and their incorporation to this structure is important for OFT remodeling and division into aorta and pulmonary arteries (Keyte *et al*, 2014).

Postnatal heart maturation

During the first week of life, the heart still undergoes important genetic and metabolic changes. In the last decades, many studies have focused on the description of those changes and their regulation.

After birth, the CMs proliferative rate is dramatically decreased in mice and humans (FIG. 3) (Soonpaa *et al*, 1996; Mollova *et al*, 2013). However, in a few days, the size of the heart is duplicated due to a hypertrophic process of the CMs (Li *et al*, 1996). This hypertrophy is linked to an increase in CM ploidy that results predominantly in binucleation of CMs in mice and nuclear polyploidization in humans (FIG. 3) (Bergmann *et al*, 2015). Whereas developing CMs are mononucleated, around P21 85-90% of CMs are binucleated in mice (Soonpaa *et al*, 1996; Walsh *et al*, 2010). In general, genes promoting CM cell cycle are strongly downregulated while genes inhibiting the cell cycle are upregulated during this process (Engel *et al*, 2005; Quaife-Ryan *et al*, 2017). The reasons for these changes are still under study. It has been proposed, that the increase in oxygen levels after birth might lead to the activation of the oxidative stress damage response and the subsequent cell cycle arrest (Puente *et al*, 2014; Kimura *et al*, 2014).

In addition, it has been recently discovered that the neonatal mouse heart presents the capability to regenerate after injury during the 3-4 first postnatal days, although at P7 this ability is lost (Porrello *et al*, 2011). This was a very encouraging finding because it opened the possibility of activating adult CM proliferation to stimulate cardiac injury repair. Many efforts have been concentrated on understanding the molecular mechanisms underlying CMs cell cycle arrest (Tzahor & Poss, 2017). Activation of Hippo signaling is one of the mechanisms shown to inhibit postnatal CMs proliferation (Heallen *et al*, 2011; von Gise *et al*, 2012) and administration or upregulation of extracellular matrix proteins has been shown to modify the regenerative capacity of the heart (D'Uva *et al*, 2015; Bassat *et al*, 2017). Recently, Meis1 was identified as negative regulator of postnatal CMs cell cycle (Mahmoud *et al*, 2013). More studies in

this field are still needed to achieve adult CM regeneration, although recent advances in the pig model are encouraging (Gabisonia *et al*, 2019).

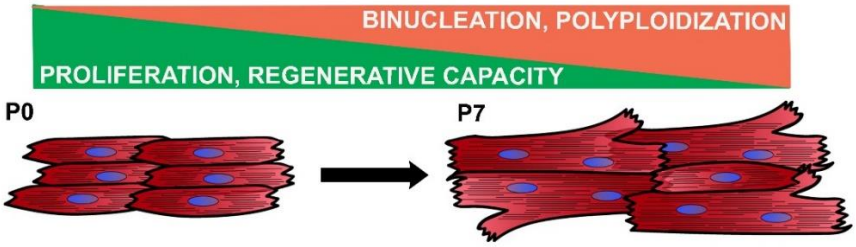

Figure 3. Postnatal cardiomyocyte maturation. Changes between P0 and P7 in mammalian cardiomyocytes. Cell cycle is arrested and the regenerative capacity is lost, while the binucleation and polyploidization become predominant in cardiomyocytes.

The cardiac conduction system

The formation of a proper functional heart requires not only the accomplishment of complex and varied morphogenetic processes, but also the establishment of the adequate cardiac rhythm. In mammals, the nervous system and hormones regulate the cardiac rate to adapt it to the needs of body's cells for oxygen and nutrients.

However, there are specialized CMs with the capability of automaticity in electrical pacing, known as the pace-maker cells, which, in the absence of extrinsic influences, can maintain constant basal heart rhythm (Gordan *et al*, 2015). These CMs present few sarcomeres, less mitochondria and T tubules and enriched glycogen content (Virágh S, 1977; Myers & Fishman, 2003).

Heartbeats originate as a spreadable rapid rise and fall of voltage across the cellular membrane which is called action potential (AP). The AP is generated in the sinoatrial node (SAN) and spreads through a system of specialized CMs known as the Cardiac Conduction System (CCS). All CCS CMs can generate action potentials, although the SAN has the fastest rate of spontaneous depolarization and, therefore, acquires the role of pacemaker. The SAN is located at the dorsal part of the right atrium, close to the superior cava vein entrance (FIG. 4A). From the SAN, the impulse spreads throughout the atria inducing their contraction. Then, the AP reaches the atrio-ventricular node (AVN), where it suffers a delay before entering the His Bundle (HB) at the base of the ventricles (FIG. 4A). The delay created by the AVN is essential to allow

blood flow from atria to fill the ventricles during atrial systole and before ventricular systole. The atrial and ventricular myocardium are electrically isolated from each other by the annulus fibrosus and central fibrous body. The HB is the only CCS element that crosses this insulation, running through the crest of the ventricular septum and transmitting the electrical impulse from atria to ventricles.

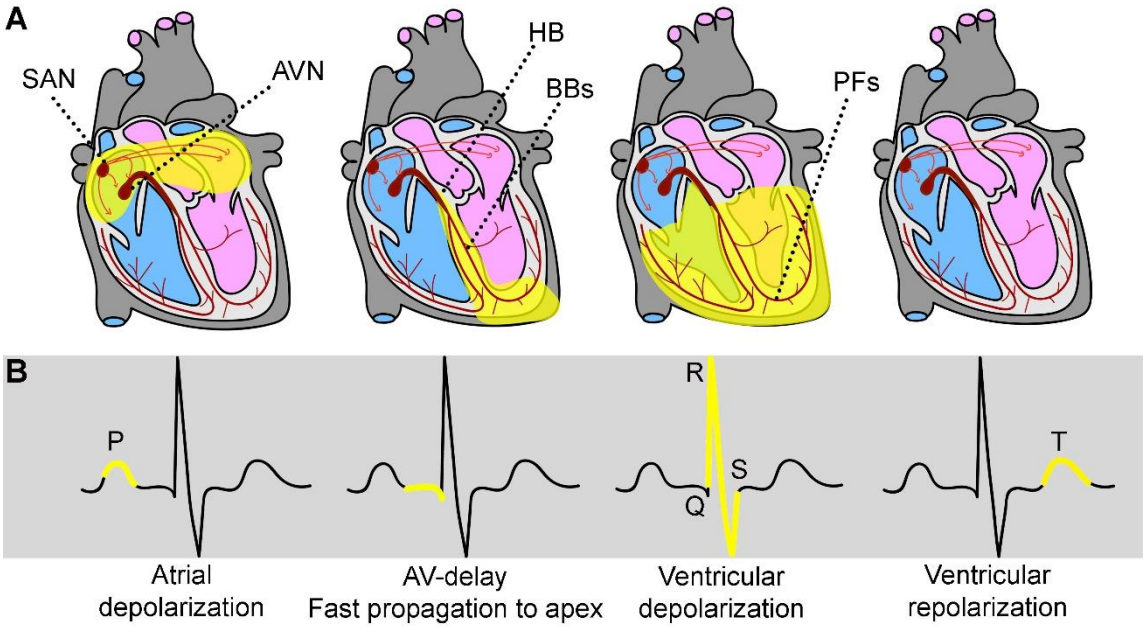

Figure 4. Cardiac conduction system and electrocardiogram interpretation. A. Adult heart representation with cardiac conduction system anatomy in red. From left to right, yellow areas represent the sequence of activated regions upon electrical impulse generation in the sinoatrial node (SAN). Atrioventricular node (AVN), Hiss Bundle (HB), right and left Bundle Brunches (BBs) and Purkinje Fibers (PFs). B. Example of human electrocardiogram with highlighted areas in yellow that correspond to the phases represented in (A).

Two branches arise from the HB, right and left bundle brunches (RBB; LBB) located at either side of the interventricular septum. BBs prolong from the top of the septum towards the apex and connect to the Purkinje Fiber network (PF) at the tips (FIG. 4A). Then, the AP is rapidly transmitted to the whole ventricles, from apex to base, leading to subsequent ventricular contraction and ejection of blood through the great arteries. PFs are distributed throughout the ventricular walls and they are mainly located in a sub-endocardial position (Van Weerd & Christoffels, 2016). The ventricular conduction system (VCS), composed of the HB, the BBs and the PFs is electrically isolated from the working myocardium by connective tissue, so that the electrical impulse only reaches the working myocardium through the Purkinje-Myocyte junctions. This

ensures the proper timing and the apex-to-base contraction of the ventricles for efficient blood pumping (Munshi, 2012).

Electrophysiology of the adult heart

The adequate function of the CCS is essential for life. Perturbations of heart rhythm lead to an important proportion of morbidity and mortality in the human population. Nowadays, the overall prevalence of arrhythmias is approximately 3.4% (Andersson *et al*, 2013; Zoni-Berisso *et al*, 2014; Clauss *et al*, 2019), however, the pathophysiology of arrhythmias is complex and not completely understood.

The electrocardiogram (ECG) is a diagnostic tool that allows the study in detail of CCS function. It is widely used in humans and also in animal experiments. It consists on the measurement of voltage versus time, which generates a pattern with several waves and isoelectric segments, each one reporting the activity of a particular part of CCS and working myocardium electrical activity (FIG. 4B). A proper interpretation of the electrocardiogram is essential for a good description of CCS function. The human ECG was described for the first time in 1895 by Einthoven and eighty-three years later, in 1968, the first description of the mouse ECG was published (Fye, 1994; Goldbarg *et al*, 1968). Comprehension of both ECGs is of crucial importance for the extrapolation of the results in mouse models to human health.

Before ECG interpretation, it is necessary to explain the molecular basis of the action potential. The AP is produced by the interchange of ions between the cell and the intercellular space (FIG. 5A). AP shape varies between species and also between different regions of the heart. In general, the resting voltage potential across the CM plasma membrane is usually -90mV with higher concentrations of Na^+ outside the cell and of K^+ inside. When the action potential is generated, fast sodium channels are opened creating an inward Na^+ current that rapidly increases voltage across the plasma membrane (sarcolemma) to values of +10mV (FIG. 5A, B). This phenomenon is known as depolarization. The returning to the resting membrane voltage is called repolarization and is achieved by outward K^+ current to the intercellular space (FIG. 5A, B). In human CMs, there is and intermediate phase, after the beginning of repolarization, called plateau phase. In this phase, calcium channels are opened, so

that Ca^{2+} enters the cell while K^+ outward current occurs, keeping voltage on values of about 0mV before complete repolarization (FIG. 5A, B) (Nerbonne & Kass, 2005). Transient hyperpolarization is normally observed in human CMs due to the potassium outward current that brings the voltage to more negative values than in the resting phase. These differences in AP between mice and humans creates different ECG patterns.

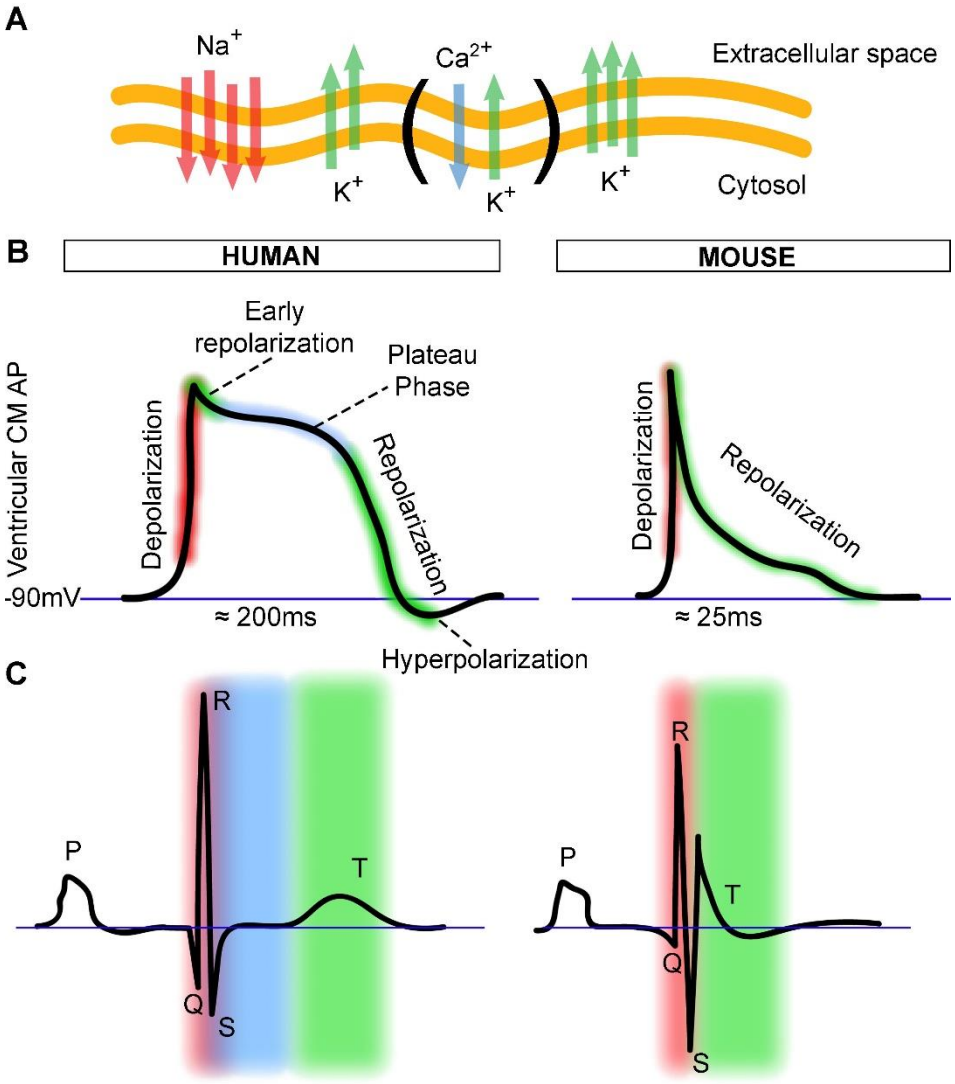

Figure 5. Electrophysiology of human and murine ventricular cardiomyocytes. A. Schematic representation of ion exchange during AP phases in CMs. Brackets indicate the plateau phase that is exclusive of human CMs. B. Action potential shapes in human and mouse ventricular CMs. C. The ECG profile in human and murine hearts with indication of each wave. Colors indicate the phases of AP: red, depolarization, green, repolarization and blue, plateau phase.

The time between the end of P wave and the initiation of Q wave corresponds to the delay between atrial and ventricular conduction (FIG. 4B, 5C). Prolongation of this segment might indicate an atrio-ventricular conduction delay or block. Then, the QRS complex appears, reflecting ventricular depolarization, with a morphology that differs between mice and humans (FIG. 4B, 5C).

In mice, ventricular repolarization occurs immediately after the QRS, however, in humans, ventricular repolarization takes a longer time and generates the T wave after and isoelectric segment (FIG. 4B, 5C) (Boukens *et al*, 2014). In mice, the T wave voltage is negative and ends when it reaches the isoelectric line (FIG. 5C) (Boukens *et al*, 2014). The atrial repolarization wave is not seen probably because is hidden by the QRS complex.

Molecular and cellular bases of cardiac conduction

Synchronous impulse propagation and contraction requires proper excitation-contraction coupling. Calcium signaling is a key regulator of this process allowing to pair depolarization with mechanical contraction. When electrical impulse reaches working CMs and depolarization starts, L-type Voltage-operated Ca^{2+} channels (VOCC) (Cav1.2) are opened (Fearnley *et al*, 2011). Ca^{2+} flows into a restricted space between sarcolemma and sarcoplasmic reticulum (SR) known as “dyadic cleft”. Ca^{2+} accumulation in this micro domain induces opening of RyR2 (Type 2 Ryanodine Receptor) located in the SR and produces a Ca^{2+} release signal known as “Ca^{2+} spark” in a processed called “calcium-induced calcium release” (CICR) (FIG. 6). Ca^{2+} ions diffuse to engage the Troponin C, which is the Ca^{2+} binding component of the contractile machinery, and contraction occurs. After activation of contractile units, Ca^{2+} is rapidly removed from the cytosol causing relaxation and preparing the cell for the next action potential (Shannon and Bers, 2004). The main mechanisms for calcium efflux from the cytosol is the Ca^{2+} ATPase2 (SERCA2) pump located at the SR (FIG. 6). There are also sodium/calcium exchanger channels (NCX) in the sarcolemma that contribute to this process in a smaller percentage (FIG. 6) (Fearnley *et al*, 2011). It has been shown this system has high adaptability robustness, since SERCA2 cardiac-

specific knockout mice showed minimal cardiac dysfunction due to a compensatory increase in NCX activity (Andersson *et al*, 2009).

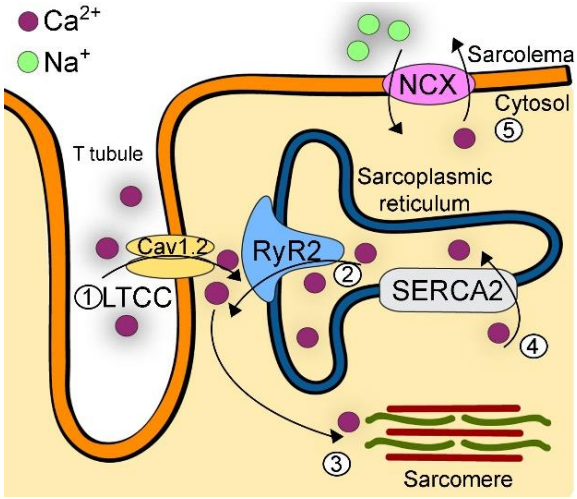

Figure 6. Calcium-Induced Calcium Release. (1) Extracellular calcium enters cytosol through L-type Calcium Channels (LTCC) inducing Calcium release from the sarcoplasmic reticulum (SR) by RyR2 (2). Increased cytosolic calcium concentration allows contraction of the sarcomeres (3). Initial calcium levels are recovered via SERCA2 and NCX, which recruit calcium in the SR and extracellular space, respectively (4 and 5).

The contractile and electrical forces spread readily between adjacent CMs thank to the intercalated disc (ID). IDs are located at the ends of the rod shaped CMs and are composed of desmosomes (intercellular adhesion), fascia adherens (transmission of contractile forces) and Gap junctions (AP propagation) (FIG. 7) (Estigoy *et al*, 2009). It has recently been observed that these elements are in close interaction, so defects in the structural part of IDs can affect excitability of the cells and vice versa (Moncayo-Arlandi & Brugada, 2017).

In vertebrates, gap junctions are formed by connexins, which are trans-membrane proteins that enable the direct cytoplasmic exchange of ions and low molecular weight metabolites between adjacent cells (Nielsen *et al*, 2012). In the adult murine heart, there are different connexin isoforms and Cx43, Cx40, Cx45 and Cx30.2 are the predominant ones (Davis *et al*, 1994; Jansen *et al*, 2010). Cx43 is the major isoform, expressed in both atrial and ventricular myocardium. Cx40 is present in the atria, AVN and VCS (Beyer et al., 1987; Davis et al., 1994). Cx45 and Cx30.2 are less studied and their expression is more restricted to the CCS (Coppen *et al*, 1999; Kreuzberg *et al*, 2009, 2005). Furthermore, sodium channels, like Nav1.5, essential for electrical impulse conduction, concentrate at the intercalated disc too (FIG. 7) (Dhar Malhotra *et al*, 2001).

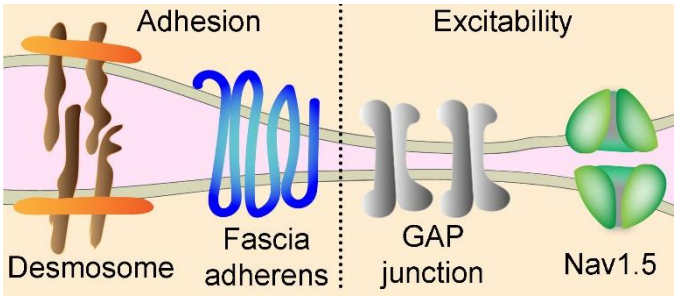

Figure 7. Intercalated disc composition. Draw of the different structures that can be found in intercalated discs separated by function: adhesion and excitability. Orange is cytosol and pink extracellular space between two couple CMs.

Disorganized intercalated discs can lead to several cardiac diseases. One example is the arrhythmogenic right ventricular cardiomyopathy (ARVC), that arises from mutations in structural proteins of the desmosomes and leads to fibrosis, reduced and mislocalized Cx43 and arrhythmias that can lead to sudden cardiac death (Gard *et al*, 2005; Cerrone *et al*, 2012a). Brugada Syndrome, is considered a channelopathy, mainly related with mutations in *Scn5a* (Nav1.5), however, mutations in proteins of the desmosomes can also affect *Scn5a* expression and reproduce several Brugada Syndrome features (Moncayo-Arlandi & Brugada, 2017). These data indicate that the structural and the excitability components of the IDs do interact with each other.

Cardiac Conduction System development

Genetic and environmental factors are both contributing to the development of arrhythmias. The comprehension of CCS embryonic development can help to elucidate the genetic origin of some types of arrhythmias.

In the mouse, as mentioned above, the CC is already a beating structure. Those beats are automatically generated by the newly formed CMs derived from the FHF. At this stage, CMs are poorly differentiated, presenting underdeveloped sarcomeres and SR, which resemble adult conducting CMs. Markers that are later exclusive for CCS, such as Hcn4 and Cx40 are expressed in the myocardial layer of the HT (Mommersteeg *et al*; Später *et al*, 2013). At E8.0, when the HT is formed, the dominant automaticity is located in the venous pole and all cells conduct similarly, so that blood is pumped towards the arterial pole or OFT in a peristaltic mode (FIG. 8). The transcription factor Nxk2.5 is initially expressed in the CC and SHF precursors, although later on, when the heart elongates and starts looping, Tbx18 is the predominant marker in the venous pole, where pacemaker CMs are formed (Christoffels *et al*, 2006; Mommersteeg *et al*;

Wiese *et al*, 2009). The SAN can be anatomically distinguished for first time at E11.5 (Challice & Virágh, 1980).

The atrioventricular canal (AVC) is the structure of the primitive tube that separates atria and ventricles and gives rise to the atrio-ventricular ring and AVN (FIG. 8). The AVC comes from $Tbx2^{+}$ cells at the IFT of the HT. Around E9, the AVC expresses Bmp2, Tbx2 and Tbx3 (Singh *et al*, 2012). This combination of TFs represses the expression of markers for chamber myocardium and keeps Cx30.2, which is important for the slow conduction phenotype of the AVN. From E12.5 onwards the annulus fibrosus insulates atria from ventricles and $Tbx3^{+}$ cells form the AVN. It has been described that Tbx5 and Gata4 also contribute to the slow conduction velocity found in the AVN (Munshi *et al*, 2009). In contrast, the ventricular conduction system is fast conducting due to expression of Cx40 and Scn5a. The HB forms from the arterial pole of the HT and the timing is similar to that of the AVN (Mohan *et al*, 2017) (FIG. 8). However, the BBs and the PFs are specified later in development, around E15.5. BBs come from sub-endocardial CMs located in the trabecules of the septum and PFs from the trabecules of the ventricular chambers, being SHF-derived in the RV and FHF-derived in the LV (Christoffels & Moorman, 2009; van Eif *et al*, 2018). The origin of the VCS has been long debated and still some aspects of it remained obscure. Clonal analysis has shown that VCS share a common progenitor with surrounding working CMs and after specification there are limited rounds of proliferation (biphasic model) (Miquerol *et al*, 2010). However, it has been suggested that CNC and epicardial derived cells can contribute to the VCS, although there are not yet definitive conclusions about this possibility (Nakamura *et al*, 2006; Aanhaanen *et al*, 2010). Nevertheless, it is clear that different elements of the CCS derive from different progenitor pools of the FHF and SHF, although in the adult heart, they are integrated in a single conduction system (Miquerol *et al*, 2011).

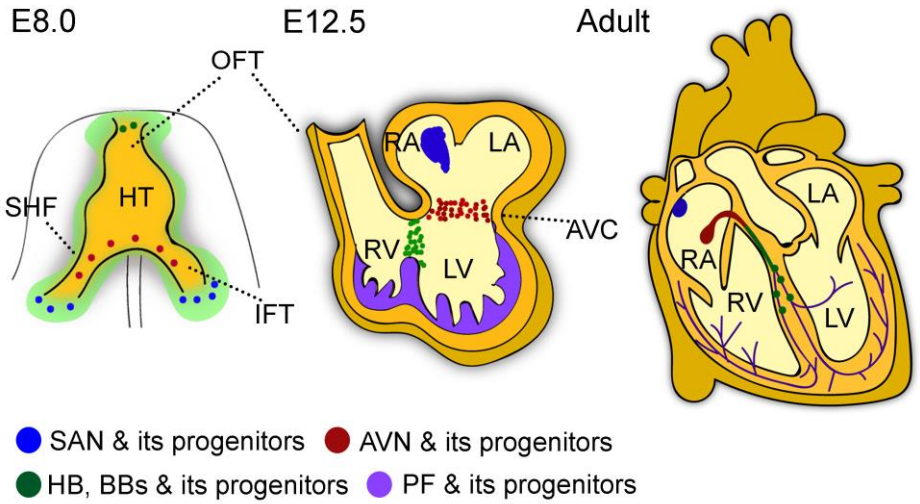

Figure 8. Cardiac conduction system development. E8.0 heart tube (HT), E12.5 and adult hearts. Each color represents a different part of the adult CCS and the location of their progenitors during cardiac development.

Meis transcription factors

As described, cardiogenesis is a complex process that requires to be tightly regulated. Transcription factors (TF) play an important role in the regulation of embryonic development, since they possess the capability to bind DNA and control the expression of a subset of genes. There are TFs whose function in heart development has been studied for decades, but many others have been recently discovered.

Meis TFs belong to the TALE family (Three Aminoacid Loop Extension) and are highly conserved among species at the molecular and functional level (Longobardi *et al*, 2014a). Meis1 (myeloid ecotropic viral integration site 1) was the first gene of the family to be identified (Moskow *et al*, 1995). In mammals, two more genes with high homology were identified; Meis2 and Meis3 (Nakamura *et al*, 1996; Oulad-Abdelghani *et al*, 1997). Except in the head, the expression patterns of Meis1 and Meis2 in embryos are highly similar and both genes encode very similar proteins, which suggests they might have redundant functions. In contrast, Meis3 expression is mainly restricted to the hindbrain, although it can be also detected in the heart, spleen and lung at later stages (Nakamura *et al*, 1996). A Meis3 knockout mouse has not been generated so very little is known about Meis3 functions in mammalian development.

Meis1 is expressed in the neural tube, the eye, the ear primordium, gut, cardiac chambers, lung, paraxial mesoderm (Hisa *et al*, 2004; González-Lázaro *et al*, 2014) and proximal domain of the forming limb (Mercader *et al*, 1999). Meis2 expression pattern overlaps with that of Meis1 in many of the areas described above. However, Meis2 is not expressed in the eye, while it does so in midbrain, forebrain and kidneys, where Meis1 has not been detected (Oulad-Abdelghani *et al*, 1997; Cecconi *et al*, 1997; Mercader *et al*, 1999).

In addition, Meis TFs function as cofactors of other TFs, such as Pbx, Prep or Hox factors (Mann & Affolter, 1998; Ryoo *et al*, 1999). They can form dimers or trimers, modifying the cofactors' affinity and selectivity for DNA-binding sites. Thus, there is increased difficulty in understanding Meis TFs function, because it varies depending on the context.

Meis1 knockout mice die around E14.5 due to failing hematopoiesis (Hisa *et al*, 2004; Azcoitia *et al*, 2005). Defects in these mutant embryos also present eye and fetal liver hypoplasia and interventricular septal defects in the heart (Hisa *et al*, 2004; Azcoitia *et al*, 2005; Stankunas *et al*, 2008; González-Lázaro *et al*, 2014). It has been reported that *Meis2* knockout mice also die around E14.5, presenting hemorrhages and *Persistent Truncus Arteriosus* (PTA) (Machon *et al*, 2015). This defect derives from the failure in separating the aortic and pulmonary trunks, and is a relatively common CHD in humans.

Meis1 functions have been also studied in adult organisms, where it is important for the maintenance of hematopoietic stem cell quiescence in the hematopoietic niche (Simsek *et al*, 2014; Unnisa *et al*, 2012). It plays a key role in the development of leukemia and other cancer diseases (Wong *et al*, 2007; Zha *et al*, 2014) and it is associated with the Restless Legs Syndrome in humans (Spieler *et al*, 2014). Moreover, regarding the heart, it has been shown that Meis1 is important for the cell cycle arrest of postnatal CMs in mice (Mahmoud *et al*, 2013) while *Meis1* genetic variants are associated with PR elongation in humans, suggesting a role in the CCS function (Pfeufer *et al*, 2010; Smith *et al*, 2011a). In addition, sporadic germline heterozygous *Meis2* mutations in humans lead to palatal defects, intellectual disability

and congenital heart defects, mainly affecting the interventricular septum and OFT positioning (Louw *et al*, 2015; Verheije *et al*, 2019; Giliberti *et al*, 2019).

OBJECTIVES

We consider there are enough evidences suggests Meis1 and Meis2 play a role in cardiomyocytes of the developing and adult heart but they have not been explored in detail yet. Moreover, understanding Meis1 and Meis2 function in the heart will generate new knowledge in the cardiovascular field that might be relevant for the understanding of certain human diseases.

Thus, the main goal of this thesis is to study the role of Meis1 and Meis2 transcription factors in the context of cardiac development and adult heart homeostasis.

To achieve this goal, we propose the following concrete objectives:

1- Describe the expression pattern of Meis1 and Meis2 in the developing and adult heart.

2- Generate mouse models for the cardiomyocyte-specific constitutive and inducible double deletion of Meis1 and Meis2.

3- Characterize the phenotype generated upon Meis1 and Meis2 constitutive and inducible loss of function in cardiomyocytes.

4- Describe molecular determinants of Meis function in cardiomyocytes.

5- Identify potential direct targets of Meis1 and Meis2 in cardiomyocytes.

MATERIALS & METHODS

ANIMAL PROCEDURES

Mouse lines

All animals in this project were handled following CNIC Ethics Committee, Spanish laws and the EU Directive 2010/63/EU. All the experiments were approved by CNIC and Universidad Autónoma de Madrid Committees for “Ética y Bienestar Animal” and the area of “Protección Animal” of Comunidad de Madrid with reference PROEX 220/15. In this study mice were maintained on a mixed genetic background.

To study the expression of Meis1 we took advantage of two knock-in mouse lines previously generated in the laboratory: Meis1-ECFP and Meis1-CreER (González-Lázaro et al., 2014). Meis1-CreER was crossed with R26RTdTomato (Madisen *et al*, 2010) line containing a STOP cassette flanked with LoxP sites, followed by Tomato fluorescence protein, in the R26 locus. Upon Cre recombination STOP cassette is removed and Tomato fluorescence protein is expressed in the recombined cell and its offspring. CreER is only active for recombination in the presence of tamoxifen. Tamoxifen was administered orally to adult mice (1mg/day for 5 consecutive days). Hearts were harvested two days after tamoxifen injection.

To understand the function of Meis1 and Meis2 in developing and adult CMs, we generated two models that allowed us to simultaneously delete both genes specifically in CMs. To generate a Meis1$^{flox/flox}$; Meis2$^{flox/flox}$ mouse line, we combined a Meis1-flox (Unnisa *et al*, 2012) gently given by Dr. Sadek and a Meis2-flox allele generated in the laboratory of Miguel Torres (Roselló and Giovinazzo, unpublished). Loxp sites flank exon 8 in Meis1 and exon 3 in Meis2. Upon recombination, Meis1 loses the homeodomain coding region, essential for Meis1 activity and Meis2 does not produce any protein. For the induction of LoxP recombination, we used two transgenic Cre lines specific for CMs, α-MHC-Cre (Agah *et al*, 1997) and α-MHC-MerCreMer, inducible by tamoxifen (Sohal *et al*, 2001).

We crossed Meis1$^{flox/flox}$; Meis2$^{flox/flox}$ females with Meis1$^{flox/wt}$; Meis2$^{flox/flox}$; α-MHC-Cre$^{tg/wt}$ males in order to obtain 25% of embryos with Meis1 and Meis2 double homozygous deletion, Meis1$^{flox/flox}$; Meis2$^{flox/flox}$; α-MHC-Cre$^{tg/wt}$ (dKO), 25% Meis1$^{flox/flox}$; Meis2$^{flox/flox}$; α-MHC-Cre$^{wt/wt}$ and 25% Meis1$^{flox/wt}$; Meis2$^{flox/flox}$; α-MHC-Cre$^{wt/wt}$ (both used as control) and 25% of Meis1$^{flox/wt}$; Meis2$^{flox/flox}$; α-MHC-Cre$^{tg/wt}$ (M1Het;M2KO).

In the case of Meis1 and Meis2 deletion in adult CMs, we continued using the same Meis1$^{flox/flox}$; Meis2$^{flox/flox}$ mice but crossing them with Meis1$^{flox/flox}$; Meis2$^{flox/flox}$; α-MHC-MerCreMer$^{tg/wt}$ to obtain 50% of Meis1$^{flox/flox}$; Meis2$^{flox/flox}$; α-MHC-MerCreMer$^{tg/wt}$ (inducible-dKO or idKO) and 50% of Meis1$^{flox/flox}$; Meis2$^{flox/flox}$; α-MHC-MerCreMer$^{wt/wt}$ (Control). As an extra control for possible Cre toxicity we used α-MHC-MerCreMer$^{tg/wt}$ (CRE) compared to their wild type (WT) littermates. Tamoxifen was administered through oral-gavage (1mg/day for 5 consecutive days) to mice around 10 weeks of age. All experimental groups of this model were given tamoxifen.

Animals were genotyped by PCR following protocols detailed in the publication of each line. In the case of Meis2$^{flox/flox}$, here are explained the primers and program used:

Fw: CAA GGA CGC AAT CTA TGG GTA

Rv: TGC AGA AAA CTT TCC TCT TAA TCA

PCR program: (3´95º, 35x (30´´95º, 30´´51º, 1´30´´72º) 7´72º and 4º)

Tamoxifen preparation

200mg of tamoxifen (Sigma-T5648-1G) were dissolved in 20ml of corn oil (Sigma-C8267) for a final concentration of 10mg/ml. The solution was sonicated for 1 hour in ice with ultrasonic homogenizer (Bandelin) and then aliquoted to store at 4ºC. When the stock solution preparation was older than 1 week, the aliquots were re-sonicated for 15 min before use. 100ul were given by oral-gavage to the mice per day, during 5 days.

Embryo harvest

Mice were mated in the afternoon and females were checked in the morning for the presence of vaginal plug. The stage of the embryos was defined by the day when the plug was observed, considering at noon of that day embryonic day 0.5 (E0.5). Pregnancy was always checked again before sacrifice, to avoid false positives. Pregnant females were euthanized by CO_2 inhalation and the uterus was extracted through an incision of the abdominal cavity and transferred to PBS. Then, in a petri dish containing PBS, the muscular layer of the uterus was removed with forceps. For embryos at E13.5 or younger, a piece of the yolk sac was collected for genotyping and from E14.5 onwards the tip of the tail was used instead. After removing the yolk sac and amnion, embryos were decapitated and the thorax was opened to collect the heart. Hearts were quickly wash in PBS and fixed in paraformaldehyde (PFA) (Merck) 2% in PBS overnight at 4ºC.

Adult mouse sacrifice

Heparin (ROVI 1000UL/mL) was injected intraperitoneal in mice (200µL), 30 minutes before sacrifice to improve blood removal. Adult mice were sacrificed at different experimental points by CO_2 inhalation and hearts were harvested by opening the thorax with scissors and forceps. Hearts were place in a petri dish with a KCl 30mM solution to stop beating in the phase of diastole. After removing lungs and thymus, hearts were weighted and placed in another petri dish with PBS for cannulation. A 5ml syringe (Beckton Dickinson) with a blunt needle was introduced in the left ventricle through the aorta and PBS was infused slowly until blood was removed. Then, hearts were fixed in PFA 2% in PBS 24 hours at 4ºC. The left posterior leg of every mice was cut, and skin and muscle removed, to measure tibia length with a caliber.

BrdU treatment

Adult mice were treated with BrdU (5-Bromo-2'-desoxyuridine; Merck B5002) dissolved at 0.5mg/mL in drinking water for 3 weeks. The treatment started one week after tamoxifen administration.

TISSUE PROCESSING

Cryo and paraffin-sectioning

After fixation, tissues were washed several times in PBS and cryopreserved with 15% sucrose overnight at 4ºC. Then, tissues were incubated in a solution with 15% sucrose and 7.5% gelatin in PBS at 37ºC for at least 4 hours, changing the solution and agitating occasionally. Gelatin blocks were prepared in a P6 dish at room temperature for gelatin solidification. Blocks were cooled down at 4ºC and frozen in isopentane at -80ºC for 1 minute and kept stored at -80ºC until cryo-sectioning. 8 µm-thick sections were obtained using a Leica CM1950 automated Cryostat and stored at -20ºC.

If the objective was to do paraffin sections, tissues were directly washed with 70% ethanol after fixation. Then, samples were incubated in different solutions at room temperature with increasing percentage of ethanol, until incubation with xilol. Samples were embedded in paraffin at 65ºC and after orientation, left at 4ºC to solidify. The dehydration process was usually done in a Thermo Excelsior SA processor at the Histopathology Unit at CNIC. Paraffin blocks were cut at 4 µm (10 µm for in situ hybridization) using a Leica RM2245 semi-automatic microtome. Sections were stored at 4ºC.

In both cases sections were collected on Superfrost+ slides (Fisherbrand).

IN SITU HYBRIDIZATION ON SECTIONS

Paraffin sections were rehydrated from xilol to PBS passing through sterile solutions with decreasing concentrations of ethanol. Sections were digested with proteinase K (10µg/ml) at 37ºC for 10 minutes. Riboprobe hybridization was performed at 65ºC overnight. The next day, sections were washed and incubated with anti-DIG antibody at 4ºC overnight. Then, sections were developed with BM-purple (Roche, ref 11442074001) at room temperature or 37ºC. Time of development was about 5 days.

IMMUNOFLUORESCENCE

In paraffin sections

Slides were incubated in xilol and solutions with decreasing concentrations of ethanol, washed in distilled water and PBS. Antigen retrieval was performed to break methylene bridges formed with fixation that cross-link proteins and mask the antigen sites. We used the heat-induced method with two different buffers. The most common was the sodium citrate but Meis antibodies worked better with Tris-EDTA buffer.

Here are the recipes for each buffer.

Citrate Buffer		
Citric Acid Monohydrate	Sigma-33114	10mM
Distilled water		1L
Adjust pH to 6.0 with NaOH		
Tween 20		0.05%
Store at room temperature for 1 month		

Tris-EDTA Buffer		
Trizma Base	Sigma-93350	10mM
EDTA solution	Sigma-E6758	1mM
Distilled water		1L
Adjust pH to 9.0		
Tween 20		0.05%
Store at room temperature for 1 month		

For antigen retrieval, the buffer was pre-heated in the microwave for 5 minutes. Samples were immersed in the buffer and heated for 20 minutes. Then, buffer with samples was let to temper for 20 minutes. Permeabilization was done with Triton X-100 0.5% in PBS for 30 minutes. In the case of Cx43, Triton concentration was reduced to 0.25%. Peroxidase block was done, if needed, after permeabilization, using H_2O_2 3% in methanol for 1 hour in darkness. To avoid unspecific binding of the antibody, sections were incubated with the universal TNB blocking reagent FP1012-Perkin Elmer, 1 hour at room temperature. Primary antibodies were incubated in the same TNB solution overnight at 4ºC. Secondary antibodies were incubated in PBS 1 hour at room temperature. Slides were always washed several times between every step with

Tween 0.1% in PBS. Finally, slides were mounted with Dako fluorescence mounting medium (s3023).

In gelatin sections

Slides were incubated in Tween 0.1% in PBS at 37ºC for 15 minutes and washed several times at room temperature until gelatin was removed. Then continued with the steps explained before without performing antigen retrieval.

Isolated CMs

After fixation, PFA was carefully washed several times with PBS. Then we followed the same steps explained before, starting with permeabilization. For BrdU staining a step of DNAse digestion was needed. It was performed after permeabilization, with DNAse I 1:20 (Roche) for 1 hour at 37ºC. After secondary antibody, Vectashield mounting medium (Vector Laboratories) was added to the dishes.

Whole mount atria from fetuses

Atria were washed with PBS after fixation and incubated with Triton X-100 0.5% in PBS for 24 hours at 4ºC. Blocking reagent was incubated for 8 hours and solution with Wheat Germ Agglutinin (WGA-Thermo Scientific-W21404) and DAPI for three days. Before confocal acquisition atria were transparent with CUBIC 1 for 1 day at 4ºC (Susaki *et al*, 2015).

Primary antibodies used:

TARGET	HOST	CONCENTRATION	REFERENCE
Meis a *	Rabbit	1:500	Torres' Lab
Meis 2 *	Rabbit	1:500	Torres' Lab
Hcn4	Mouse	1:100	Abcam ab85023
c-TnT	Mouse	1:200	MS-295 Thermo Scientific
Cx43	Rabbit	1:200	Sigma C6213
CFP	Goat	1:200	Acris R1091P
BrdU	Mouse	1:50	Invitrogen 347580
PH3	Rabbit	1:100	Millipore 06-570

* Anti-Meis-a antibody and anti-Meis2 were generated in rabbits with a synthetic peptide corresponding to the conserved C-terminal domain of Meis1 and Meis2 (GMNMGMDGQWHYM) and to a Meis2-specific N-terminal domain of Meis2 (HAPRPIPPVHHLNHGPP), respectively (Mercader, 2005).

Secondary antibodies used:

REACTIVITY	CONJUGATED	CONCENTRATION	REFERENCE
Rabbit	A633	1:500	Life technologies A21071
Rabbit	A594	1:500	Life technologies A11012
Rabbit	HRP	1:500	Dako P0448
Mouse	A488	1:500	Life technologies A11029
Mouse	A568	1:500	Life technologies A11004
Mouse	A647	1:500	Life technologies A21052
Goat	Biotin	1:500	Jackson 705-065-003

HEMATOXILIN & EOSIN AND SIRIUS RED STAINING

H&E and Sirius Red staining were performed at the CNIC Histopathology Unit. H&E staining was carried out using the Leica Automated Slide Stainer ST5020. For Sirius Red staining, the sections were brought to water and the nuclei were stained with Wiegerts hematoxylin. The tissue was then stained with Sirius red solution for one hour followed by differentiation in acetic acid and finally dehydrated and mounted in DPX.

IMAGE ACQUISITION

Images of the in situ hybridization were acquired with a Nikon Eclipse 90i microscope. H&E and SR stained sections were scanned with Hamamatsu Nanozoomer 2.0 RS and NDP.Scan 2.5 software. Analysis and quantifications were performed with NDP.Analyzer software. Immunofluorescence sections were acquired with a Zeiss LSM 700 confocal microscope and a Leica TCS SP8 coupled to a DMi8 inverted confocal microscope Navigator module equipped with white light laser. Whole-mount images of hearts were acquired with Nikon DXM1200F coupled to a Leica MZFLIII scope with a Plan Apo 1x objective.

ECHOCARDIOGRAPHY

In pregnant females

In a first approach, pregnant females, with the belly shaved were anesthetized with 2% isoflurane in oxygen. Abdominal surgery was then performed for uterus exposure. After surgery, isoflurane was adjusted to maintain a heart rate at 450±50 bpm and fetuses were exposed one at a time to keep them as warm as possible. An infrared

heat lamp was used for the same purpose during acquisition. Echocardiography was performed by an expert operator using a high-frequency ultrasound system (Vevo 2100, Visualsonics, Canada) with a 50-MHz probe on a heating platform. Bidimensional (2D), M-Mode and Doppler echocardiography were used to visualize the hearts in long and short axis view (LAX and SAX, respectively). Left and right ventricular ejection fraction (EF), wall thickness and diastolic and systolic chamber dimensions were assessed from the M-Mode SAX view. Color flow Doppler was placed at the base of the left or right ventricle to visualize simultaneously the inflow and outflow blood pattern. Heart rate was calculated using three consecutive outflow waves. The position of the fetuses was recorded, so that fetal identity could be tracked for genotyping. This procedure was therefore blinded to the genotype of the fetuses.

In the second approach, pregnant females were lightly anesthetized with 0.5-2% isoflurane in oxygen, adjusting the isoflurane to maintain heart rate at 450±50 bpm. Abdominal palpation was done to identify number of fetuses and position before image acquisition. Transabdominal echocardiography was performed by an expert operator using the same ultrasound system and acquiring the same images as explain above. Afterwards, a small incision was done in the abdominal cavity to confirm embryo number and position and track fetal identity for genotyping.

Adult mice

Transthoracic echocardiography was performed blinded by an expert operator using a high-frequency ultrasound system (Vevo 2100, Visualsonics, Canada) with a 40-MHz linear probe on a heating platform. Mice were lightly anesthetized with 0.5-2% isoflurane in oxygen, adjusting the isoflurane to maintain heart rate at 450±50 bpm. A base-apex electrocardiogram was continuously monitored. Images were analyzed using Vevo 2100Workstation software. Parasternal standard, 2D and MM, long and short axis views at the level of the papillary muscles (LAX and SAX view, respectively) were acquired.

OPTICAL MAPPING

The optical mapping technique provides action potential recordings at the tissue level with a high temporal and spatial resolution, and can be used from the subcellular level to the whole heart in vivo. We performed the technique in hearts from E14.5 and E16.5 fetuses following similar protocol to previous publications by Dr. Sedmera's group (Benes *et al*, 2014).

Pregnant females were sacrificed by cervical dislocation and embryos were harvested as explained above. While hearts were dissected, embryos were placed on a petri dish with ice-cold Tyrode's Buffer to prevent ischemic damage. Harvested hearts were placed in wells of a P12 dish on ice and incubated for 15 minutes in 500mL of cold Tyrode's Buffer with 2µL of di-4-ANEPPS (Invitrogen) (dye with fluorescence voltage dependent) and 15µL of blebbistatin (it stops heart beat and avoids movements during recording) in darkness. After staining, hearts were place on a special warm dish (37ºC) with Tyrode's Buffer and constant oxygen flow. Hearts were pinned and oriented for the desired acquisition view. Data was recorded using Ultima L high-speed camera and bundled software.

Tyrode's Buffer	
NaCl	145mM
KCl	5.9mM
HEPES	5mM
$CaCl_2$	1.1mM
$MgCl_2$	1.2mM
Glucose	11mM
Adjust pH to 7.4 at 37ºC	

Schematic representation of optical mapping procedure:

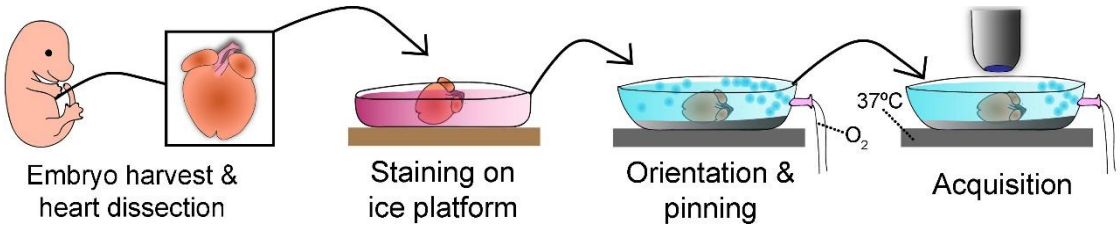

Data analysis and maps were done with BrainVision Analysis software. AP recordings were processed with Medium (3x3) and High Pass (0.5) filter to reduced noise and derivatives were calculated. Usually, the first beat was selected for mapping and a spatial filter of 3x3 was applied to improve map resolution. For activation curves calculations, the area of each color band in each ventricle was measured and expressed as percentage of whole ventricular area. Limit between left and right ventricles was defined by hand from apex aperture to base following the septum shadow in bright field pictures. Heart rates were calculated from the distance between one AP maximum pic and the next one (data are mean of 6 beats/per heart). A-V delay time was determine by the time between the beginning of atrial AP and the beginning of ventricular AP (data are mean of 3 beats/heart).

ADULT CARDIOMYOCYTE ISOLATION

Adult mice were sacrificed by CO_2 inhalation and the thoracic cavity was opened to expose the heart. Hearts were dissected and cannulated in a petri dish with Perfusion Buffer. The cannula was secured to the aorta with surgical thread and then placed in the Langendorff system (Obame *et al*, 2008), where Perfusion Buffer was infused for approximately 5 minutes until blood was removed.

The Langendorff system enables the buffer to enter the heart through the aorta with a constant flux achieved by a peristaltic pump and constant temperature at 37ºC. After cleaning the blood, the Digestion Buffer was infused to digest the extracellular matrix and isolate cardiac cells. Digestion was performed for about 20 minutes. Once the heart was completely digested, the cannula was removed and the cardiac tissue placed in a petri dish for complete disaggregation with a Pasteur pipette. From this point onwards, steps were carried out at room temperature. Cardiac cells were filtered through a 100µm strain net for extracellular matrix removing and transferred to a 50mL Falcon tube with Stopping Buffer I. After 15 minutes of decantation, the supernatant was discarded and cells newly resuspended in Stopping Buffer II in a 15mL Falcon tube for 10 minutes. CMs are the largest cells in the adult heart, so they are the first to reach the bottom. Thus, short steps of decantation allow an enrichment in CMs of the final pool of cells. Then, cells were transferred to a new 15mL Falcon tube containing

T2 buffer for calcium reintroduction for 10 minutes and the step was repeated to incubate cells in T5 buffer. CMs were then plated on laminin-coated MatTeK glass-bottom dishes with plating medium and incubated at 37ºC for about 2-4 hours. When CMs were attached to laminin, the medium was washed with PBS and 2% PFA was added overnight at 4ºC for fixation before immunostaining.

	REAGENT	COMPANY	CONCENTRATION
PERFUSSION BUFFER	Sodium chloride	Sigma - Aldrich	113mM
	Potassium choride	Sigma - Aldrich	4,7mM
	Potassium phosphate monobasic	Sigma - Aldrich	0,6mM
	Sodium phosohate dibasic	Sigma - Aldrich	0,6mM
	Magnesium sulphate heptahydrate	Sigma - Aldrich	1,2mM
	Sodium bicarbonate	Sigma - Aldrich	12mM
	Potassium bicarbonate	Sigma - Aldrich	10mM
	Phenol Red	Sigma - Aldrich	0,032mM
	HEPES salt	Sigma - Aldrich	10mM
	Taurine	Sigma - Aldrich	30mM
	Butanodione monoxime (BDM)	Sigma - Aldrich	10mM
	Glucose	Sigma - Aldrich	5,5mM
	H_2O		
DIGESTION BUFFER	Perfussion buffer		1X
	Liberase TM 100mg	Roche Appl. Biosc	0,2mg/ml
	Trypsin 2,5%	Gibco	0,14mg/ml
	Calcium Chloride 100mM	Sigma - Aldrich	12,5µM
	H_2O		
STOPPING BUFFER I	Perfussion buffer		1X
	Fetal Bovine Serum	Gibco	5%
	Calcium Choride 10mM	Sigma - Aldrich	12,5µM
STOPPING BUFFER II	Perfussion buffer		1X
	Fetal Bovine Serum	Gibco	10%
	Calcium Choride 10mM	Sigma - Aldrich	12,5µM
T2	Stopping Buffer II		1X
	Calcium Choride	Sigma - Aldrich	100µM
T5	Stopping Buffer II		1X
	Calcium Choride	Sigma - Aldrich	1mM

	REAGENT	COMPANY	CONCENTRATION
PLATING MEDIUM	Medium 199	Invitrogen	
	PEN-STREPT	Lonza	100U/ml
	L-Glutamine	Lonza	1%
	BSA	Sigma-Aldrich	0,2%
	NaHCO3	Sigma-Aldrich	22mM
	FBS	GIBCO	5%
	BDM (2,3-Butanedione monoxime		10mM
	Blebbistatin		25uM

PLOIDY ESTIMATION IN ISOLATED CMs

To measure nuclear volumes and DAPI intensity in isolated CMs we acquired confocal z-stacks at high magnification (63X) with steps of 2µm using Zeiss LSM 700 confocal microscope. Image J (https://imagej.nih.gov/ij/) was used for image analysis. The first step was to segment the DAPI channel, for which images were filtered with Gaussian Blur to improve automatic recognition of nuclei. The green channel (autofluorescence) was used to subtract background signal in the DAPI channel and the threshold tool was used to create a 3D binary file. If necessary, the "fill holes" tool was applied and "analyzed particles" tool was used to eliminate small dots from background. The next step was to use 3D ROI manager to create a 3D selection around the nuclei (Ollion *et al*, 2013). Objects touching the border of the pictures were not consider for analysis. Finally, objects created were placed on the original DAPI channel to measure their volume and intensity. The same objects were used to measure BrdU intensity in the red channel.

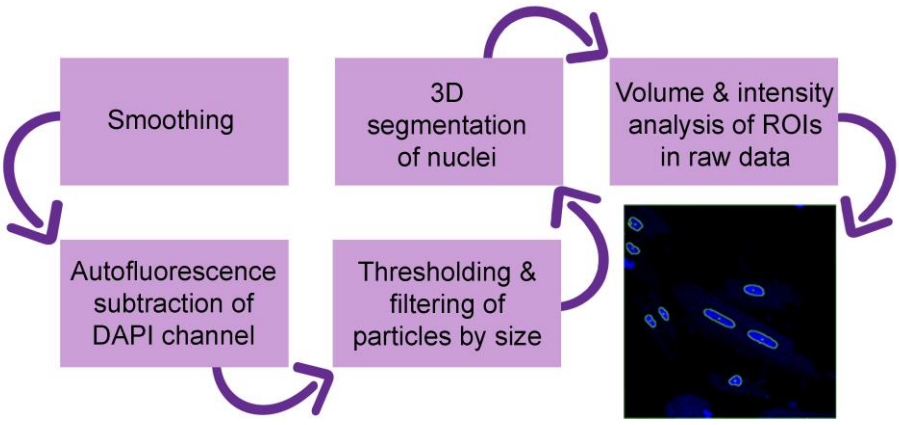

ELECTROCARDIOGRAM

Adult mice were lightly anesthetized with 1.5% isoflurane in oxygen and placed facing up on a metallic platform. Electrodes were introduced subcutaneously in each limb and ECG was record for about 2 minutes.

When mice were challenged with isoproterenol, 5 minutes were recorded before treatment. Then, isoproterenol (3mg/kg) was injected intraperitoneal and heart beats were recorded for additional 20 minutes. During the last minute the isoflurane was turned off to observe heart conduction during the recovery phase. Experiments always finished before animals were completely awake, to avoid stress. Moreover, an infrared heat lamp was used to keep normal body temperature in mice and protective cream was apply in the eyes before starting the experiment.

Analysis were performed on manually selected 40-second-fragments containing about 300-400 beats of stable ECG. Measurements were calculated with custom MatLab scripts design by the group of Dr. David Filgueiras at CNIC. To detect the R-peak of the QRS complex we used parabolic fitting of the coiflet wavelet transformation and further detection of the maximum magnitude point. All R-peak detections were supervised to ensure accuracy of ECG segmentations. After detection of QRS complex, P and T waves, ECG intervals were extracted using adaptive windowing depending upon beat-to-beat R-R changes. Specifically: PR intervals were measured from the beginning or the P wave to the beginning of the R wave; QRS intervals were measured from the beginning of the Q wave until the lowest amplitude point of S wave; QT intervals were measured from the beginning of the Q wave until the point where the T-wave declines to 90% (T90) from the peak; QTt intervals were measured from the beginning of the Q wave to the point where the tangential from the beginning of T wave crosses the baseline. Adaptive heart-rate-corrected QT and QTt values (QTc; QTtc) were derived using a modification of Bazzet's formula for murine electrocardiography (Mitchell *et al*, 1998).

Here is an example of how the ECG is visualized and automatically analyzed in the program:

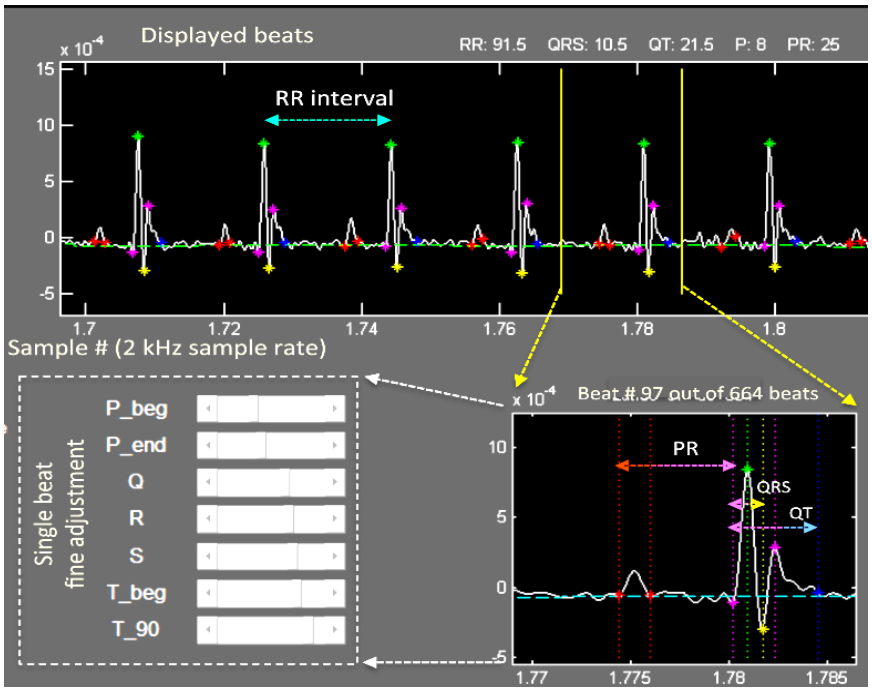

RNA SEQUENCING

RNA-seq was performed in four different conditions, atria and ventricles from fetal hearts at E15.5 and from adult hearts to compare Meis1 and Meis2 double deletion (constitutive or inducible) with control littermates. In all cases, 4 replicates were used for each condition.

RNA isolation

Fetuses were harvested at E15.5 from four independent litters and a Control and a dKO were selected from each litter. Hearts were dissected in ice-cold sterile PBS. Atria and ventricles were separated and OFT removed, to be immediately frozen with liquid nitrogen and stored at -80ºC until all the samples were collected. Tissue lysis was performed with TissueLyser LT (Quiagen) and RNA isolation with RNeasy Mini Kit (Quiagen).

Adult hearts from 8 male littermates were harvested two weeks after tamoxifen induction, as explained in previous chapters, and cannulated to clean the blood with

ice-cold sterile PBS. Atria and ventricles were separated and OFT removed before being frozen at -80ºC. Tissue lysis was done with TriReagent (Trizol; Sigma-T9424) using TissueLyser LT (Quiagen). Total RNA isolation was completed following RNeasy Midi Kit (Quiagen) protocol for RNA cleanup.

RNA-seq library production and sequencing

It was performed at CNIC Genomic Unit.

20ng of total RNA were used to generate barcoded RNA-seq libraries using the NEBNext Ultra RNA Library preparation kit (New England Biolabs). Briefly, poly A+ RNA was purified using poly-T oligo-attached magnetic beads followed by fragmentation and then first and second cDNA strand synthesis. Next, cDNA ends were repaired and adenylated. The NEBNext adaptor was then ligated, followed by uracil excision from the adaptor and PCR amplification. Finally, the size and the concentration of the libraries was checked using the TapeStation 2200 DNA 1000 chip. Libraries were sequenced on a HiSeq2500 (Illumina) to generate 60-base single reads. FastQ files for each sample were obtained using bcltofastQ software 2.20.

RNA-seq data analysis

Read quality was assessed with FastQC (http://www.bioinformatics.babraham.ac.uk/projects/fastqc/). Over-represented sequences were trimmed with Cutadapt 1.7.1 (Martin, 2012), which also discarded reads that were shorter than 30 bp. The resulting reads were mapped against the mouse transcriptome (GRCm38, release 91; aug2017 archive) and quantified using RSEM v1.2.20 (Ritchie et al., 2015). Data were then processed with a differential expression analysis pipeline that used Bioconductor package LIMMA (Ritchie et al., 2015) for normalization and differential expression testing, using a paired strategy.

Genes with at least 1 count per million in at least 4 samples were considered for statistical analysis. We considered as differentially expressed those genes with Benjamin-Hochberg adjusted p-value<0.05. Fold change and log (ratio) values were calculated to represent gene expression differences between conditions.

Gene Set Enrichment Analysis was performed with genes differentially expressed using the Broad Institute GSEA “Molecular Signatures Database”

(http://software.broadinstitute.org/gsea/msigdb/index.jsp) computing overlaps with KEGG and Gene Ontology gene sets.

STATISTICS

Parametrical T student test was performed to compare two groups of data. For comparisons with more than two groups of data, Two-way ANOVA was used. In this analysis the influence of two factors, time and genotype, in the distribution of the sample, were studied. Chi square test was used for comparisons between observed and expected frequencies. Data are indicated as means ± SEM except for ECG data which are expressed as median ± SEM.

All comparisons and graphs were made using Prism 7.0 statistical analysis software. In all cases values of $P<0.05$ were considered statistically significant.

RESULTS

MEIS EXPRESSION PATTERN IN THE HEART

Meis1 And Meis2 Are Expressed In Cardiac Progenitors And The Three Layers Of The Developing And Adult Heart: Endocardium, Myocardium And Epicardium.

Determining the expression pattern of a gene is crucial to be able to understand its function. Thus, we performed in situ hybridization for *Meis1* and *Meis2* mRNAs at different embryonic days in the mouse heart (FIG. 9). Similar expression patterns were found for *Meis1* and *Meis2* in the developing heart. At early stages, both genes are expressed in second heart field progenitors, epicardium and endocardium (FIG. 9). However, at E14.5 we detected strong signal of *Meis2* RNA in the valves while *Meis1* is almost absent in this area.

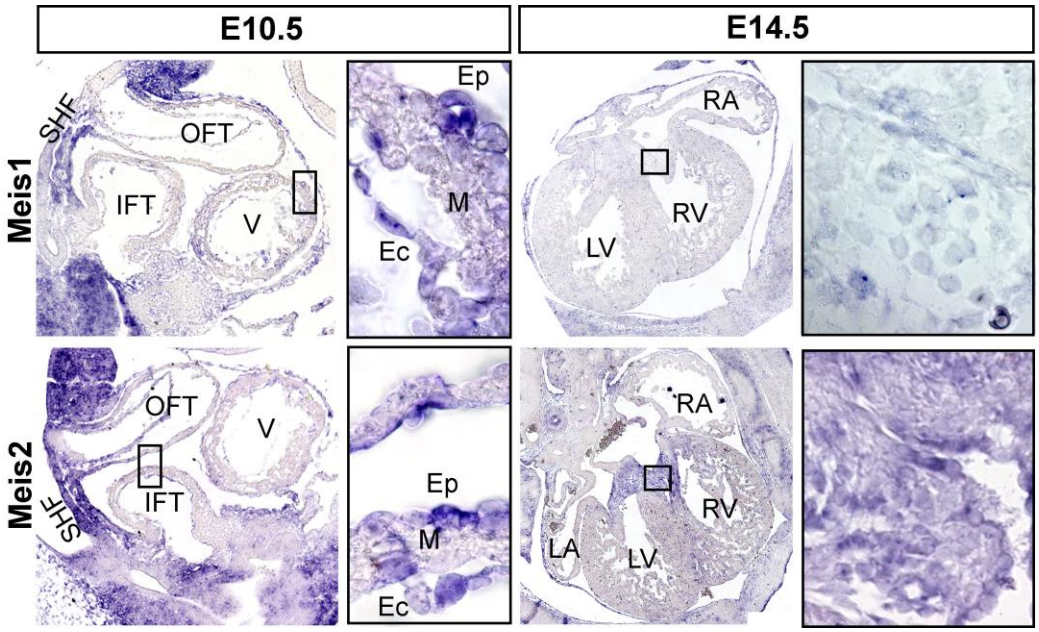

Figure 9. *Meis1* and *Meis2* mRNA in situ hybridization. *Meis1* and *Meis2* mRNA was detected in the second heart field (SHF), pericardium, endocardium (Ec) and epicardium (Ep) in E10.5 wild type embryos. Boxed regions indicate magnifications shown to the right. Panels on the right show *Meis1* and *Meis2* expression at E14.5. Magnified boxes show that expression pattern in the atrio-ventricular valves. Inflow tract (IFT), Outflow tract (OFT), Ventricle (V), Myocardium (M), Right Atrium (RA), Left Atrium (LA), Left Ventricle (LV), Right Ventricle (RV).

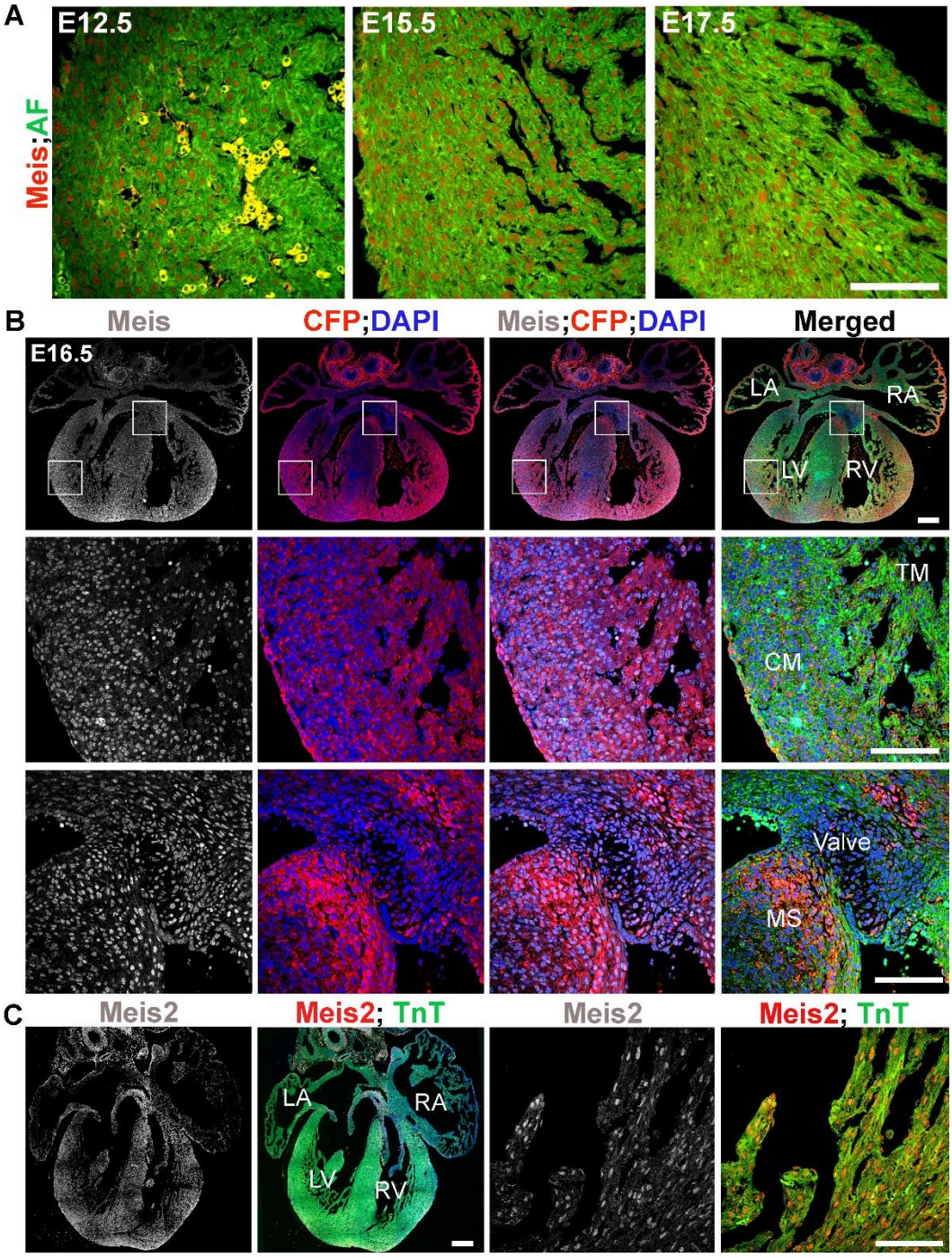

Figure 10. Meis1 and Meis2 are expressed in developing cardiomyocytes. A. Confocal images of embryonic ventricles at different time points. Immunofluorescence anti-Meis-a is shown in red. B. Confocal sections of E16.5 hearts of the Meis1-ECFP line combined with Meis-a immunofluorescence. Boxes indicate magnified regions shown below corresponding to ventricular myocardium and sub-membranous area of the septum. C. Immunofluorescence with anti-Meis2 antibody. Right panels show a high magnification of a ventricular myocardium region. Scale bars: 100µm in all pictures.

We were not able to observe a clear signal in the myocardium area with this technique so we tried with immunofluorescence using an antibody that recognizes Meis1 and Meis2 proteins. A nuclear signal for Meis was found in compact and trabecular myocardium throughout development (FIG. 10A).

In order to better understand the expression dynamics of Meis in the myocardium, we took advantage of a *Meis1-ECFP* knock-in line and compared the ECFP fluorescence with a Meis antibody immunofluorescence at E16.5 (FIG. 10B). The ECFP signal was detected in myocardium of the atria and ventricles. The pattern is quite homogeneous, except in the septum, where a strong ECFP signal is present in the sub-membranous and sub-endocardial layers (FIG. 10B). The central part of the septum showed weak ECFP signal, while the Meis antibody stains this region. This suggests that Meis2 could be the prevalent factor in the central septum area as well as in the valves. Moreover, we confirmed these results using and antibody specific for Meis2 protein, which detected a nuclear signal in the valves, the septum and also the compact and trabecular myocardium (FIG. 10C).

We next addressed the same question in the adult heart. We continued using the Meis1-ECFP tool and observed a strong signal in the sinoatrial and atrio-ventricular nodes and the His Bundle (FIG. 11A). The atria were also labeled, but this was not clear in the case of ventricular myocardium (FIG. 11A). IF for Meis and Hcn4 confirmed the preferential expression of these transcription factors in the CCS and in atrial and ventricular cardiomyocytes (FIG. 11B). To further confirm our results, we used *Meis1-CreER; R26-TdTomato* as a reporter of Meis1-expressing cells upon adult tamoxifen administration. Hearts were harvested right after the tamoxifen induction (1mg/day for 5 days). TdTomato reporter expression was found in the CCS, including the VCS and the atrial CCS with its nodes. The strongest recombination was found in the SAN (FIG. 11C). In addition, many CMs from the atria were labeled and several in the ventricles (FIG. 11C). We consider that not all CMs were labeled due to low Cre recombination efficiency, and the usual variability associated to the use of tamoxifen.

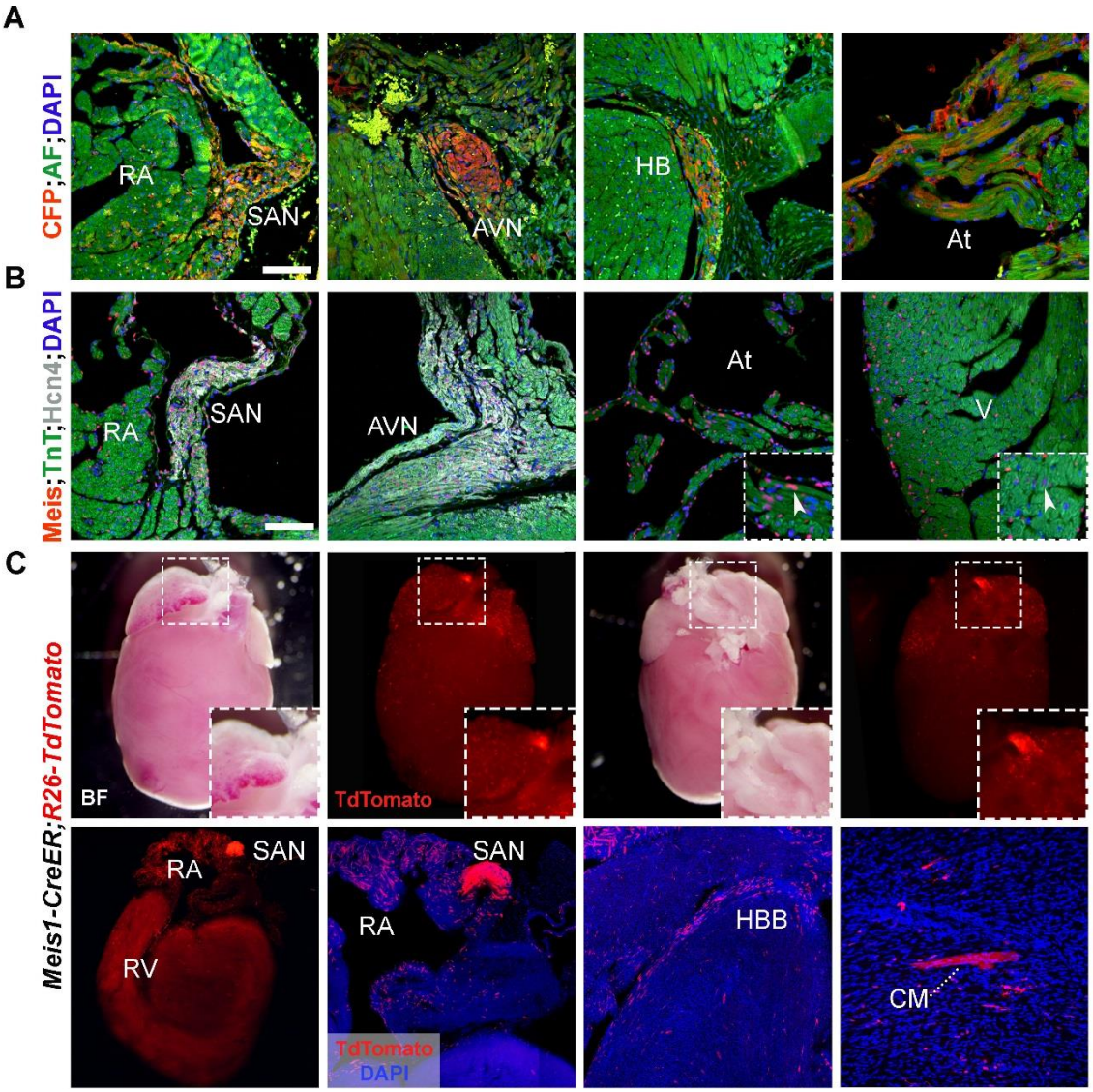

Figure 11. Meis1 and Meis2 are expressed in adult cardiomyocytes of the working and conducting myocardium. A. Confocal images showing expression of Meis1-ECFP in CCS and atrium myocardium. Sinoatrial node (SAN), Atrio-Ventricular node (AVN), His Bundle (HB) B. Left panels show co-immunofluorescence of Meis-a and Hcn4 in the SAN and AVN. Right panels show Meis-a signal in atrial (At) and ventricular (V) CMs. Arrowheads in boxes point to CMs positive for Meis-a. Scale bar in A and B is 100µm C. Upper panels show whole-mount *R26TdTomato;Meis1-CreER* hearts. Boxes show a magnification of the SAN area. Bottom panels show thick sections of a *R26TdTomato;Meis1-CreER* heart.

MEIS FUNCTION IN CARDIOMYOCYTES DURING HEART DEVELOPMENT

Meis1 And *Meis2* Double Deletion In CMs Causes Perinatal Death

We generated a mouse model to study the function of Meis TFs in cardiomyocytes. *Meis1* and *Meis2* were simultaneously deleted by recombination with *α-MHC-Cre* (FIG. 12A).

The recombination pattern of *α-MHC-Cre* is very specific for CMs (Agah *et al*, 1997) and it starts to recombine at E8.5 with some patches. We studied the recombination using the *R26R-LacZ* reporter line and observed at E10.5 the whole left ventricle is already recombined, while atria and right ventricle take one or two days longer for full recombination (FIG. 12B).

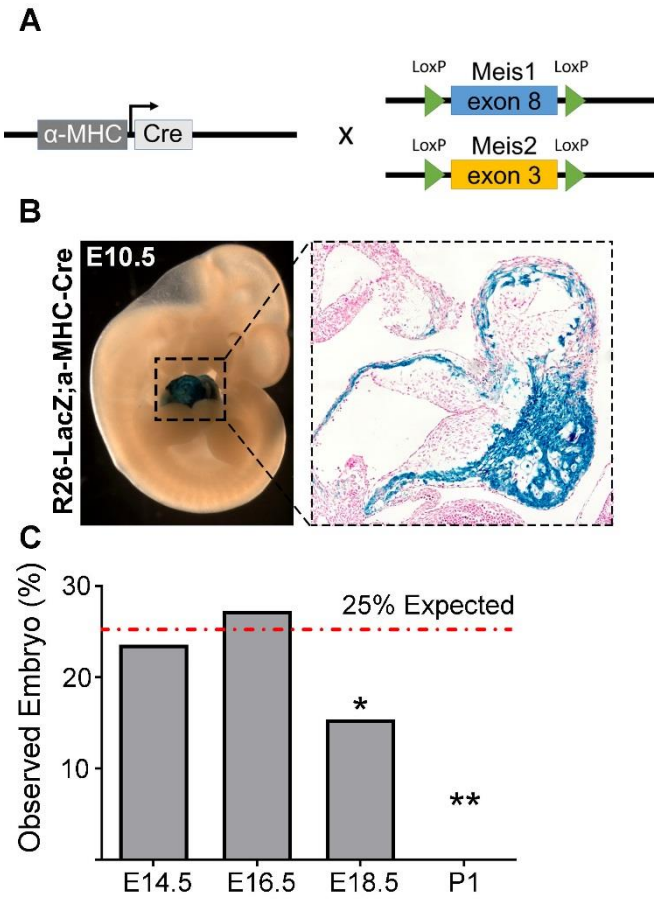

Figure 12. *Meis1* and *Meis2* double deletion in developing CMs causes perinatal death. A. Model for simultaneous constitutive deletion of *Meis1* and *Meis2* in CMs. B. Recombination pattern of *a-MHC-Cre* in E10.5 whole-mount embryo and a heart section. C. Graph showing expected and observed frequencies of dKO fetuses at different embryonic days.

We analyzed the frequencies of the different genotypes at several time points. We noticed that at the latest stages of development, the frequency of dKO embryos was below the expected value (FIG. 12C). At postnatal day 1 we were not able to recover any dKO (FIG. 12C). These results indicate that Meis1 and Meis2 TFs are essential in CMs for survival at birth.

Meis1; Meis2 dKO Hearts Present Morphological Alterations

The next step was to analyze in detail the phenotype of dKO hearts to elucidate what are the alterations derived from Meis loss of function in cardiomyocytes.

We harvested hearts at E18.5 and described external morphological alterations in the atria of dKOs compared to controls (FIG. 13A). The left atrium is the most affected presenting finger-like protrusions and a reduced size (FIG. 13B). The right atrium also showed finger-like structures but they were less prominent than those in the left atrium (FIG. 13B). The junction between right and left ventricle, at the apex, is not properly closed. We performed histological analysis to study internal structures and observed ventricular septal defects and a non-significant tendency to present thinner compact myocardial walls (FIG. 13C). VSD was present in 40% of the dKO fetuses at E18.5 (FIG. 13D) and in some cases was accompanied by overriding aorta. Wall-thickness was measured on sections and dKO hearts showed a tendency to present thinner ventricular compact myocardium (FIG. 13Es).

Harvesting hearts at earlier stages we found that dKO hearts can be clearly identified at E14.5 by atrial malformations, while at E12.5 only in some cases small finger-like protrusions can be observed in left atria (FIG. 14). Altogether, these data suggest Meis TFs play a role in cardiac morphogenesis.

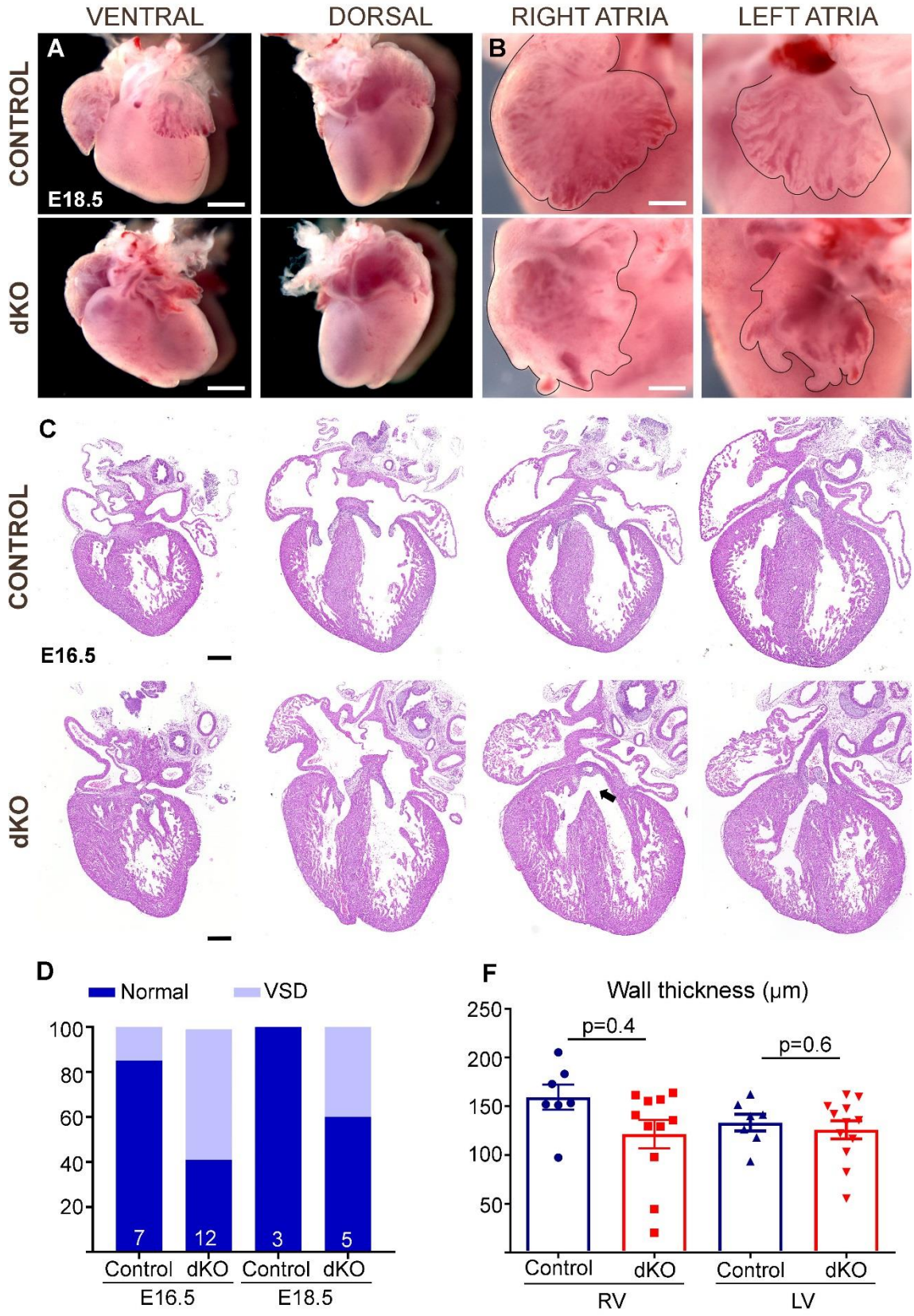
VENTRAL
DORSAL
RIGHT ATRIA
LEFT ATRIA
A
B
CONTROL
dKO
E18.5
C
CONTROL
dKO
E16.5
D
Normal
VSD
100
80
60
40
20
7
12
3
5
Control
dKO
Control
dKO
E16.5
E18.5
F
Wall thickness (μm)
250
200
150
100
50
p=0.4
p=0.6
Control
dKO
Control
dKO
RV
LV

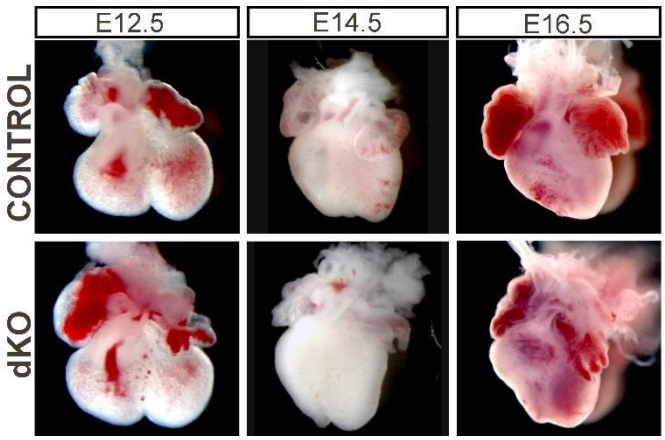

Figure 14. External malformations in dKO hearts are visible at E14.5. Whole mount images of Control and dKO hearts at three different embryonic days. Atrial finger-like protrusions are already present at E14.5.

In order to better understand atrial malformations we dissected atria from E18.5 hearts and stained them in whole mount for tissue visualization in confocal. 3D reconstruction highlighted the different morphology in dKO atria compared to control siblings (FIG. 15A). Studying confocal sections in detail, we observed thinner and disorganized pectinate muscles in dKO when compare to control (FIG. 15B).

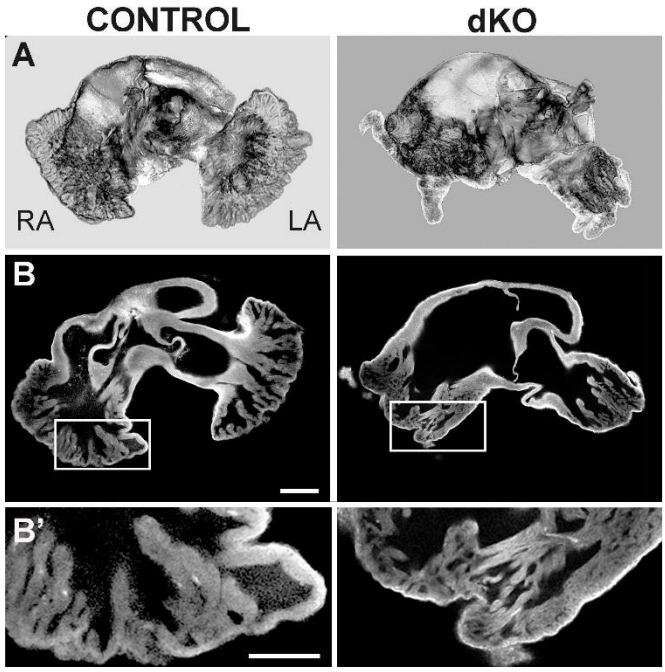

Figure 15. Atrial malformations affect pectinate muscles. A. 3D reconstruction of whole mount confocal images from Control and dKO atria stained with WGA at E18.5. B. Confocal section of atria in panel A. Box regions indicate magnification shown in B'. Scale bar: 400µm. B'. Right atria magnification showing pectinate muscles. Scale bar: 200µm.

Figure 13. Cardiac morphological alterations produced by CM-specific Meis1 and Meis2 deletion. A. Whole-mount E18.5 hearts from control and dKO littermates. Scale bar 500um. B. Left and right atrium from control and dKO hearts. Scale bar 500um.C. H&E staining on sections from control and dKO E18.5 hearts. From left to right the sectioning plane progresses from dorsal to ventral. Arrow point to VSD. Scale bar 200um. D. Percentage of fetuses with VSD at E16.5 and E18.5. E. Graph showing compact myocardium thickness of control and dKO hearts at E16.5 measured in sections.

Constitutive *Meis1* And *Meis2* Deletion Leads To Smaller Hearts And Stress-induced Cardiac Rhythm Alteration.

The morphological defects found do not necessarily explain the lethality of dKOs embryos at birth. Thus, we decided to explore by echocardiography the morphology and function of mutant fetal hearts *in utero*. For these experiments, pregnant females were anesthetized and the uterus was directly exposed for trans-uterine echocardiography (FIG. 16A). First, we measured the size of the interventricular septum and found a reduction in dKO hearts at E18.5, although it was not detected at earlier stages (FIG. 16B). Moreover, left and right ventricular masses were also reduced by the end of gestation but not before (FIG. 15B). These data, together with our previous result on wall thickness, determines Meis loss of function in CMs leads to smaller hearts. Thus, we decided to explore the possibility of defective proliferation in dKOs as an explanation for the smaller size. However, dKO hearts presented a non-significant tendency to proliferate more than control hearts at E16.5 (FIG. 17).

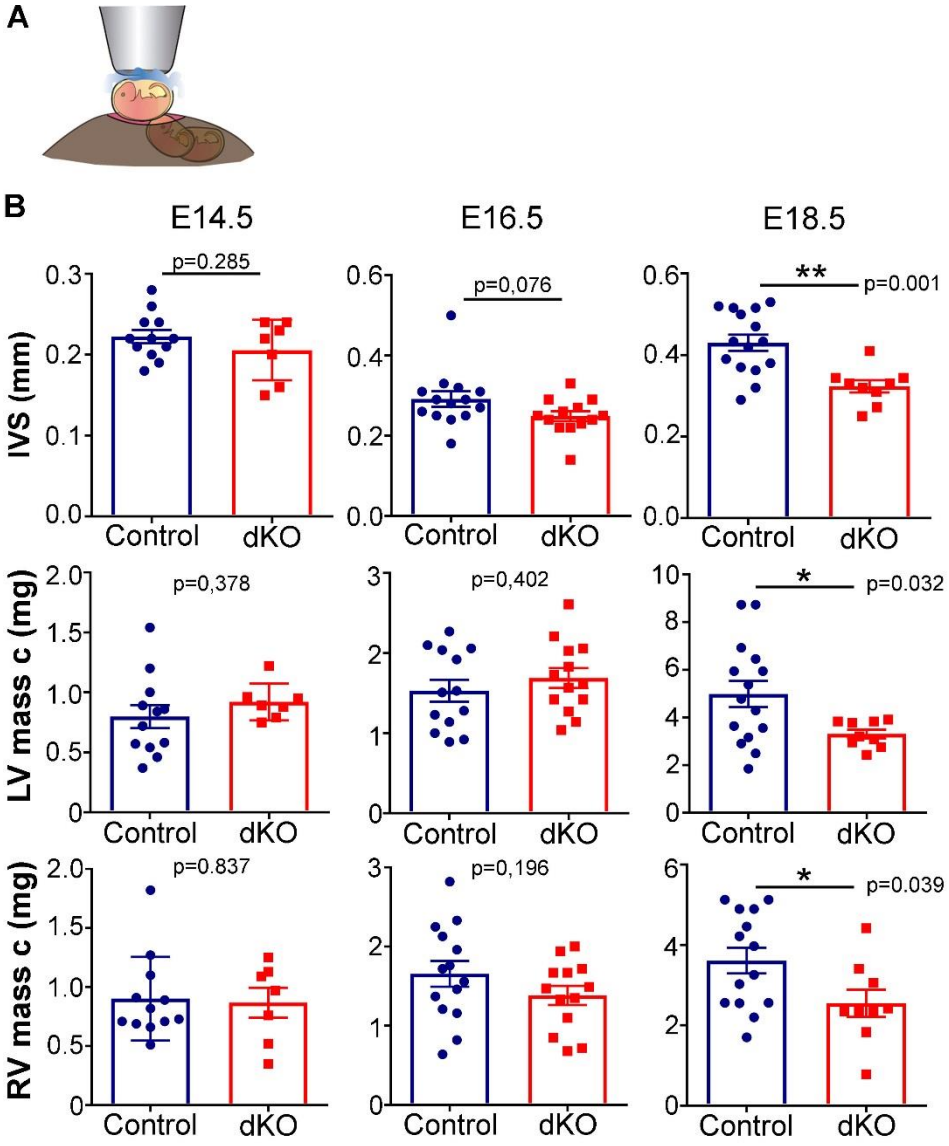

Figure 16. Echocardiography reveals smaller hearts in dKO fetuses. A. Schematic representation of Echo-Doppler procedure in pregnant females. B. Graphs summarizing results obtain from interventricular septum (IVS) thickness, and left and right ventricular masses at three different embryonic days in Control and dKO fetuses.

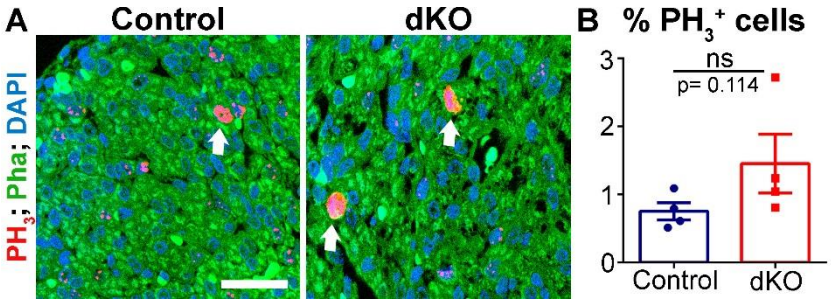

Figure 17. Proliferation rate in the myocardium of control and mutant fetuses. A. Confocal section of control and dKO ventricle stained with PH3 in red and Phalloidin in green. Arrows indicate mitotic cells. Scale bar: 25µm B. Graph showing quantification of cells PH3 + per total number of nuclei in terms of percentage. Data are means from 6 sections per embryo.

Regarding cardiac function, we were not able to detect any difference in left ventricular ejection fraction, at any of the developmental points analyzed (FIG. 18A). This observation, together with the moderate reduction in heart size suggest insufficient cardiac output is not the cause of lethality. However, heart rate was found significantly higher in dKO embryos at the end of gestation, suggesting alterations in cardiac rhythm (FIG. 18B).

Then, we decided to focus on flow pulse records through which we can detect passive filling of the ventricle when it is relax (E wave), the atrial contraction by the flow of blood coming into the ventricle (A wave) and ventricular contraction by blood flow going out through great vessels (Ejection wave) (FIG. 19B). Using this methodology we found higher frequency of arrhythmias in dKOs at different developmental stages (FIG. 19B, C). Looking in detail at flow pulse records from dKO fetuses, we observed changes in atrial contraction rhythmicity, although it is difficult to determine whether atrial contraction is delay or absent in some beats (FIG. 19B). These results suggest dKO fetuses present a tendency to tachycardia (FIG. 18B, 19B) and point to the SAN as a possible origin of the arrhythmia but further studies are needed.

We next studied the influence of uterine exposure on the alterations in cardiac rhythm. For this, we implemented methodology that enabled us to record blood flows in embryonic hearts without surgical procedures and without losing track of fetus identity (FIG. 20A, B). This technique allows us to longitudinally analyze the same litter from E16.5 to E18.5, keeping track of individual fetuses. In this case no differences were found on heart rate (FIG. 20B, C), and arrhythmias did not appear in any genotype (FIG. 20B; 20D). These results indicate that Meis loss of function in CMs render hearts more sensitive to certain stress conditions associated to surgery. We hypothesize that the stress of delivery and adaptation to extra-uterine life leads to cardiac rhythm alterations in Meis mutants that can lead to death.

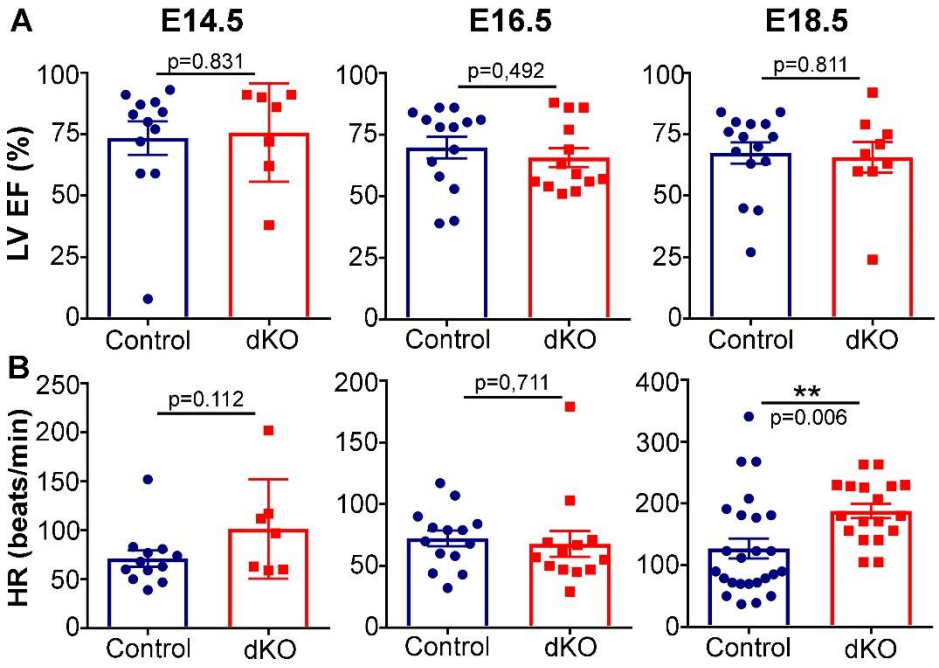

Figure 18. dKO fetuses present normal cardiac function and higher heart rates. A-B. Left ventricular ejection fraction and heart rate measurements during Echocardiography, in Control and dKO hearts at the indicated embryonic days.

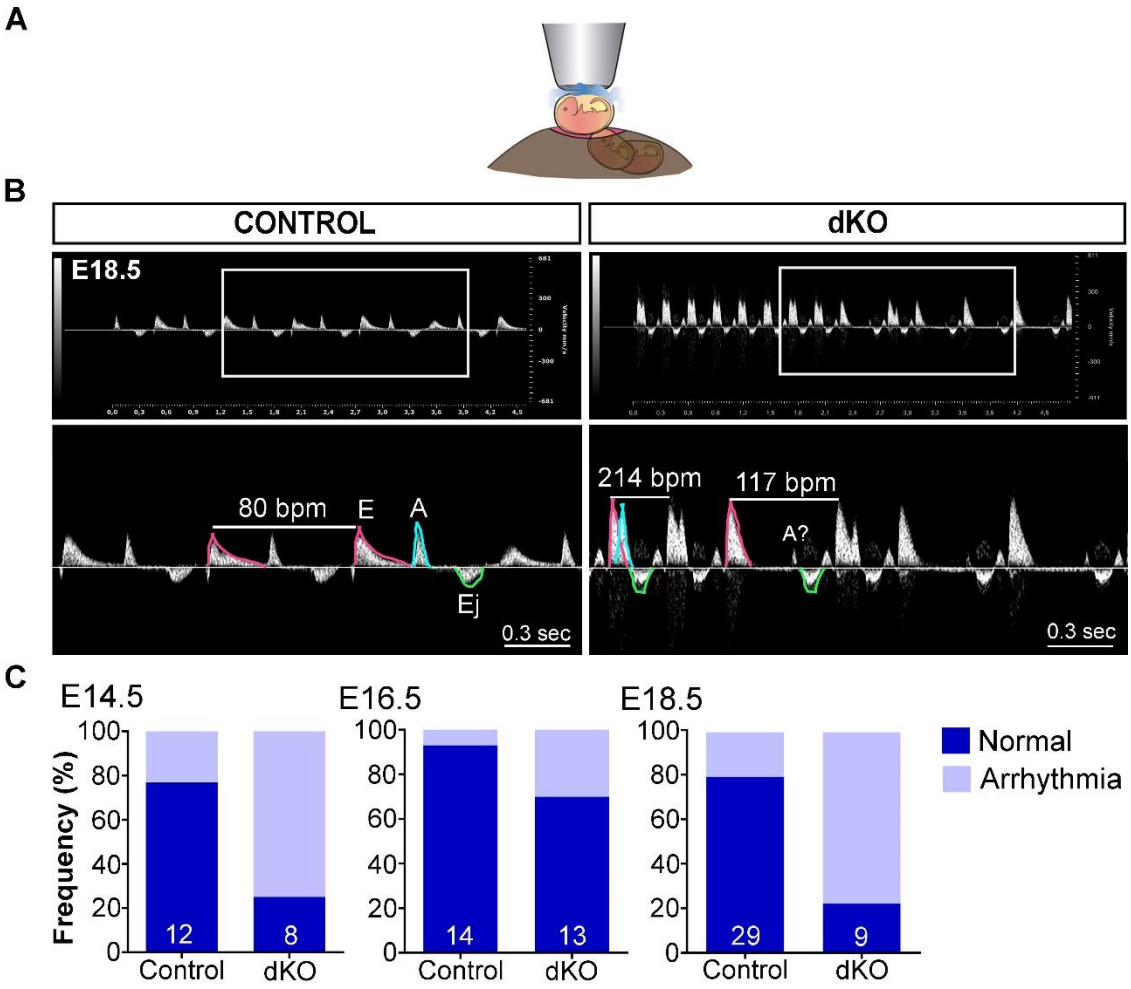

Figure 19. dKO hearts manifested arrhythmias during trans-uterine echo acquisition. A. Schematic representation of trans-uterine Echocardiography. B. 5 seconds recording of blood flows in Control and dKO hearts upon uterus exposure. Low panels are magnification of areas in white rectangles. E-wave (E) corresponds to the passive filling of the ventricle, A-wave (A) corresponds to the active filling of the ventricles upon atrial contraction. Ejection (Ej) corresponds to the blood exiting from the ventricles through great arteries after ventricular systole. Beats per minute (bpm). dKO heart show beats with no clear A wave (A?). C. Percentage of fetuses for each genotype that present some arrhythmic episode during Echo-Doppler acquisition after uterus exposure.

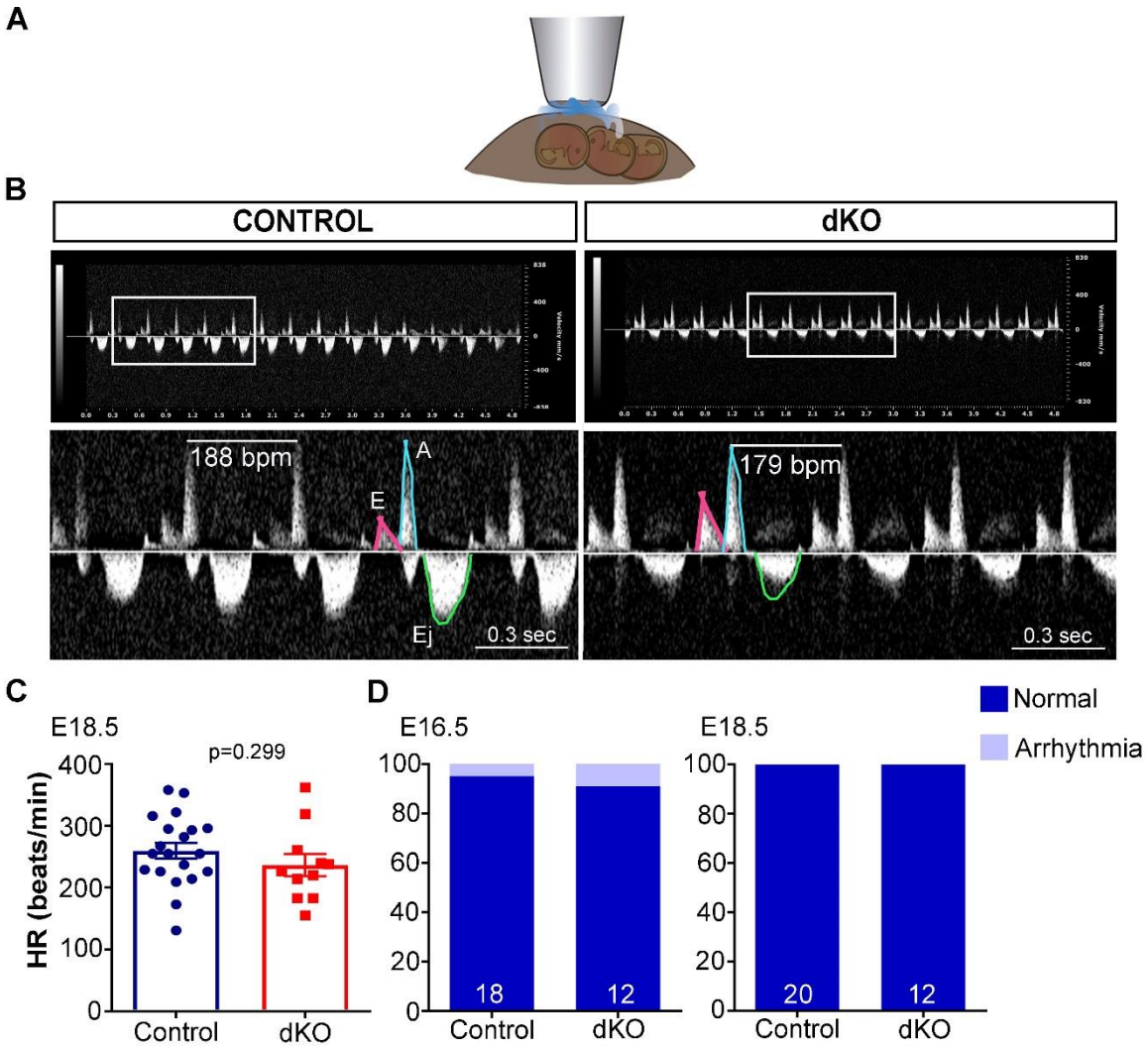

Figure 20. Normal beating heart rate and cardiac rhythm in fetuses during trans-abdominal Echocardiography. A. Schematic representation of trans-abdominal Echocardiography. B. 5 Seconds blood flows of Control and dKO fetuses acquired in pregnant females without uterus exposure. Low panels are magnification of areas in white rectangles. Pink line indicates E wave, blue, A and green, Ej. C. Control and dKO hearts beating rates during Trans-abdominal Echocardiography. D. Percentage of normal and arrhythmic hearts found during Trans-abdominal Echocardiography.

Meis Deletion In CMs Leads To Slower Electrical Impulse Propagation Through The Ventricles

In light of these results, we wanted to further explore cardiac conduction physiology in dKO hearts. Thus, we decided to characterize the electrical activity of the fetal hearts using the optical mapping technique (In collaboration with Dr. David Sedmera, Prague). Optical mapping allowed us to study the changes in voltage membrane that occur during the transmission of the electrical impulse through the heart.

We first started with E14.5 hearts when technically optical mapping is more likely to succeed and Meis should already be completely deleted but no overt morphological alterations are found in ventricles. We recorded approximately 16 seconds per heart and measured different parameters. Heart rates were similar between controls and mutants (FIG. 21A, B). We observed a non-significant tendency to a shorter delay between atrial and ventricular depolarization in mutants (FIG. 21C, D).

Analysis of voltage maps revealed a slower activation curve in the left and right ventricle of hearts lacking Meis compared to controls, mostly due to a delay during the first two milliseconds of ventricular depolarization (FIG. 22A,B). This parameter reflects the conduction velocity and therefore suggests an impairment of electrical propagation in mutants. We studied the atrial activation curve but we did not detect significant differences in this case (FIG. 22C). However, we cannot discard conduction anomalies in atria because of a very high variability among maps of the same experimental group due to the irregular atrial surface.

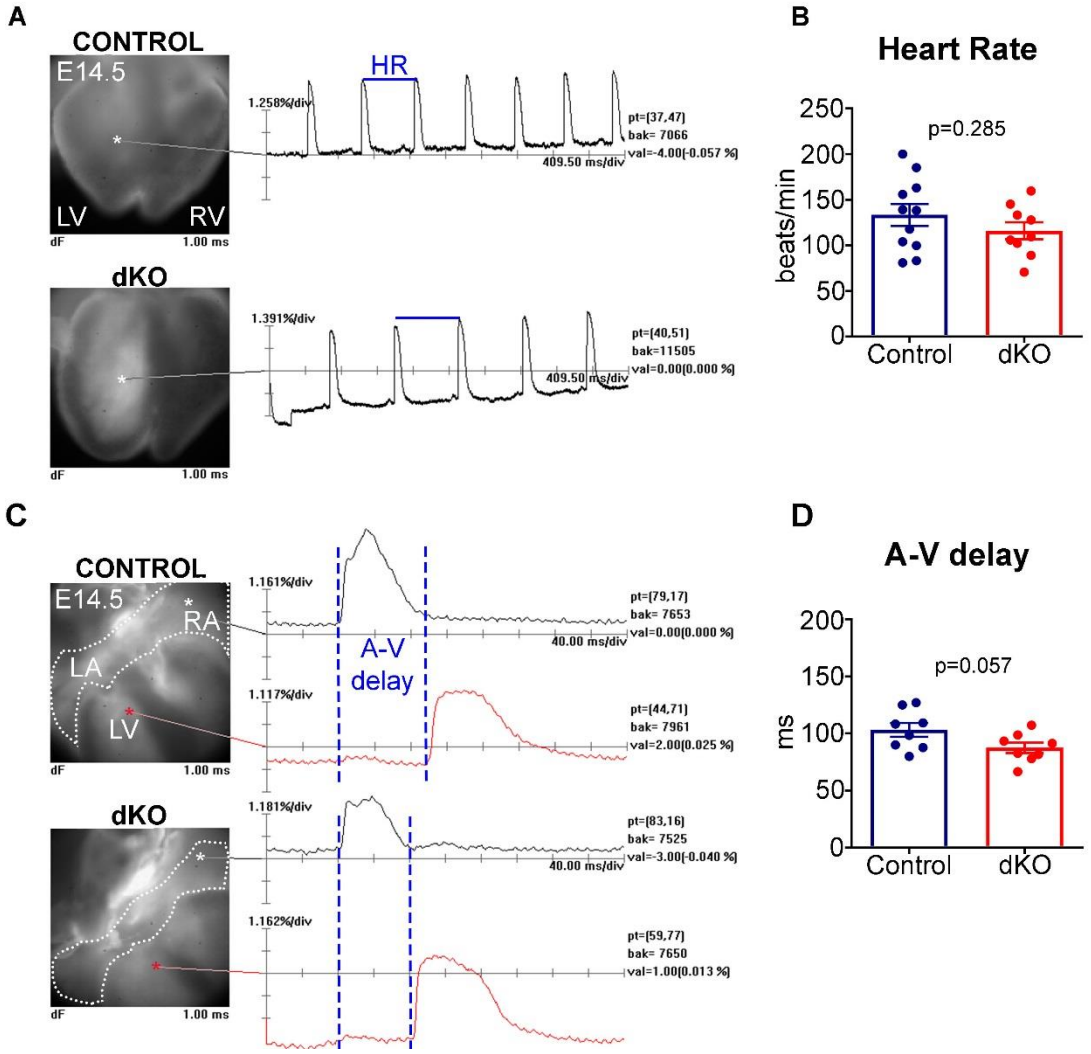

Figure 21. Heart beat rate and Atrio-Ventricular delay measured by Optical Mapping. A. Bright field image of Control and dKO hearts (dorsal view) during optical mapping. Peaks on the right show action potentials of a particular dot in the ventricles (*) along 400 ms. B. Quantification of heart beat rate (HR) in Controls and dKOs during optical mapping at E14.5. Data are means of 5 consecutive beats per heart. C. Bright field image of Control and dKO hearts (dorsal view angled to visualize the atria) during optical mapping. Peaks on the right show one action potential from atrium (white *) and ventricle (red *) of a selected dot along 40 ms. D. Quantification of time between atrial and ventricular activation in Control and dKO hearts during optical mapping. Data are means of 3 consecutive beats per heart.

Moreover, we calculated total area of ventricles and atria to assure the changes in activation curve are reflecting changes in depolarization velocity and not in heart size (FIG. 22D). These results suggest that constitutive double deletion of *Meis1* and *Meis2* in cardiomyocytes impairs electrical impulse transmission through the ventricles.

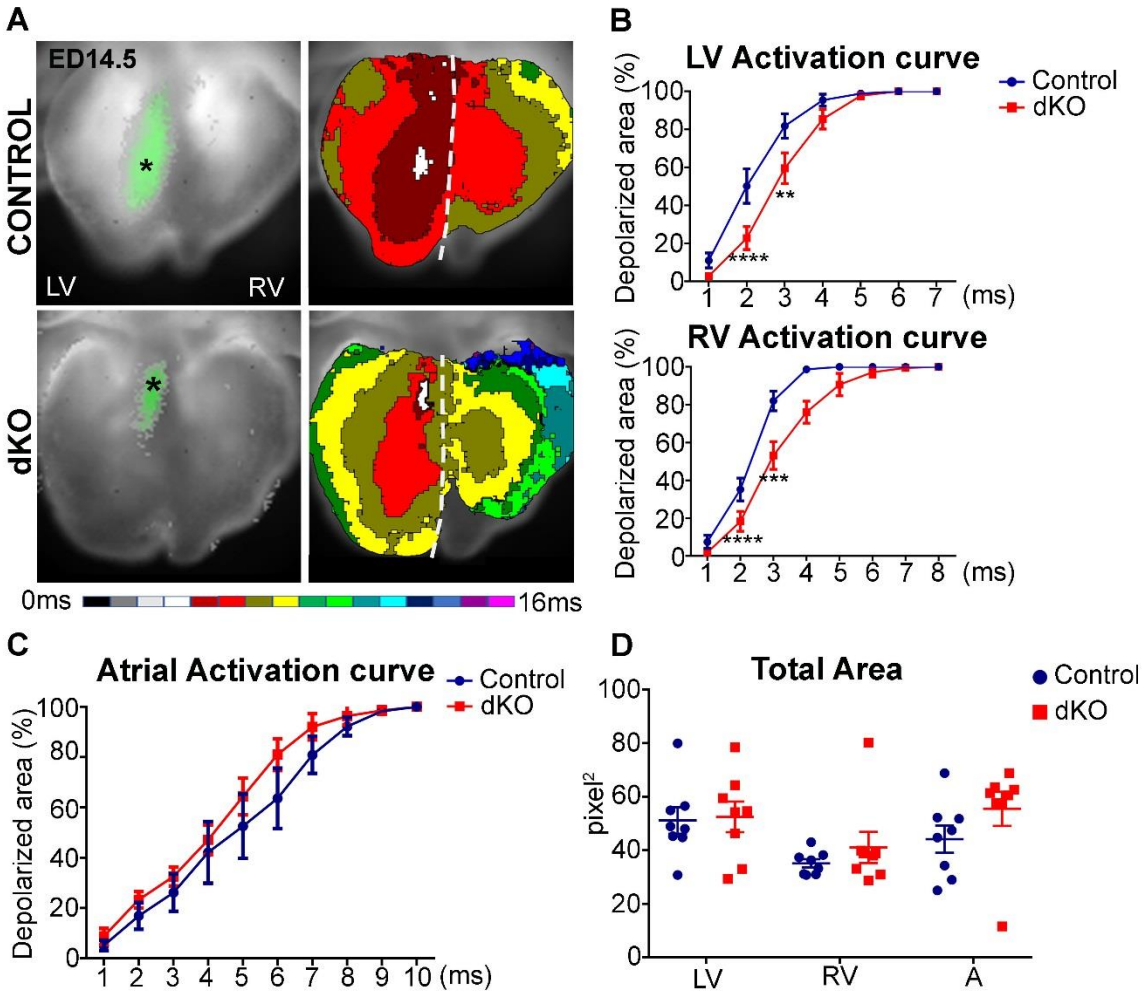

Figure 22. dKO hearts present slower ventricular activation curves. A. Representative Control and dKO optical maps of ventricular depolarization. * indicates the area where the first AP appears. White line shows manual division of left and right ventricle for analysis. Color bar shows temporal scale in the maps (1 color= 1ms). B. Left and right ventricular activation curves showing depolarized area (%) per millisecond obtain from optical mapping data (n=8/group). C. Atrial activation curve from atria (n=8/group). D. Total area of left and right ventricles and atria in Control and dKO groups. All data are from more than three independent litters.

We next studied the same parameters two days later in development, at E16.5. We noticed dKO hearts were frequently not beating by the time of recording (FIG. 23A), suggesting dKO hearts were extremely sensitive to the technique. Measurements of heart rate and A-V delay were similar in both groups (FIG. 23B, C) and activation curves too (FIG. 23D, E). We speculate that we were not able to find significant differences because, likely, the non-beating hearts were the ones presenting a more severe phenotype. It is important to mention that, even though the time of recording was very short, we detected three dKO hearts that were temporally arrhythmic, two at

E14.5 and one at E16.5 (FIG. 24). None of the control hearts showed changes in rhythm.

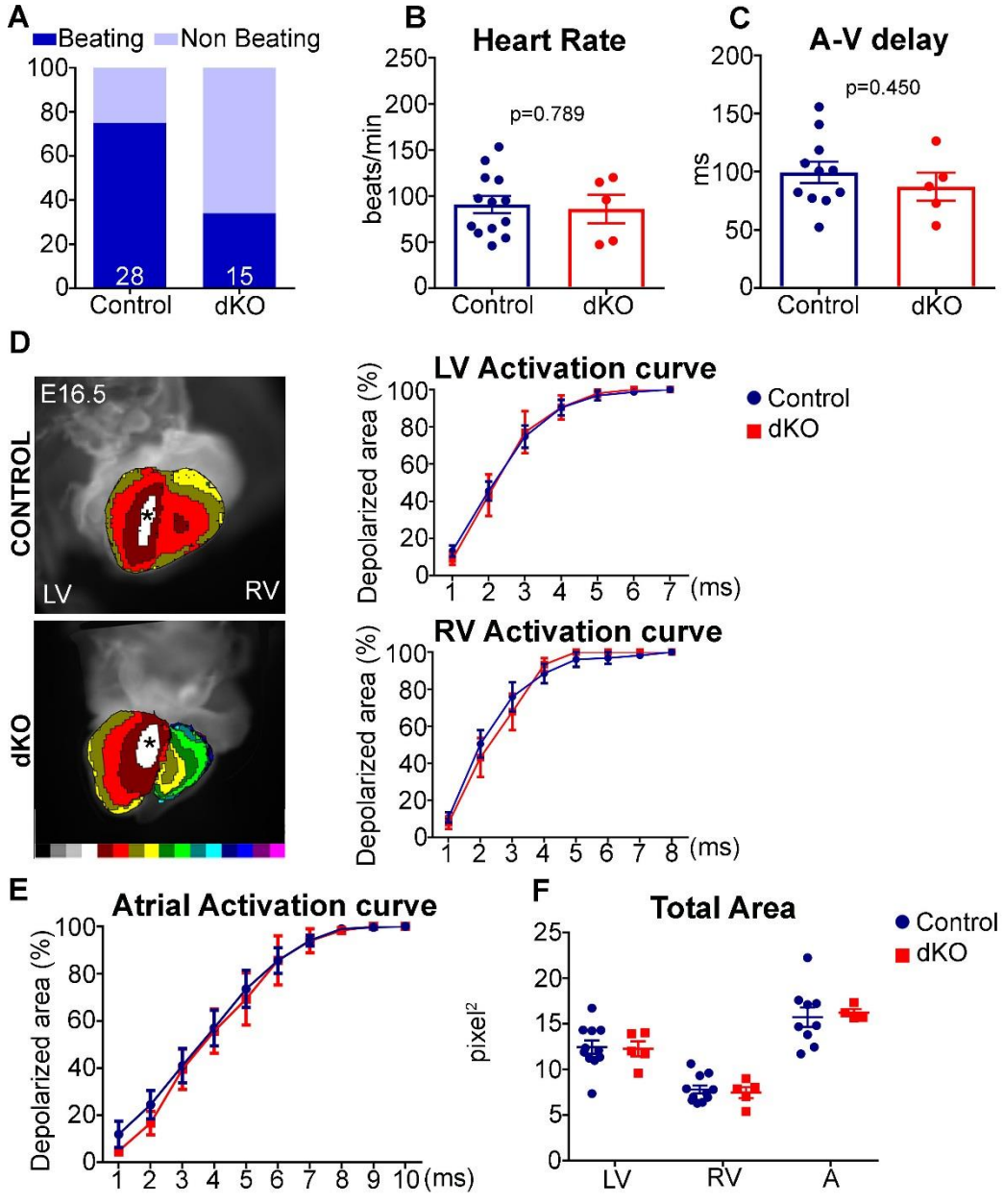

Figure 23. Optical mapping at E16.5 did not show any significant difference between Control and dKO hearts. A. Beating proportion of hearts at E16.5 by the time of optical mapping recording. B-C. Heart rates and A-V delay times of Control (n=11) and dKO (n=5) beating hearts. D. Maps and curves of left and right ventricular activation times in Control and dKO at E16.5. * indicates the area where the firs AP appears. Color bar shows temporal scale from 0 to 16ms. E. Atrial activation curve. F. Total area measured in each heart from every region analyzed.

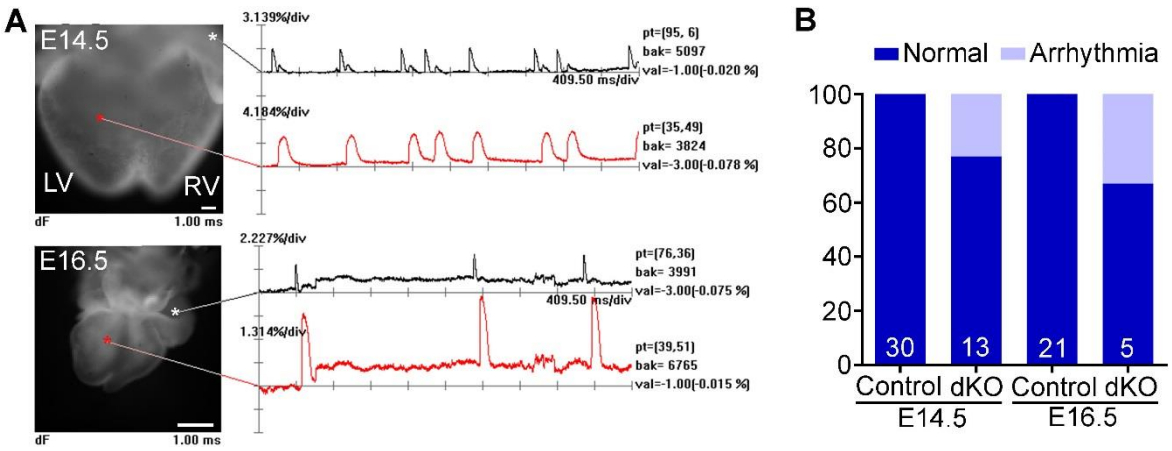

Figure 24. Arrhythmic dKO hearts detected by optical mapping. A. Bright field pictures and signals recorded by optical mapping in two E14.5 (10x) and E16.5 (4x) dKO hearts. B. Percentage of arrhythmic dKO hearts found at each time point.

MOLECULAR MECHANISMS GOVERNING *MEIS1* AND *MEIS2* DKO PHENOTYPE.

Meis Deletion In CMs Alters The Expression Of Genes Related To Cardiac Conduction

Our last objective was to unravel the molecular mechanisms responsible for the mutant phenotype. We performed RNA-seq analysis in atria and ventricles separately, at E15.5. We found more differentially expressed genes (DEGs) in atria (1281) than in ventricles (268) (Supp. table 2, 3), which might explain the morphological alterations affecting atria. GSEA analysis of DEGs in the KEGG database showed downregulation of important genes for calcium signaling *(RyR3, Cacna1h, Cacna1c*) and cardiac muscle contraction (*Myl2, Myh7*) in the ventricles (FIG. 25A). The changes detected in the atria were more pronounced, including not only calcium and contraction alterations but also genes involved in focal adhesion, Wnt signaling and genes associated with various cardiac pathologies (FIG. 25B).

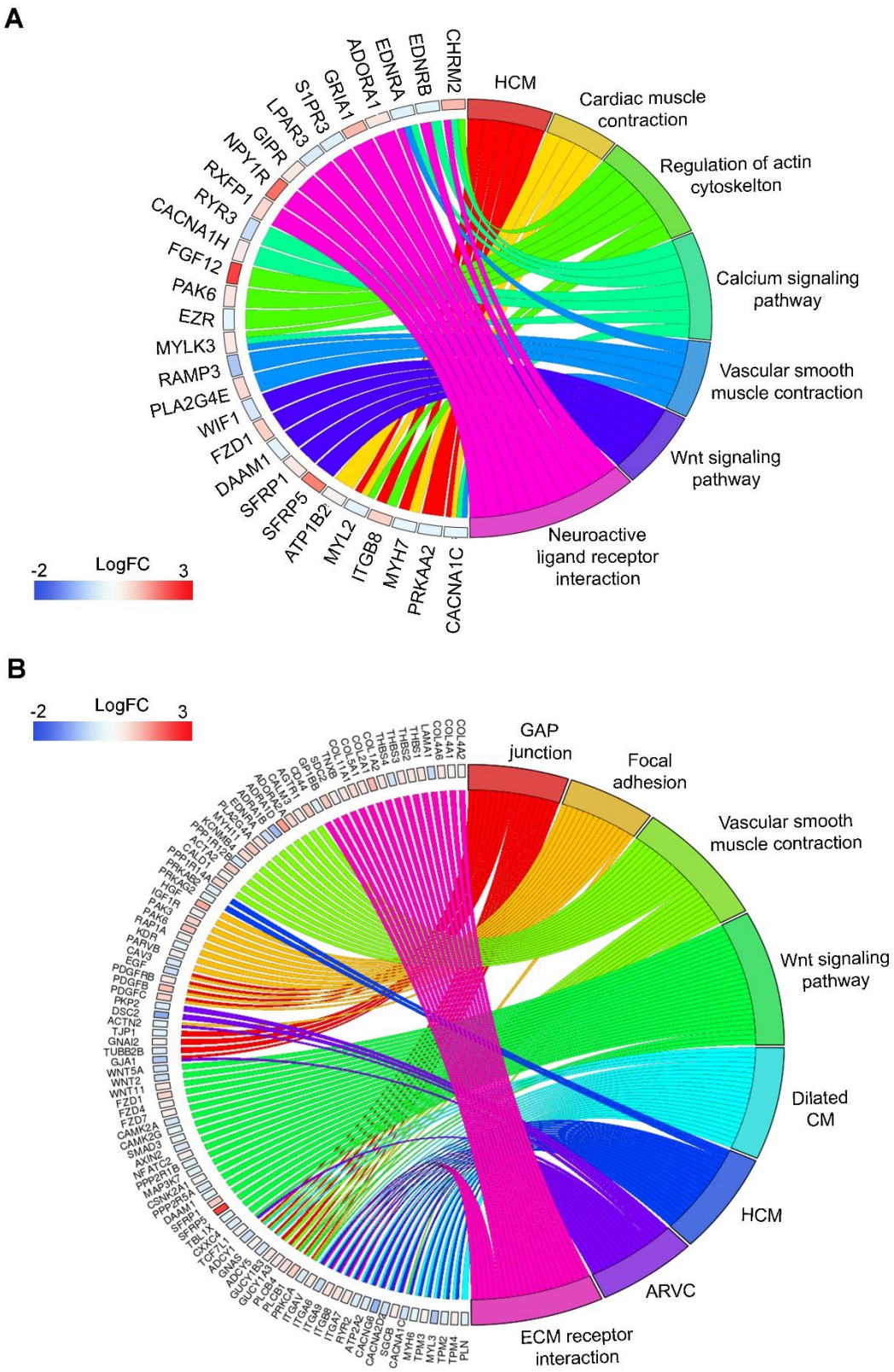

Figure 25. RNA-seq analysis of E15.5 Control vs dKO atria and ventricles. A-B. GO plots showing DEGs in dKO ventricle (A) and atria (B) that belong to significantly enriched KEGG database categories, as indicated.

In addition, we found that *Gja1*, the gene encoding Cx43, was significantly downregulated in atria and ventricles of dKO hearts at E15.5. Immunofluorescence of Cx43 supported the RNA-seq finding (FIG. 26A, B) and is consistent with the slower ventricular depolarization observed by optical mapping.

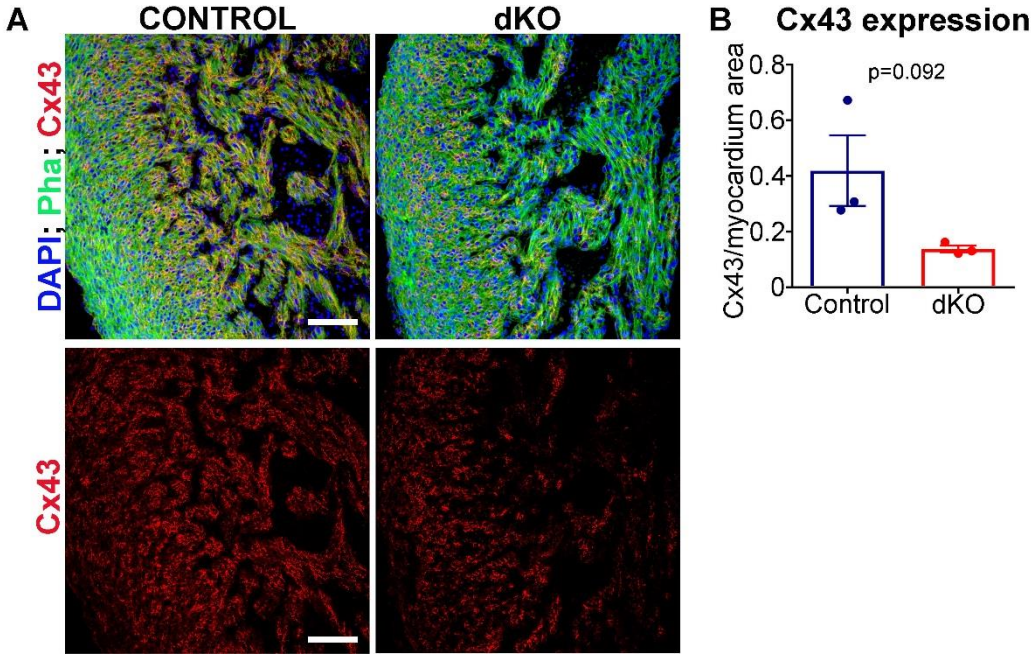

Figure 26. dKO hearts present reduced Cx43 expression. A. Confocal images of ventricular myocardium stained for Cx43 in red and phalloidin in green. Scale bar: 100µm B. Graph showing the quantification of Cx43 expression/myocardium area (pixel^2).

There are different studies relating downregulation of Cx43 with the appearance of arrhythmias. Thus, we hypothesize that downregulation of *Meis1* and *Meis2* in developing cardiomyocytes leads to misregulation of calcium signaling and downregulation of Cx43, which contributes to the development of lethal cardiac arrhythmias by the end of gestation.

MEIS FUNCTION IN CARDIOMYOCYTES DURING ADULTHOOD

To further explore the function of Meis in cardiomyocytes we developed an inducible mouse model that allowed us to study Meis role in adult CMs. We used the driver *α-MHC-MerCreMer*$^{tg/wt}$. This Cre driver is also specific for CMs but recombination will only be induced in the presence of tamoxifen (Tx) (FIG. 27A). We used mice around 10 weeks of age and oral-gavage tamoxifen was administered at 1mg/day for five consecutive days (FIG. 27B).

Meis1 And *Meis2* Double Deletion In Adult CMs Causes Cardiac Hypertrophy And Interstitial Fibrosis

Echocardiography analysis showed increased left ventricular mass and left ventricular posterior wall thickness in *Meis1*$^{flox/flox}$*;Meis2*$^{flox/flox}$*;α-MHC-MerCreMer*$^{tg/wt}$ (idKO) hearts compared to *Meis1*$^{flox/flox}$*;Meis2*$^{flox/flox}$*;α-MHC-MerCreMer*$^{wt/wt}$ (Control) (FIG. 27C, D). The change was evident two weeks after tamoxifen induction and was maintained along the time-course of the experiment (FIG. 27D). Nonetheless, left ventricular ejection fraction was conserved between groups, indicating normal systolic function (FIG. 27D). The E/A ratio was preserved, also indicating absence of diastolic dysfunction (FIG. 27D). 12 weeks after tamoxifen induction, heart weight to tibia length ratio showed a non-significant tendency of idKO hearts to present larger size compared to controls (FIG. 27E, F).

Histological analysis revealed that Meis deletion in adult CMs induced interstitial fibrosis (FIG. 28A). Fibrosis was present at 4w after tamoxifen induction and maintained without further increase during 12 weeks of follow-up. Since it was described that *α-MHC-MerCreMer* may produce cardiac toxicity in the presence of tamoxifen (Koitabashi *et al*, 2009; Bersell *et al*, 2013), we decided to characterize a model of Tx administration to MerCreMer carriers of this allele in the absence of Meis floxed alleles. Sirius red staining at 4 weeks upon tamoxifen administration revealed slightly more interstitial collagen deposition in *α-MHC-MerCreMer*$^{tg/wt}$ mice (CRE) than in their wild type siblings (WT) (FIG. 29A, B).

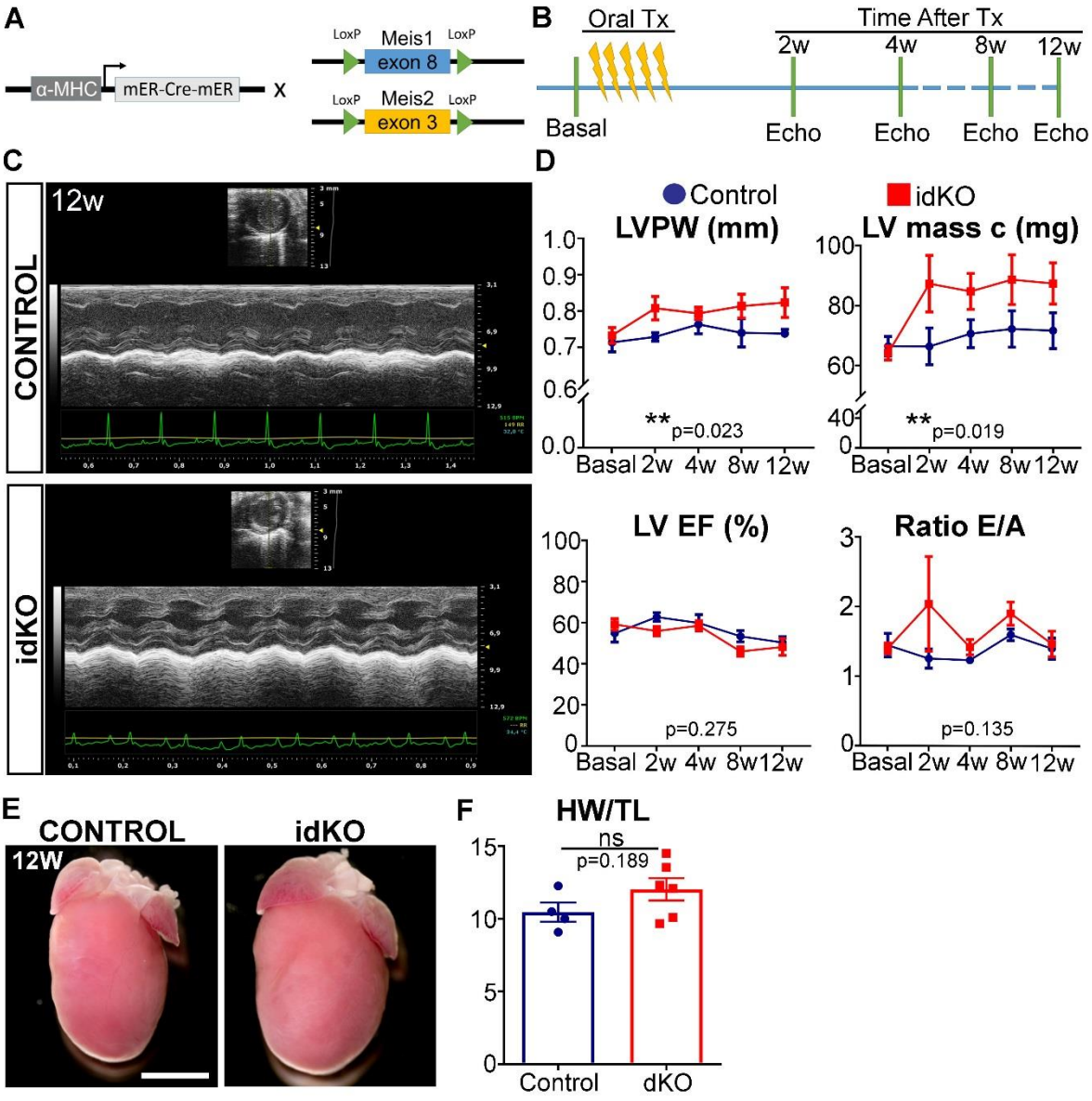

Figure 27. *Meis1* and *Meis2* inducible deletion in adult hearts leads to mild-hypertrophy. A. Mouse model for the simultaneous deletion of Meis1 and Meis2 in adult CMs. B. Schematic representation of analysis timing and tamoxifen treatment during the experiment. C. Echocardiography images of ventricular walls in short axis and mono-dimensional mode 12 weeks after tamoxifen treatment in Control and idKO. Green line shows ECG of the mouse during the study. D. Graphs summarizing the results obtained after Echo analysis regarding left ventricular posterior wall thickness (LVPW), left ventricular mass (LV mass), Left ventricular ejection fraction (LV EF) and ratio E/A. P values represent Two-way ANOVA results for genotype factor. E. Whole-mount images of hearts harvested 12 weeks after Tx administration. F. Graph showing ratio between heart weight and tibia length of Control and idKO hearts harvested 12 weeks after Tx.

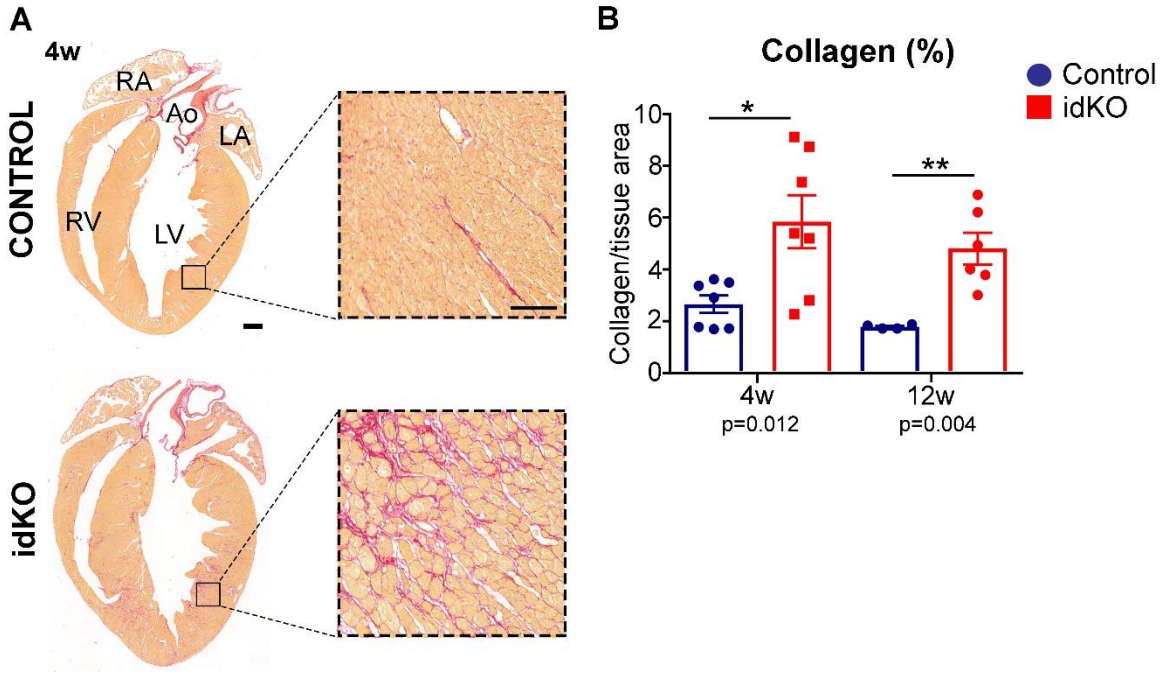

Figure 28 Meis1 and Meis2 loss of function in adult CMs induces interstitial fibrosis. A. Adult heart sections stained with Sirius Red to study collagen deposition. Scale bar: 500 µm. Black boxes show magnification of ventricular myocardium. Scale bar: 100µm. B. Graph indicating the area percentage positive for Sirius Red, 4 and 12 weeks after Tx. Data obtained as mean of positive area in ventricles from 3 sections per heart.

The amount of collagen deposition was, however, much below that observed in idKO hearts and similar to mice used as Control, so we considered unlikely that the toxicity of the MerCreMer significantly influences the histological characterization of idKO hearts. Collagen deposition alone could explain the mild hypertrophy developed in idKOs, however it is also possible that cardiomyocyte hypertrophy or proliferation contribute to the phenotype.

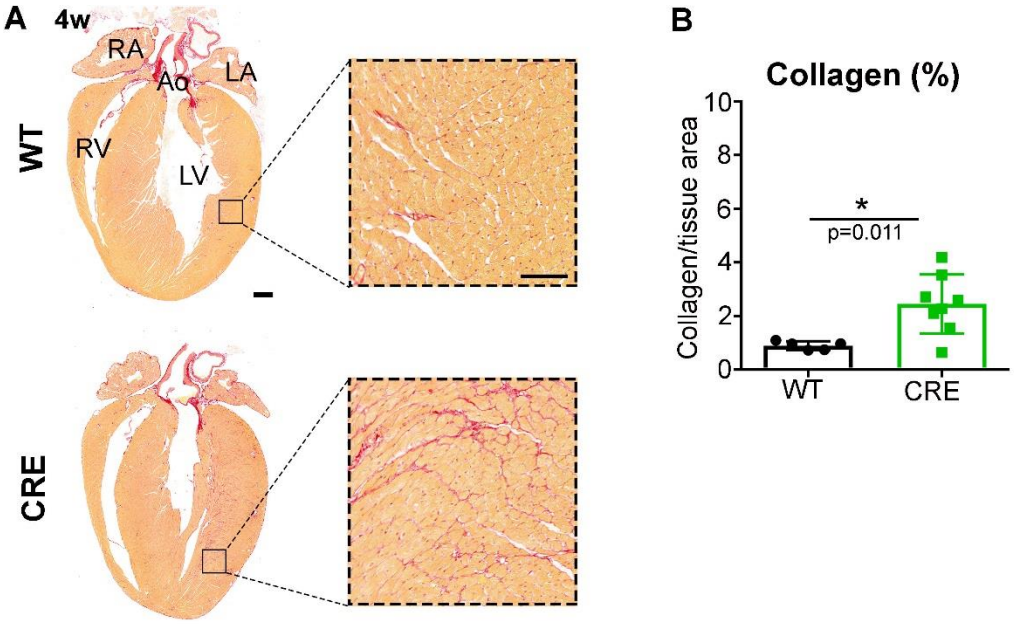

Figure 29. *α-MHC-MerCreMer* carrier mice develop mild interstitial fibrosis . A. Adult heart sections stained with Sirius Red (SR) to study collagen deposition in *α-MHC-MerCreMer*$^{tg/wt}$ and their wild type siblings. Black boxes show magnification of ventricular myocardium. B. Graph indicating area percentage positive for Sirius Red.

Loss Of Function Of *Meis1* And *Meis2* In Adult CMs Leads To Polyploidization Of Mononucleated CMs

Trying to sort out the origin of mild-hypertrophy in idKO mice, we administered BrdU in the drinking water for three weeks (starting 1 week after tamoxifen induction ceased) and isolated CMs by Langendorff perfusion, immediately after BrdU administration ended (FIG. 30A). After they adhere to the culture dish, areas occupied by single cardiomyocytes were measured on CMs populations classified by their nucleation (mononucleated, binucleated and polynucleated). No significant size differences were found between control and idKO cardiomyocytes (FIG. 30B, C).

Then, we evaluated the proliferation status of CMs in both groups. Quantification of BrdU positive CMs revealed a significant increase of BrdU-positive CMs in idKO hearts that was preferential for the mononucleated population (FIG. 30D, E). The percentage of bi and polynucleated CMs that incorporated BrdU in the nuclei were also elevated in idKO hearts, although not significantly (FIG. 30E).

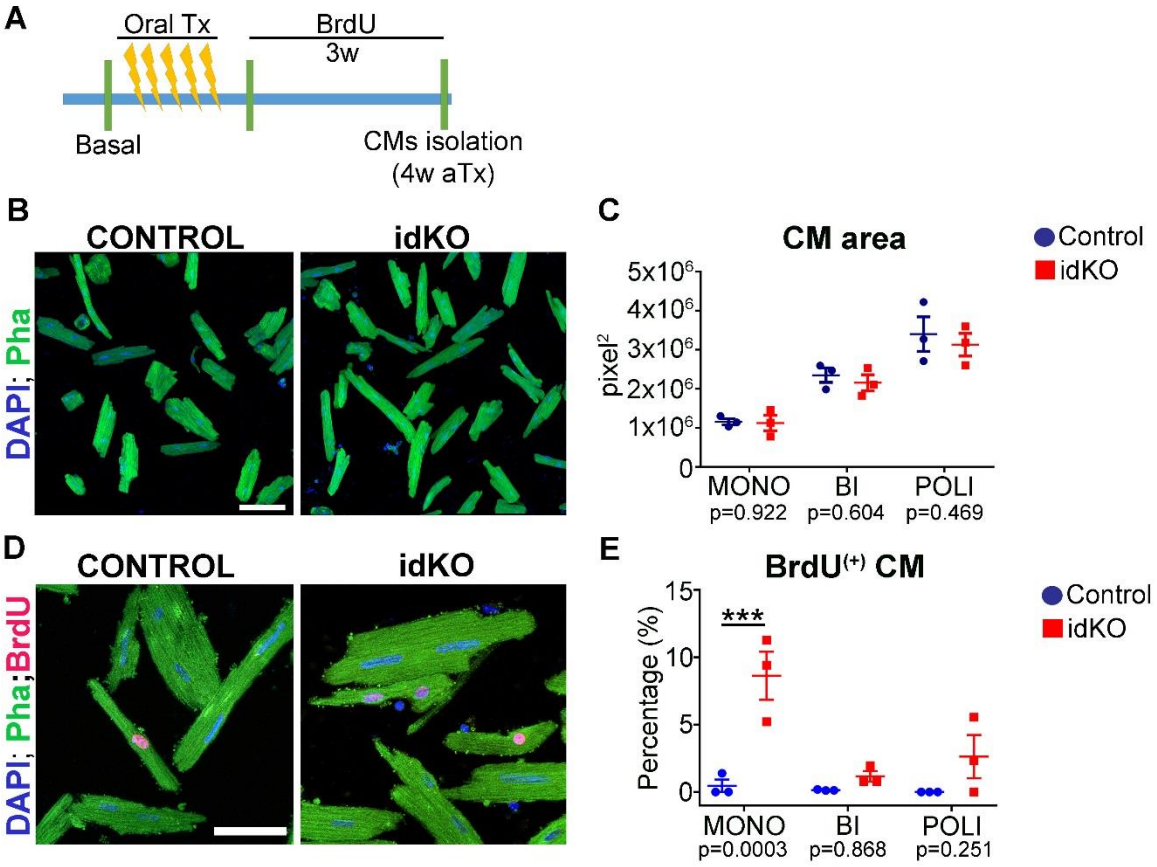

Figure 30. idKOs show normal CM size and increased BrdU incorporation in mononucleated CMs. A. Schematic summary of the experimental design. B. Confocal images of isolated CMs from Control and idKO hearts. Scale bar 50µm. C. Quantification of single CM areas, classified by number of nuclei per cell. D. Confocal images of isolated CMs from Control and idKO hearts showing BrdU incorporation. Scale bar 50µm. E. Quantification of BrdU+ CMs classified by number of nuclei per cell. MONO, n≈250 cells; BI, n≈3000 cells; POLI, n≈150 cells.

In order to determine whether this DNA synthesis was linked to proliferation or to endoreplication, we estimated the ploidy of mononucleated CMs by DAPI intensity, nuclear volume and cell size. We found that the nuclei that had incorporated BrdU exhibited approximately double DAPI intensity and double cell size compared to BrdU-negative cardiomyocytes (FIG. 31A, B, C). However, we were not able to detect differences due to genotype in this parameters. Classification of mononucleated CMs according to their nuclear volume showed roughly two cell populations –likely 2n and 4n– with similar distributions in control and idKO hearts (FIG. 31D, E). These results suggest that the majority of spontaneous BrdU incorporation by mononucleated adult cardiomyocytes is related to polyploidization and not proliferation.

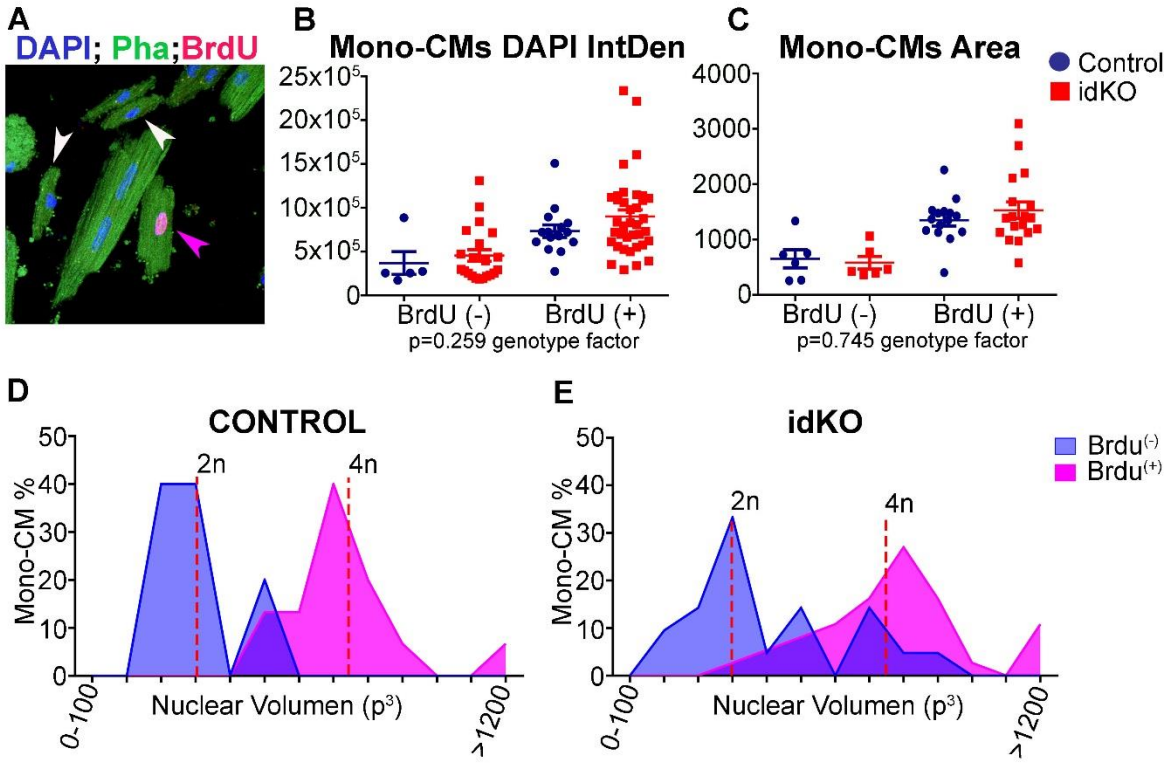

Figure 31. The majority of BrdU+ mononucleated CMs undergo DNA endoreplication and not proliferation. A. Confocal image of isolated CMs from idKO adult hearts showing differences in mononucleated CM size. Arrowheads point to mononucleated CMs, in pink for BrdU+ CMs and in white for BrdU- CMs. B. Quantification of the DAPI intensity of mononucleated CM nuclei from Control and idKO hearts. C. Graph showing mononucleated CM size depending on BrdU incorporation and genotype. D-E Histogram of nuclear volume of BrdU+ and BrdU- mononucleated CMs from Control and idKO mice.

Double Inducible Deletion Of *Meis1* And *Meis2* In Adult CMs Causes Slower Ventricular Conduction

Taking into account that we found that Meis TFs are preferentially expressed in adult CMs of the conduction system and that are necessary for the establishment of ventricular conduction during development, we decided to perform electrocardiograms of the inducible deletion adult model.

We followed the same experimental timing as before (FIG. 32A), performing ECG at different time points after Tx induction. We found progressive elongation of the QRS complex in the idKO mice (FIG. 32B, C). P, PR and QTc showed no significant differences between genotypes (FIG. 32C). However, QTtc which is a more robust measurement for QT interval, showed and increased in idKO at 2 weeks, that seems

to be ameliorated along time (FIG. 32C). Moreover, QRS amplitude significantly dropped in mutant mice at the first point analyzed and the decreased is maintained during the experiment (FIG. 32B, C). This result suggest that atrial and atrio-ventricular conduction are normal while ventricular conduction is impaired in idKOs mice.

We also checked whether QRS and QTtc intervals were normal in MerCreMer carrier animals. Comparing CRE and WT animals we did not detect any significant QRS and QTtc elongation (FIG. 33A, B), supporting the idea that slower ventricular conduction is a consequence of Meis1 and Meis2 double inducible deletion in the adult heart. In addition, we measured QRS amplitude, which appeared significantly decreased in MerCreMer carriers after Tx treatment. This indicates that Meis loss of function may not be responsible for QRS amplitude drop.

Altogether, these data demonstrate Meis TFs are necessary for normal adult heart homeostasis and electrical conduction. Moreover, it suggests that Meis could be controlling similar processes in development and adulthood, related to normal ventricular impulse propagation.

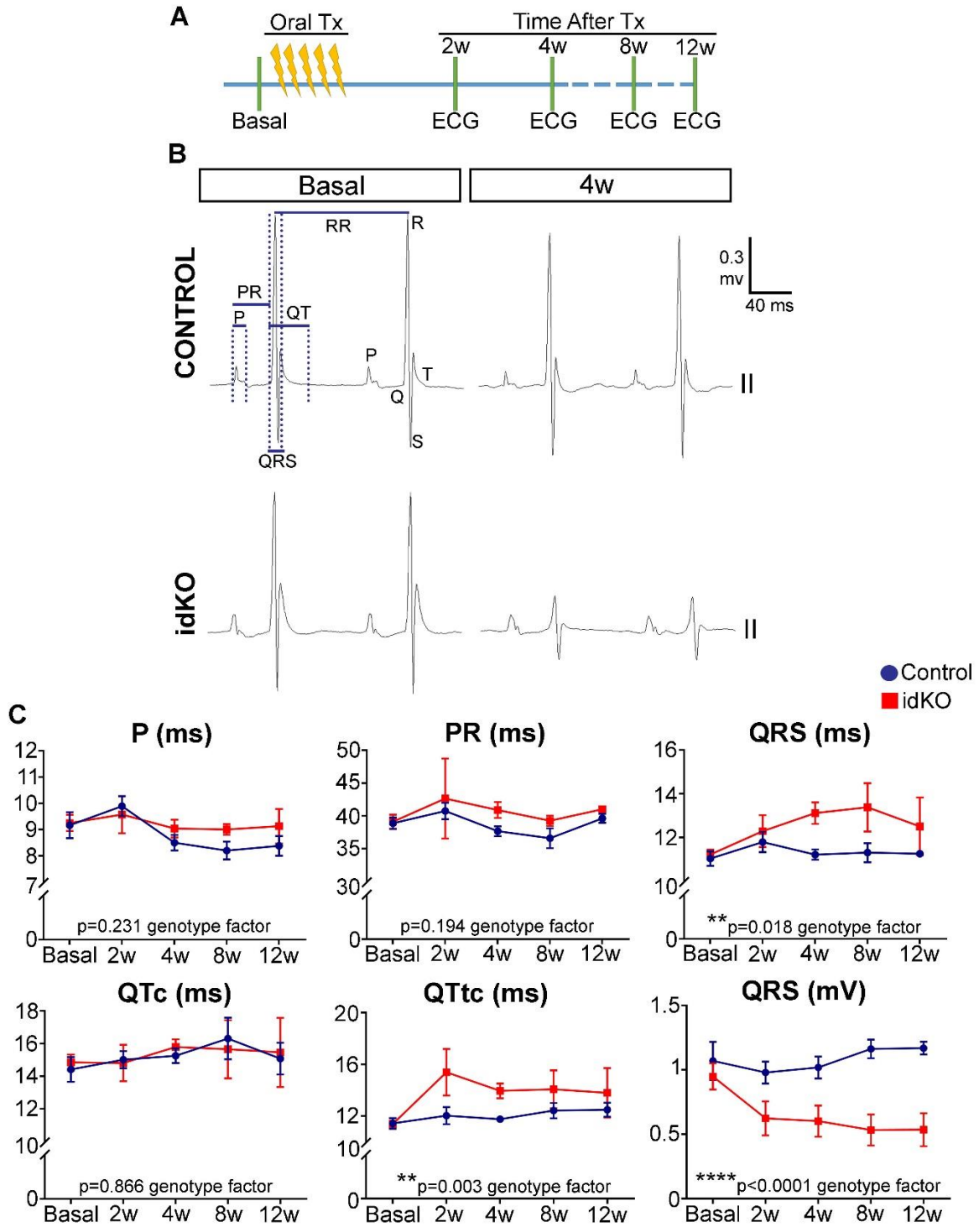

Figure 32. QRS complex is elongated upon Meis1 and Meis2 double deletion in adult CMs. A. Representation of experimental design. B. Control and idKO ECGs from anesthetized adult mice at basal and 4w experimental points. C. Graphs indicating measurements of the duration of the different ECG intervals (P, PR, QRS, QT and QTt) and QRS amplitude (mV) in controls and idKOs at the indicated experimental time points.

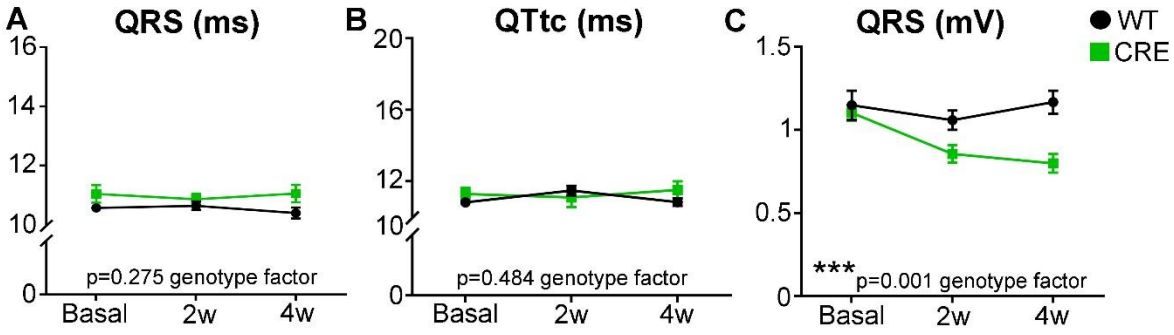

Figure 33. Measurement of ECG intervals in MerCreMer carriers. Graphs showing comparisons between CRE mice and their WT siblings before and after Tx treatment for QRS (A) and QTc times (B) and QRS amplitude (C).

MOLECULAR MECHANISMS UNDER THE CONTROL OF *MEIS1* AND *MEIS2* IN ADULT CARDIOMYOCYTES.

Meis1 And *Meis2* Regulate Calcium Signaling And Conduction System Markers

To further explore the function of Meis TFs in adult CMs we aimed to understand what molecular changes take place upon inducible deletion of *Meis1* and *Meis2.* We performed RNA-seq analysis 2 weeks after Tx administration separately from adult atria and ventricles. 263 DEGs were found in the ventricles, while only two changed in atria (FIG. 34A) (Supp. Table 4, 5). Therefore, we studied the possibility of low efficiency Cre recombination in the atria. Specific quantification of *Meis1* exon 8 and *Meis2* exon 3 in the RNAseq showed efficient deletion of both exons in ventricles, but almost no reduction in atria (FIG. 34B). These findings suggest low efficiency of MerCreMer in atria and could explain the absence of changes in that region.

We performed gene set enrichment analysis in the KEGG database and found that DEGs are mainly related to cardiomyopathies and calcium signaling pathway (FIG. 35A). Genes regulating sodium currents in CMs, *Scn5a* and *Scn10a*, are significantly downregulated, suggesting sodium current might be also deficient in idKO mice (Supp. Table 5).

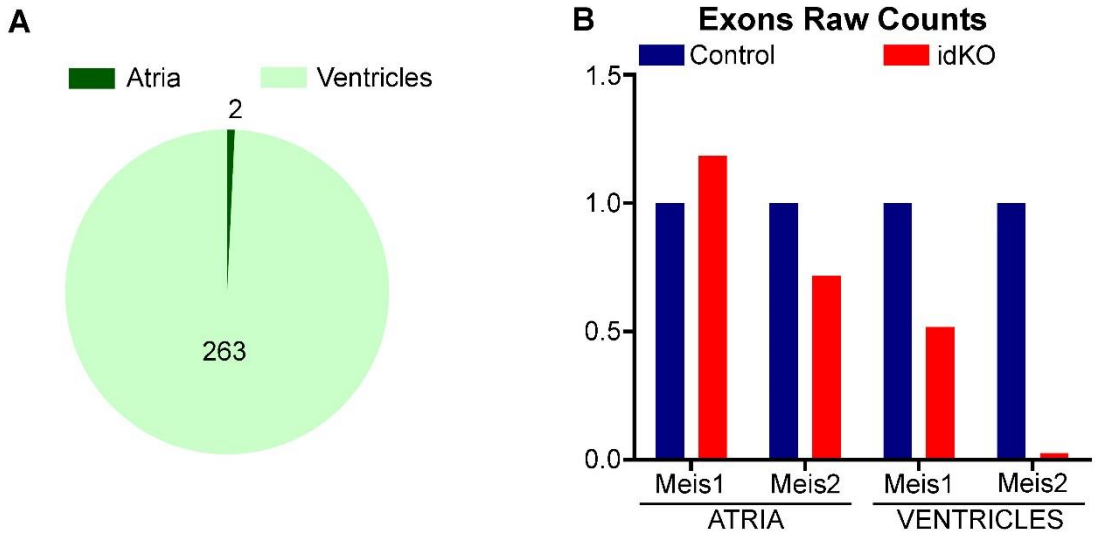

Figure 34. The *α-MHC-MerCreMer* allele does not recombine efficiently in the atria of adults. A. Number of DEGs found in atria and ventricles by RNA-seq analysis of Control vs idKO hearts. B. Quantification of *Meis1* exon8 and *Meis2* exon 3 in RNA-seq from atria and ventricles. C. Number of statically significant upregulated and downregulated genes in idKO ventricles.

Moreover, genes related to Arrhythmogenic Right Ventricular Cardiomyopathy (ARVC) appeared as the most related gene set. We decided to compare our RNA-seq data with a published RNA-seq from an ARVC mouse model in which *Pkp2* has been conditionally deleted in cardiomyocytes (Cerrone *et al*, 2012b). Pkp2 is a desmosomal protein important for the assembly of CMs. In this model, *Meis1* and *Meis2* appeared significantly downregulated (FIG. 35B green color). Moreover, when we compared the differentially expressed genes in both models we found a correlation between the genes that were changing, especially when focused on the most significantly downregulated ones, such as *Cacna1c* or *RyR2*, essential for calcium signaling (FIG. 35B). *Gja1*, appeared downregulated in both models too. Furthermore, *Hcn4* and *Cntn2*, which are CCS markers, were reduced in idKO ventricles, suggesting a possible affection of the VCS.

Altogether, it is possible that, alterations both in working and conducting myocardium are contributing to QRS elongation in idKO adult hearts.

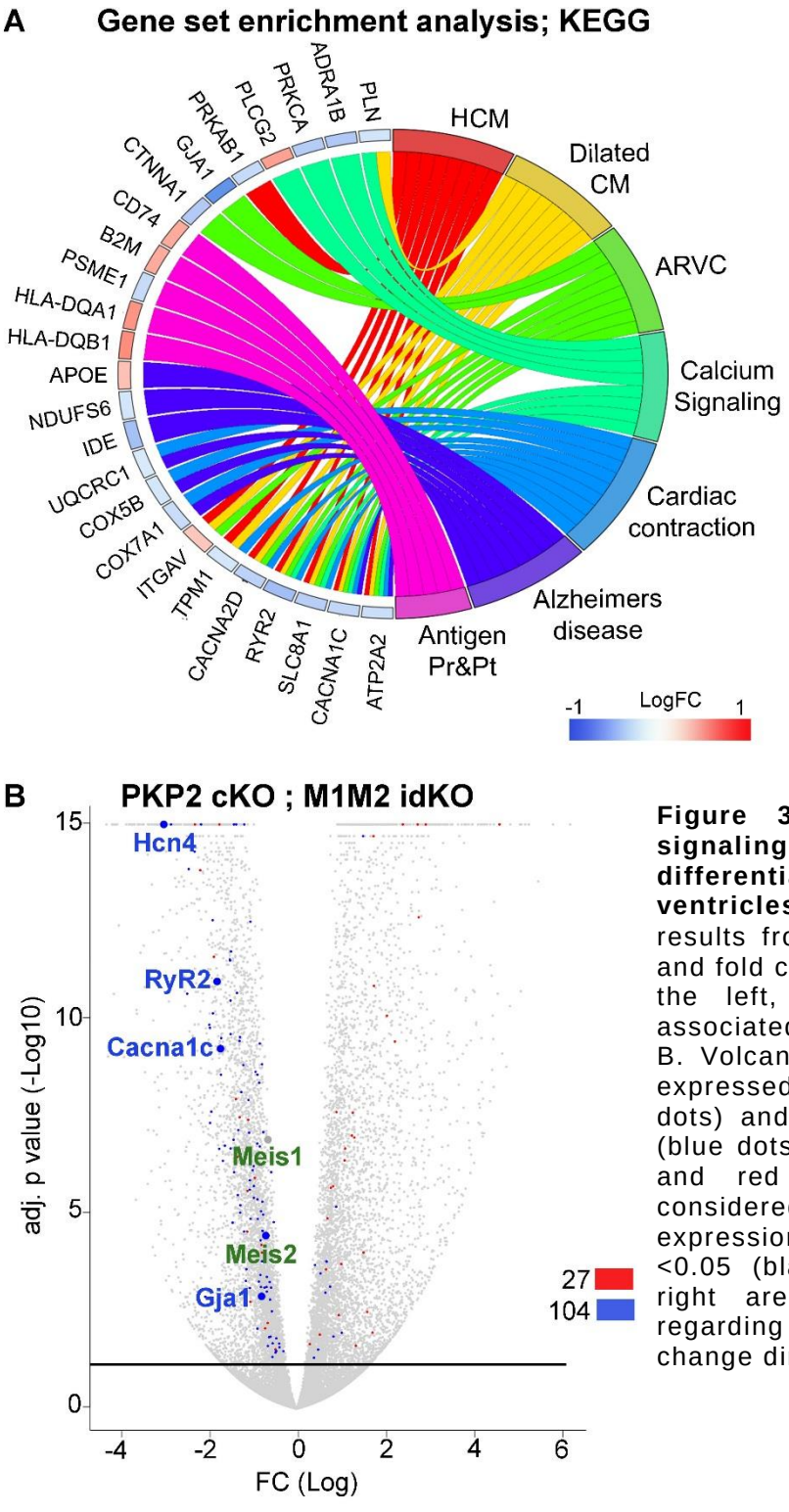

Figure 35. ARVC and calcium signaling related genes appeared differentially expressed in idKO ventricles. A. GOplot summarizing results from GSEA analysis. Genes and fold changes are represented on the left, and on the right, the associated categories to each gene. B. Volcano plot representing genes expressed in PKP2 cKO model (grey dots) and DEGs in idKO ventricles (blue dots are downregulated genes and red upregulated). We only considered for this analysis expression changes with adj. p-value <0.05 (black line). Number in the right are the overlapping genes regarding significance and fold change direction.

Cx43 Is Reduced And Mislocalized In idKO Ventricular Myocardium

We decided to study Cx43 expression because it was reduced in developing CMs when Meis1 and Meis2 were absent, and appeared downregulated in RNA-seq data from adult idKO. Immunofluorescence of Cx43 revealed a significant reduction of the protein in idKO ventricles (FIG. 36A, B). The reduction was already evident 4 weeks after tamoxifen administration. On the contrary, analyzing the atria, the same levels of expression were found between controls and idKO (FIG. 36C, D). These results are consistent with RNA-seq data, since DEGs genes where mainly found in the idKO ventricles.

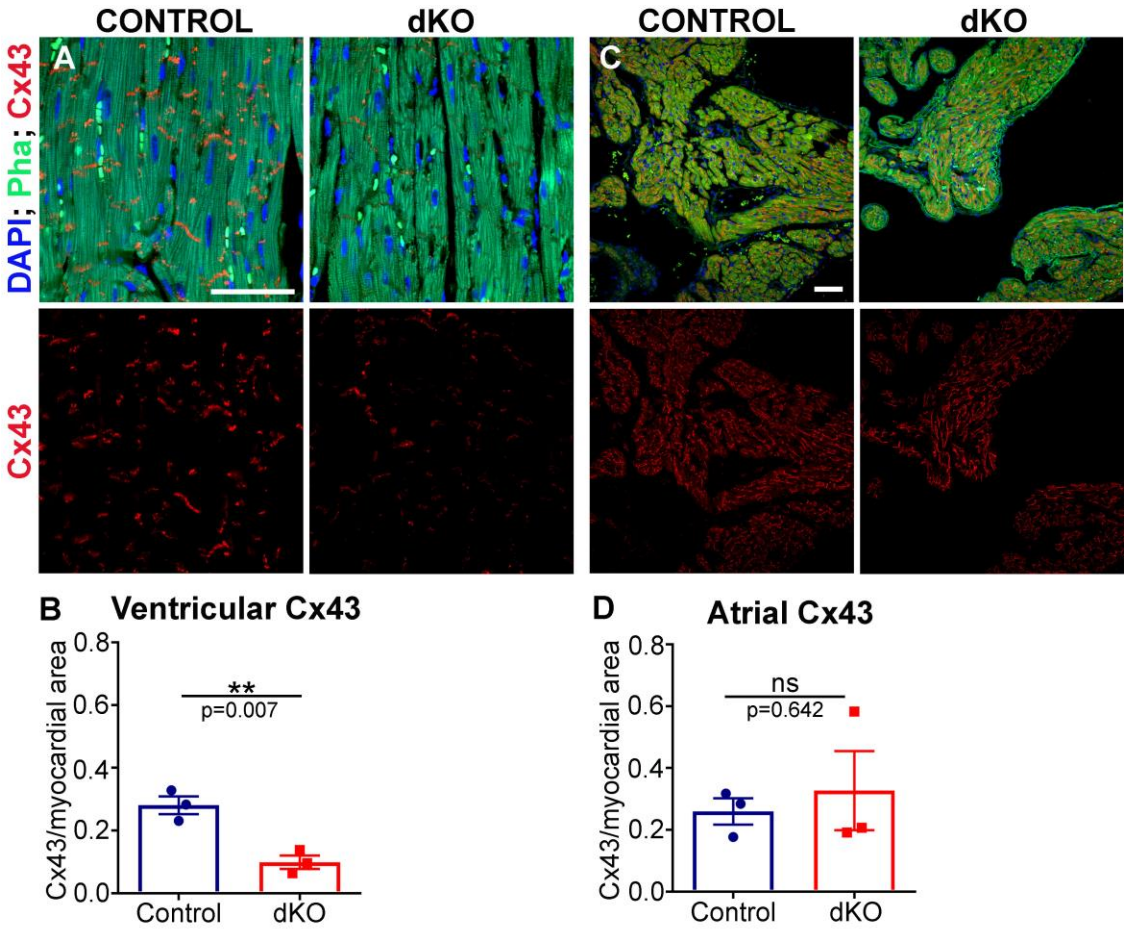

Figure 36. Cx43 expression is reduced in idKO ventricular myocardium. A. Confocal images of Control and idKO ventricular myocardium 4 weeks after Tx, stained for Cx43 (red) and Phalloidin (green). B. Quantification of Cx43 signal per myocardial area (pixel^2) in ventricles. C. Confocal images showing atria sections with the same staining as in A. Scale bars in A and B are 50µm. D. Quantification of Cx43 signal per myocardial area (pixel^2) in Atria.

Acute Isoproterenol Treatment Does Not Preferentially Induce Arrhythmias in *Meis1* and *Meis2* idKO.

In the light of these results, we wondered whether idKOs could be more prone to the development of arrhythmias under certain conditions. The mouse model for ARVC mentioned above, developed arrhythmias after being challenged with the beta adrenergic receptor, isoproterenol. Thus, we decided to reproduce the same challenge in idKOs (FIG. 37A). To corroborate that the treatment was affecting the hearts we measured the RR segment and found a reduction in length without differences between mutant and control mice. Since isoproterenol increases heart rate, the reduction in RR time corroborated the treatment was effective. (FIG. 37B, C). No significant differences between control and idKO hearts were found either in QRS elongation or any other ECG segments, although idKOs showed normalized QRS length by T2 (FIG. 37D). Sporadic arrhythmias were observed in some mice but were not related to the genotype (Table 1).

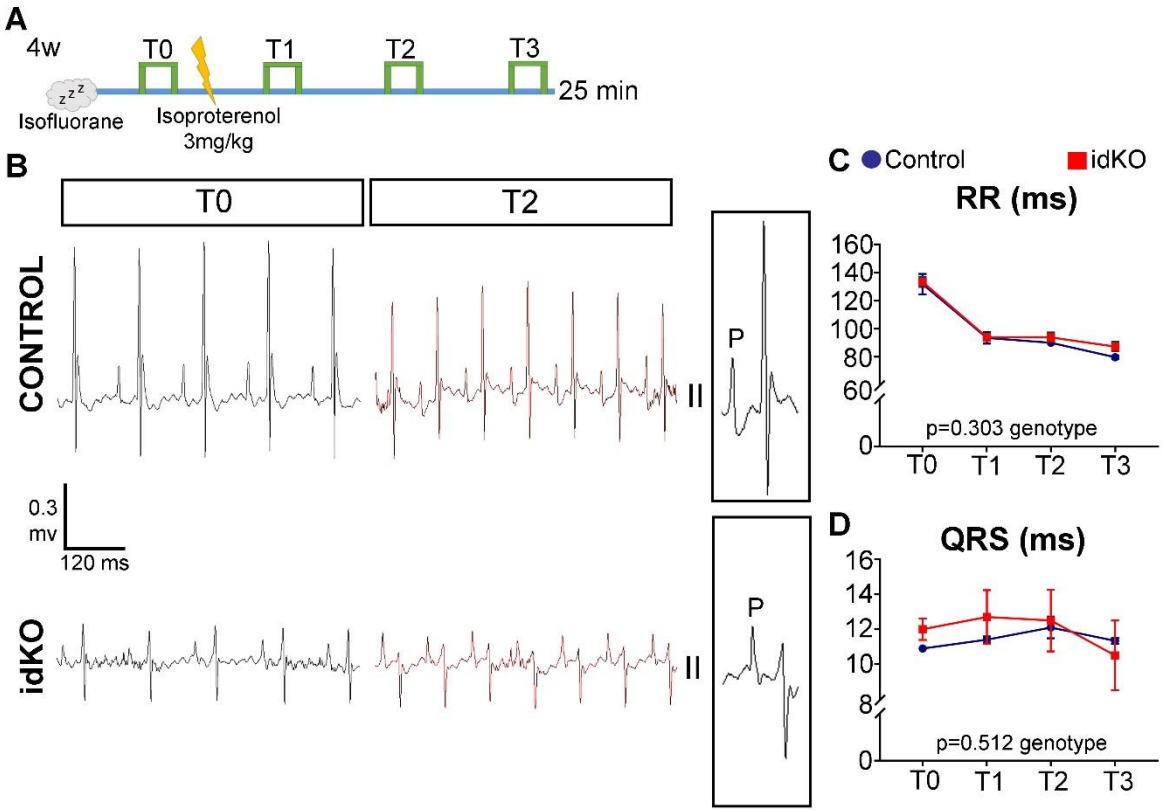

Figure 37. idKO mice respond similar to Controls after acute isoproterenol treatment. A. Schematic representation of ECG recording timing in anesthetized mice with isoproterenol induction. T0-T3 represent fragments selected for analysis. B. Representative ECG fragments of Control and idKO mice before and after isoproterenol injection. Boxes represent magnifications of a representative cardiac cycle. C-D. Graphs representing RR and QRS duration in Control and idKOs at the different time points analyzed.

	Mice with arrhythmic episodes	Total mice nº
CONTROL	3	5
idKO	2	5

Table 1. Arrhythmic episodes after isoproterenol injection where not related to genotype. Table shows the number of mice with sporadic arrhythmic events during ECG recording after acute isoproterenol treatment.

POSSIBLE DIRECT TARGETS OF MEIS TFS IN CARDIOMYOCYTES

Taking advantage of all the RNA-seq data collected in this thesis we looked at genes differentially expressed in all the tissues and conditions studied. We found 28 genes that changed expression in developing atria and in both developing and adult ventricles (FIG. 38A). The fact that these genes change expression in different contexts suggests they could represent direct targets of Meis TFs in CMs. Gene ontology analysis for biological processes related 16 of those genes with regulation of transport, secretion, heart development and contraction (FIG. 38B). *Gja1, Nppa*, *Wnk1, Corin* and *Cacna1c* were implicated in the majority of the processes altered, suggesting they could play a central role in the phenotype (FIG. 38B). On the other hand, *Fhl2, Lrrc10* and *Efnb3* appeared as the most downregulated genes (FIG. 38B). Thus, we decided to look at previous Meis ChIP-seq data from the lab (Longobardi *et al*, 2014; Delgado I *et al.* unpublished) to elucidate whether Meis TFs could bind directly to some of those genes or their previously described regulatory regions (Shen *et al*, 2012). ChIP-seq data from E10.5 embryos and E11.5 embryo trunks, including the heart, revealed putative binding sites of Meis in 5 of the 28 genes and regulatory regions studied: *Cacna1c, Clic4* (Chloride intracellular channel)*, Gpc1* (Glypican 1)*, Pam* (Peptidylglycine-alpha-amidating-monooxygenase) and *Prps2* (Phosphoribosyl pyrophosphate synthetase 2) (FIG. 39). In addition, we detected putative Meis binding sites in *Scn5a* and *Wnt11* genes, which although not included in the 28 genes commonly changed in all conditions, might also have an important relation with the phenotype describe.

These results suggest that these identified genes could be directly regulated by Meis transcription factors, thereby playing a central role in the development of the phenotypes describe in this project.

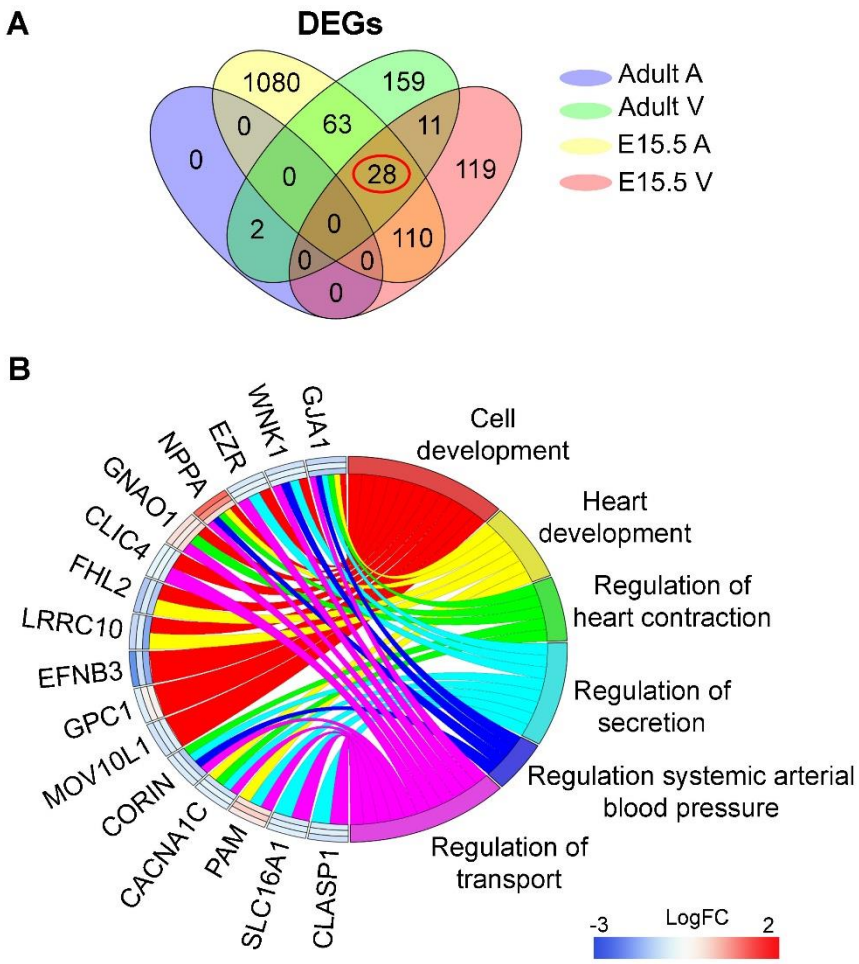

Figure 38. Analysis of coincident DEGs in the 3 RNA-seq experiments performed reveals putative direct targets of Meis TFs. A. Comparison of DEGs found in all RNA-seq studies performed in this project (atria and ventricles from adult and embryonic hearts). B. GO biological processes enrichment analysis performed with the 28 common DEGs found between adult ventricles and developing atria and ventricles. Fold changes rectangles, from outer to inner, correspond to: Adult ventricle, embryonic ventricle and embryonic atria, respectively.

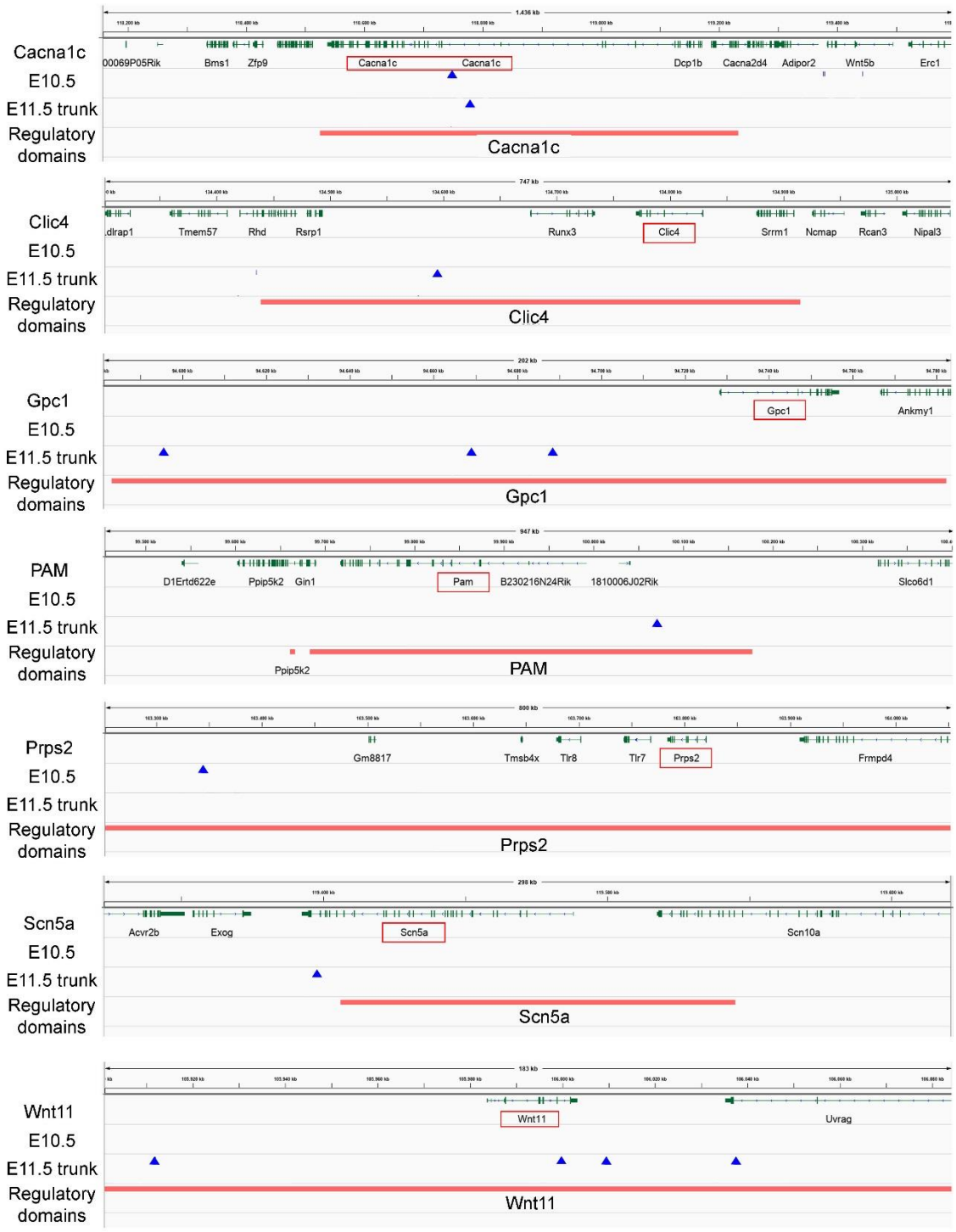

Figure 39. Putative binding sites of Meis found by ChIP-seq analysis. Representation of the genes with statically significant peaks in Meis-a ChIP analysis from E10.5 embryos and E11.5 trunks. Blue triangles represent the peaks and salmon line the regulatory regions described in Shen et al., 2012, for each gene.

DISCUSSION

In this thesis project we have investigated the role of Meis1 and Meis2 transcription factors in the developing and adult cardiomyocytes. We have found Meis1 and Meis2 co-expression in developing CM is essential for perinatal survival and in adult CMs to maintain a normal tissue homeostasis. Nonetheless, discussion is needed to put in context the value of these results, elucidate possible controversial results and propose future directions suggested by this research.

MEIS EXPRESSION PATTERN IN THE HEART

Using mRNA *in situ* hybridization in wild type mouse embryos, we have described for the first time that Meis1 and Meis2 are expressed in SHF progenitors, epicardium and endocardium. Moreover, combining two different approaches, immunofluorescence and a Meis1-CFP reporter line, we have been able to describe in detail the expression pattern of Meis1 and Meis2 in the developing myocardium. Previous studies relating Meis1 function with heart development did not analyze protein expression in this organ (Stankunas *et al*, 2008; González-Lázaro *et al*, 2014). In addition, we have identified that Meis2 is expressed in cardiac valves while Meis1 is not. These results are in accordance with previous data published by the group of Dr. Kozmik in 2015, where the Meis2 expression pattern was analyzed in embryos at E13.5 and showed expression in the valves and surrounding cardiomyocytes (Machon *et al*, 2015) .

Regarding Meis1 and Meis2 expression in the adult heart, nothing was previously reported. The work of Dr. Sadek, in 2013, studied the expression of Meis1 in the neonatal heart. They proposed that Meis1 is expressed after birth in CMs, but located in the cytoplasm around the nuclei and at P7 Meis1 is translocated to the nucleus (Mahmoud *et al*, 2013). However, in our experiments we always detect Meis signal in the nucleus, both in E18.5 fetuses and adult hearts.

Our expression studies show a previously undescribed preferential expression of Meis TFs in the adult CCS. Meis IF and lineage tracing of Meis-expressing cells in adult hearts, showed that the expression of Meis TFs is stronger in CCS CMs than in the

working myocardium. This indicates that Meis could play an important role in CCS function or homeostasis, which is in accordance with GWAS studies in different human cohorts that have associated intronic Meis1 SNPs with PR interval elongation (Pfeufer *et al*, 2010; Smith *et al*, 2011a; Butler *et al*, 2012b).

MEIS IN DEVELOPING CARDIOMYOCYTES

In this study, we have determined that double Meis1 and Meis2 deletion in developing CMs leads to perinatal death, probably due to ventricular cardiac arrhythmias. We described morphological alterations in dKO hearts that are not sufficient to explain the lethality of the fetuses, provided the EF is preserved. However, these results also pointed out to a role of Meis TFs in cardiac morphogenesis and in particular, in atrial and interventricular septum formation. Previous studies on Meis1, already described IVS defects upon Meis1 complete deletion (Stankunas *et al*, 2008; González-Lázaro *et al*, 2014). Nevertheless, in the first study cardiac defects were though to derive from a possible role of Meis1 as a partner of Pbx in CNC progenitors, but in our model *Meis1* is deleted specifically in CMs and this is sufficient to reproduce the IVS defects.

The atrial finger-like protrusions described in Meis1 and Meis2 dKO hearts have never been reported before, suggesting that Meis1 or Meis2 loss of function, independently, are not enough to produce this phenotype. We do not know the exact mechanisms underlying this malformation. RNA-seq data allowed us to speculate that extracellular matrix, CM coupling and focal adhesion, might be involved. Plakophilin 2 (PKP2) and Desmocollin 2 (Dsc2) are important proteins for desmosome formation and both are downregulated specifically in the developing atria. In addition, *Wnt5a* and *Wnt11*, regulators of planal cell polarity, are significantly downregulated. Thus, we hypothesize that defects in non-canonical Wnt signaling directly regulated by Meis could lead to CM misalignment and failure to form proper intercalated discs, which might contribute to disorganized tissue growth. We plan to study more in detail the atria, regarding relative pectinate muscles volume-to-lumen proportions, orientation of division planes and CM ultrastructure by electron microscopy, in order to unravel the mechanisms of the atrial malformation in *Meis1*; *Meis2* dKOs.

RNA-seq data also revealed alterations of *Gja1* (coding for Cx43 gap junction) in embryonic atria and ventricles. In addition, important genes for calcium signaling such us *Cacna1c* (coding for $Car_v1.2$), *RyR2* (coding for Ryanodine Receptor 2) and *Atp2a2* (coding for SERCA2), where downregulated upon *Meis1* and *Meis2* double deletion in CMs. A mouse model with a *Cacna1c* mutation leads to lethal arrhythmias at birth (Domes *et al*, 2011) and different studies in mouse models reported that more than 50% reduction in *Gja1* expression can lead to ventricular arrhythmias and sudden death around P21 (Gutstein *et al*, 2001).

All these data, together with the fact that we did not detect an impairment in cardiac function, support our hypothesis on postnatal lethal cardiac arrhythmias occurring in dKO embryos. Moreover, the reduction in Cx43 expression and the slower depolarization rates observed by optical mapping strongly support this view. Nevertheless, we have not been able to detect cardiac rhythm alterations by non-invasive echocardiography on pregnant females. It was only after surgically exposing the uterus when the alterations appeared. One possibility is that dKO embryos might be more sensitive to temperature changes, so when the temperature drops, the heart rate is slower and cardiac arrhythmias manifest. This might also be the explanation for the low proportion of mutants that show beating after cesarean dissection of fetuses at E16.5 during optical mapping.

An interesting future experiment, would be harvesting fetuses at E18.5 and reanimate them to perform ECG and record the possible arrhythmic events before death. We also plan to better investigate blood flows recorded in embryonic hearts by echocardiography, where we can visualize atrioventricular blocks, changes in SAN rhythm and heart rate variability. Thus, we will have more information about the possible origin of the arrhythmia.

MEIS IN ADULT CMs

We showed that *Meis1* and *Meis2* double inducible deletion in adult CMs leads to an increase in ventricular mass and wall thickness with preserved ejection fraction. The mild hypertrophy observed might not be a primary effect of Meis loss of function and it does not progress to heart failure in the temporal window explored in this work. A

possible explanation for the preserved cardiac function is that the increase in cardiac size is not as severe as in other models of hypertrophic cardiomyopathy (Nakamura & Sadoshima, 2018; You *et al*, 2017). Moreover, we were not able to detect significant differences in the size of CMs of idKO hearts. One possibility is that the mild increase in heart size might be mainly due to the interstitial fibrosis observed with preserved number of CMs and contractile function. Nonetheless, it is important to mention that histological images with SR staining in control and idKO (FIG. 27A) suggested that a local CM hypertrophy, not detected in the global quantifications, could be happening close to the regions with higher increase in collagen deposition. This opens the possibility that there is local CM death leading to fibrosis and hypertrophy of the surrounding CMs for function compensation. If this was the case, the percentage of hypertrophic CMs would be small and upon Langendorff isolation, they would dilute out in the sample so that the differences may not be detectable. We are currently measuring CMs area in sections to address this possibility.

An alternative to this idea would be that mild CM hyperplasia might underlie the increase in cardiac mass. This would be functionally compensatory and fit with the previous reports that link Meis activity and CM exit of the cell cycle (Mahmoud *et al*, 2013, 2014). Therefore, we also explored CM proliferation as another possible factor contributing to the increase of ventricular mass in idKOs. We described here a significant augment of BrdU incorporation in mononucleated CMs of idKOs hearts, however this did not result in actual CM proliferation. Instead, mononucleated CMs became polyploid and increased size. This increase in size of the $BrdU^{+}$ mononucleated CMs in idKOs likely has a very small contribution to the hypertrophic phenotype, since it represents a very small percentage of the total CM population. These results are apparently contradictory with those reported by the Sadek lab, where Meis1 is proposed as a negative regulator of postnatal CMs proliferation. In fact, after *Meis1* deletion in neonatal CMs, Mahmoud *et al*., found increased CM proliferation and a higher number of mononucleated CMs by P7. In addition to characterizing proliferation, we have specifically looked for the expression of genes related to cell cycle that were described in the perinatal deletion of *Meis1* by Mahmoud et al., but we did not detect changes in these factors in the *Meis1* and *Meis2* adult mutants. We think

there are two possible explanations for this, either the function of *Meis1* in adult CMs is different to that in perinatal stages, which has not been explored here, or in adult CMs the absence of Meis function is not enough to induce the complete cell division process, so it only increases DNA synthesis.

ECG analysis in control and idKOs pointed out possible alterations in conduction velocity upon *Meis1* and *Meis2* deletion in adult CMs. We detected that idKOs have a prolonged QRS complex, which correlates to what we found in dKO fetuses by optical mapping. QRS elongation in humans is a risk factor for ventricular fibrillation (Elhendy *et al*, 2005; Desai *et al*, 2006) but it does not always correspond with a slower ventricular conduction velocity. It has been reported that increased cardiac mass together with normal conduction velocity can also lead to longer QRS complexes (Wiegerinck *et al*, 2006). The most important determinant of ventricular conduction velocity is the sodium current mainly generated by channels encoded by *Scn5a*. RNA-seq data from adult ventricles showed *Scn5a* expression is significantly reduced in idKOs, suggesting that a defective sodium current might underlie the slower ventricular conduction and QRS elongation in our model. It would be very interesting to measure this current by patch-clump in both CCs and working-myocardium CMs to corroborate these results at the single-cell level.

The reduced Cx43 expression and the interstitial fibrosis might also contribute to QRS elongation. Several mouse models have shown that reduction in Cx43 expression is associated with slower ventricular conduction velocity accompanied by increased incidence of arrhythmias and sudden cardiac death (Gutstein *et al*, 2001; Danik *et al*, 2004; van Rijen *et al*, 2004; Lerner *et al*, 2000). Moreover, rapid Cx43 remodeling or redistribution to the lateral membrane has been found in patients with various cardiac diseases, such as cardiac hypertrophy or dilated cardiomyopathy (Lambiase & Tinker, 2015; Severs *et al*, 2004). Several genes related to these diseases appear altered in idKOs hearts, as the gene set enrichment analysis pointed out, however we did not observed dilation in mutant hearts.

Furthermore, it has been proposed that reduced adhesion between cardiomyocytes might lead to mechanical stress and induce cell death (Moncayo-Arlandi & Brugada,

2017; Basso *et al*, 2009). According to this idea, interstitial fibrosis could be a secondary effect of ID disorganization. Furthermore, *Scn5a* downregulation could be a secondary consequence of Cx43 alteration in the ID (Moncayo-Arlandi & Brugada, 2017). On the other hand, there are evidences of *Scn5a* loss of function in old mice leading to fibrosis and reduced expression of Cx43 (van Veen *et al*, 2005). Thus, determining which is the cause and which the consequence would need further analyses.

As mentioned above, *Meis1* genetic variants have been associated with PR interval elongation in humans (Pfeufer *et al*, 2010; Smith *et al*, 2011b; Butler *et al*, 2012a). However, we did not detect any alterations on this interval upon double inducible deletion of *Meis1* and *Meis2* in CMs. This is likely due to the low efficiency of recombination of *α-MHC-MerCreMer* in atria, although the association found in humans does not tell about the type of alteration in *Meis1* function (gain or loss function) that drives the phenotype. Nonetheless, *Meis1* and *Meis2* loss of function in adult ventricular CMs also leads to decreased expression of *Hcn4* and *Cntn2*, which are markers of the CCS, suggesting a specific function of Meis in CCS cardiomyocytes. We consider idKOs might have alterations in the VCS, although we have not been able to find any functional impairment specifically in these cells. We are currently studying the Cntn2 expression pattern in the Purkinje Fiber network in this model and the consequences of *Meis1* and *Meis2* double specific deletion in CCS, using a *Hcn4-CreERT* knockin line.

The molecular changes found by RNA-seq data in idKO ventricles indicate certain similarities between *Meis* loss of function and those observed in mouse models of ARVC. A murine model developed by Dr. Delmar (Cerrone *et al*, 2012a) consisting on *Pkp2* (desmosome structural protein) deletion in adult CMs recapitulates some features of human ARVC. In *Pkp2* conditional KO mice there is desmosome disorganization that leads to decreased levels of expression of many other proteins important for the intercalated discs, such us Cx43. The pathology starts with interstitial fibrosis that can affect only the right or both ventricles, and with time evolves to dilated cardiomyopathy, impaired cardiac function and death. Moreover, intracellular calcium homeostasis is affected due to downregulation of key regulatory genes like *RyR2* and

Cacna1c. Comparing RNA-seq data from *Meis1* and *Meis2* idKO and *Pkp2* inducible KO, we found that key genes for the ARVC phenotype where commonly affected in both models. Furthermore, PKP2 deletion leads to significant downregulation of *Meis1* and *Meis2* genes. Thus, we propose that Meis TFs could be partly under the control of the regulatory network involved in the ARVC-like phenotype present in *Pkp2* mutant hearts (Cerrone *et al*, 2012a). To further study this possibility, we are currently developing a mouse line with simultaneous *Pkp2* deletion and *Meis2* overexpression in adult CMs. We will determine whether *Meis2* can rescue aspects of the ARVC phenotype in this mouse model.

In humans, ARVC also leads to ventricular arrhythmias and sudden death (Zhao *et al*, 2019). In the murine model of *Pkp2* deletion, arrhythmias only appeared upon acute isoproterenol treatment. However, *Meis1* and *Meis2* idKO mice did not preferentially show arrhythmic episodes after the same treatment. We hypothesized that *Meis1* and *Meis2* inducible deletion in adult CMs recapitulates some features of ARVC but this is not enough to reproduce the complete phenotype found in *Pkp2* inducible KOs. Actually, in the volcano plot in FIG. 34B it can be observed that *Pkp2* deletion leads to many more gene expression changes than those observed in Meis mutants.

PUTATIVE DIRECT TARGETS OF MEIS

In the last part of this thesis project, we examined the putative direct targets of Meis1 and Meis2 in cardiomyocytes. Comparing the three RNA-seq performed in developing atria and ventricles and adult ventricles from Control and idKO hearts, we found 28 genes differentially expressed in the three conditions. Gene ontology analysis related 16 of those genes with several biological functions: heart development and contraction, regulation of transport and secretion. Despite the fact that 28 genes are a low input for a gene ontology analysis, the categories found are closely related to the phenotypes described upon Meis loss of function, which suggests this gene list is relevant to the mechanisms involved in the phenotypic alterations. Furthermore, *Fhl2* and *Lrrc10,* which are strongly downregulated, have been previously as hypertrophic growth repressor (Okamoto *et al*, 2013) and cardiac excitation-contraction coupling regulator, respectively (Chiamvimonvat & Song, 2018). By contrast, nothing has been reported

before about *EfnB3* expression or function in the heart, despite of being one of the most downregulated in Meis mutants. We are currently working on the expression pattern of this protein.

Analysis of previous Meis ChIP-seq data from the lab, performed in E10.5 embryos and E11.5 embryonic trunk (Longobardi *et al*, 2014; Delgado I *et al,* unpublished), revealed putative Meis binding sites among the genes of interest. As we have explained before, *Cacna1c* could be playing a central role in the development of arrhythmias, together with *Gja1* downregulation. However, our results only detected possible Meis direct regulation in *Cacna1c* and not *Gja1*. *Nppa*, which appears upregulated in all conditions, does not seem to be a direct target of Meis. This result fits with the role of Nppa as a general responder to a wide variety of cardiac stresses. Interestingly, we also found *Clic4* and *Gpc1* as potential targets of Meis. Clic4 is expressed in the sarcoplasmic reticulum and has been proposed to regulate ryanodine-receptors (Ponnalagu *et al*, 2016). Gpc1 is an extracellular matrix protein whose expression appeared altered in a model of induce arrhythmias in rat (Vakhitova *et al*). *PAM* and *Prps2* also presented putative binding sites for Meis. PAM is important for Nppa secretion in the atria (Eipper *et al*, 1988; Czyzyk *et al*, 2005) and Prps2 is implicated in the synthesis of purines and pyrimidines and it has been related to cancer (Mannava *et al*, 2008), but nothing is reported about its function in the heart. Using the same approach we also identified Meis binding sites in *Scn5a* and *Wnt11* whose downregulation might underlie important features of the Meis mutant phenotypes. Nevertheless, these results are not enough to determine whether Meis is directly regulating those genes or whether Meis is actually binding to some of the genes where we did not detect peaks, and further studies specific for cardiomyocytes are needed.

Overall, we propose that Meis1 and Meis2 TFs play an important role in the regulation of calcium and sodium transport and gap junction establishment in developing and adult CMs through regulation of *Cacna1c*, *Scn5a* and *Gja1* expression. The downregulation of *Cacna1c* and *Scn5a* upon Meis deletion would impair electrico-mechanical coupling and the intercalated disc structure which could lead to Cx43 downregulation. These defects result in slower ventricular depolarization. Moreover, ID disorganization and CM uncoupling might induce mechanical stress leading to cell

death, interstitial fibrosis and mild-hypertrophy, to preserve cardiac function. In the formation of the atria, these alterations in cell-cell coupling, together with misregulation of cell polarity due to decreased expression of *Wnt11* and *Wnt5a*, are probably contributing to the atrial malformations found in dKO embryonic hearts. These alterations lead to an increased susceptibility to suffer arrhythmias in newborns, while in the adult heart it seems that more factors are needed for arrhythmia manifestation.

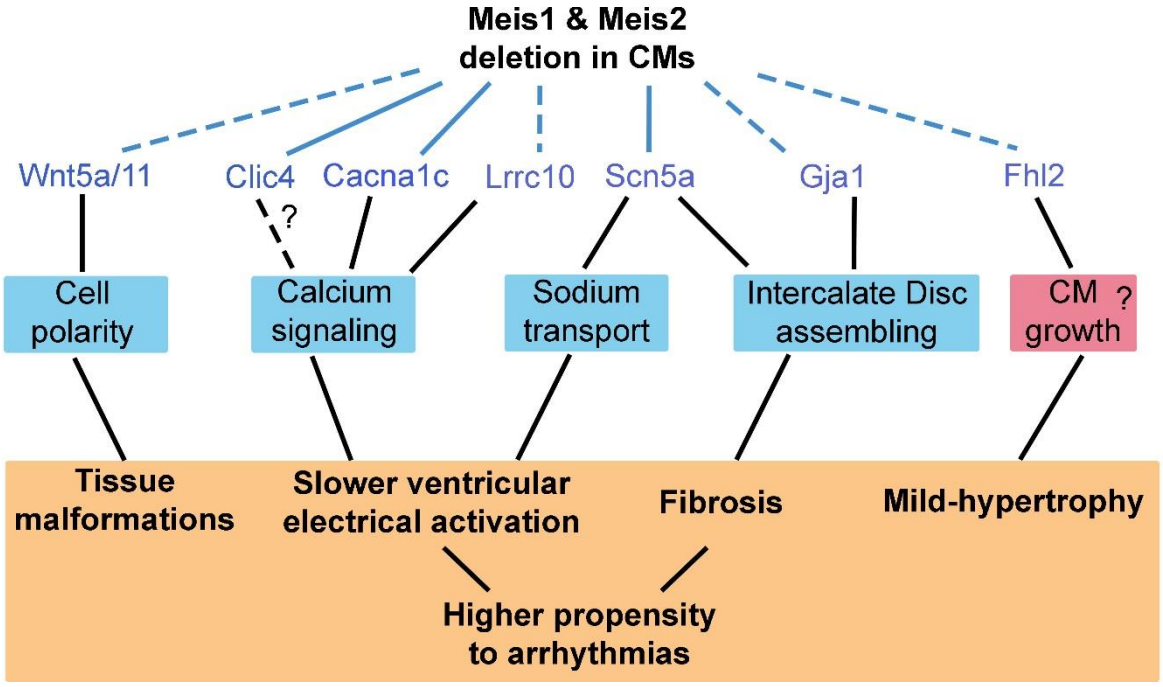

Figure 40. Summary of defects and gene expression changes found in CMs lacking *Meis1* and *Meis2*. In blue are represented genes and processes which are impaired upon Meis loss of function in CMs and in red, processed that increase. Blue lines link to potential direct targets of Meis and dashed lines to targets with no evidence of direct regulation. The orange box includes the defects found in mutant hearts.

CONCLUSIONS

1) Meis1 and Meis2 transcription factors are expressed in developing and adult cardiomyocytes and are necessary for perinatal survival and adult heart homeostasis.

2) The simultaneous deletion of *Meis1* and *Meis2* deletion in developing cardiomyocytes leads to cardiac malformations in atria and ventricles and slower ventricular conduction velocity.

3) Fetuses with *Meis1* and *Meis2* cardiomyocyte-specific loss of function show higher frequency of stress-induced arrhythmias than Control littermates.

4) Deletion of *Meis1* and *Meis2* in adult cardiomyocytes produces interstitial fibrosis and QRS enlargement, suggesting a slower propagation of the electrical impulse in ventricles.

5) *Meis1* and *Meis2* deletion in adult cardiomyocytes stimulates endoreplicative DNA synthesis preferentially in mononucleated cells but does not stimulate cardiomyocyte proliferation.

6) The expression of genes encoding calcium signaling factors, sodium channels and Gap-junction proteins are regulated by *Meis1* and *Meis2* transcription factors in cardiomyocytes.

7) *Cacna1c*, *Scn5a*, *Clic4, Gpc1, Wnt11, PAM* and *Prps2* are identified as putative direct targets of Meis1 and Meis2 in developing and adult cardiomyocytes.

CONCLUSIONES

1) Los factores de transcripción Meis1 y Meis2 se expresan en cardiomiocitos durante el desarrollo embrionario y en el corazón adulto y son necesarios para la supervivencia de los fetos al nacer y para mantener la homeostasis del corazón adulto.

2) La deleción simultánea de *Meis1* y *Meis2* en cardiomiocitos durante el desarrollo cardiaco conlleva la aparición de malformaciones en las aurículas y los ventrículos, además de ralentizar la velocidad de conducción en los ventrículos.

3) Los fetos con falta de función de *Meis1* y *Meis2* en cardiomiocitos presentan una mayor frecuencia de arritmias cuando se exponen a situaciones de estrés.

4) La doble deleción de *Meis1* y *Meis2* en cardiomiocitos adultos produce fibrosis intersticial y un alargamiento del complejo QRS, lo que sugiere que la propagación del impulso eléctrico es más lenta.

5) La falta de función de *Meis1* y *Meis2* en cardiomiocitos incrementa la proporción de endoreplicación de ADN preferencialmente en células mononucleadas, pero no incrementa la proliferación de los cardiomiocitos.

6) Genes que codifican factores implicados en la señalización del calcio en cardiomiocitos, en el establecimiento de las uniones GAP y el transporte del sodio, están regulados por los factores de transcripción Meis1 y Meis2.

7) *Cacna1c*, *Scn5a*, *Clic4, Gpc1, Wnt11, PAM* y *Prps2* se identifican como posibles dianas directas de Meis1 y Meis2 en cardiomiocitos, lo que ayudaría a explicar gran parte de los fenotipos descritos.

BIBLIOGRAPHY

Aanhaanen WTJ, Mommersteeg MTM, Norden J, Wakker V, de Gier-de Vries C, Anderson RH, Kispert A, Moorman AFM & Christoffels VM (2010) Developmental Origin, Growth, and Three-Dimensional Architecture of the Atrioventricular Conduction Axis of the Mouse Heart. *Circ. Res.* **107:** 728–736

Agah R, Frenkel P a, French B a, Michael LH, Overbeek P a & Schneider MD (1997) Gene Recombination in Postmitotic Cells. *J. Clin. Invest.* **100:** 169–179

Andersson KB, Birkeland JAK, Finsen AV, Louch WE, Sjaastad I, Wang Y, Chen J, Molkentin JD, Chien KR, Sejersted OM & Christensen G (2009) Moderate heart dysfunction in mice with inducible cardiomyocyte-specific excision of the Serca2 gene. *J. Mol. Cell. Cardiol.* **47:** 180–187

Andersson T, Magnuson A, Bryngelsson I-L, Frøbert O, Henriksson KM, Edvardsson N & Poçi D (2013) All-cause mortality in 272 186 patients hospitalized with incident atrial fibrillation 1995–2008: a Swedish nationwide long-term case–control study. *Eur. Heart J.* **34:** 1061–1067

Azcoitia V, Aracil M, Martínez-A C & Torres M (2005) The homeodomain protein Meis1 is essential for definitive hematopoiesis and vascular patterning in the mouse embryo. *Dev. Biol.* **280:** 307–320

Bassat E, Mutlak YE, Genzelinakh A, Shadrin IY, Baruch Umansky K, Yifa O, Kain D, Rajchman D, Leach J, Riabov Bassat D, Udi Y, Sarig R, Sagi I, Martin JF, Bursac N, Cohen S & Tzahor E (2017) The extracellular matrix protein agrin promotes heart regeneration in mice. *Nature* **547:** 179–184

Basso C, Corrado D, Marcus FI, Nava A & Thiene G (2009) Arrhythmogenic right ventricular cardiomyopathy. *Lancet* **373:** 1289–1300

Benes J, Ammirabile G, Sankova B, Campione M, Krejci E, Kvasilova A & Sedmera D (2014) The role of connexin40 in developing atrial conduction. *FEBS Lett.* **588:** 1465–1469

Bergmann O, Zdunek S, Felker A, Salehpour M, Alkass K, Bernard S, Sjostrom SL, Szewczykowska M, Jackowska T, dos Remedios C, Malm T, Andrä M, Jashari R, Nyengaard JR, Possnert G, Jovinge S, Druid H & Frisén J (2015) Dynamics of Cell Generation and Turnover in the Human Heart. *Cell* **161:** 1566–1575

Bersell K, Choudhury S, Mollova M, Polizzotti BD, Ganapathy B, Walsh S, Wadugu B, Arab S & Kuhn B (2013) Moderate and high amounts of tamoxifen in MHC-MerCreMer mice induce a DNA damage response, leading to heart failure and death. *Dis. Model. Mech.* **6:** 1459–1469

Blausen BE, Johannes RS & Hutchins GM (1990) Computer-based reconstructions of the cardiac ventricles of human embryos. *Am. J. Cardiovasc. Pathol.* **3:** 37–43

Bondue A & Blanpain C (2010) Mesp1: a key regulator of cardiovascular lineage commitment. *Circ. Res.* **107:** 1414–27

Boukens BJ, Rivaud MR, Rentschler S & Coronel R (2014) Misinterpretation of the mouse ECG: 'musing the waves of Mus musculus'. *J. Physiol.* **592:** 4613–26

Brown CB & Baldwin HS (2006) Neural Crest Contribution to the Cardiovascular System. In *Neural Crest Induction and Differentiation* pp 134–154. Boston, MA: Springer US

Bruneau BG (2008) The developmental genetics of congenital heart disease. *Nature* **451:** 943–948

Butler AM, Yin X, Evans DS, Nalls M a., Smith EN, Tanaka T, Li G, Buxbaum SG, Whitsel E a., Alonso A, Arking DE, Benjamin EJ, Berenson GS, Bis JC, Chen W, Deo R, Ellinor PT, Heckbert SR, Heiss G, Hsueh WC, et al (2012a) Novel loci associated with PR interval in a genome-wide association study of 10 African American cohorts. *Circ. Cardiovasc. Genet.* **5:** 639–646

Butler AM, Yin X, Evans DS, Nalls MA, Smith EN, Tanaka T, Li G, Buxbaum SG, Whitsel EA, Alonso A, Arking DE, Benjamin EJ, Berenson GS, Bis JC, Chen W, Deo R, Ellinor PT, Heckbert SR, Heiss G, Hsueh W-C, et al (2012b) Novel Loci Associated With PR Interval in a Genome-Wide Association Study of 10 African American Cohorts. *Circ. Cardiovasc. Genet.* **5:** 639–646

Cai C-L, Liang X, Shi Y, Chu P-H, Pfaff SL, Chen J & Evans S (2003) Isl1 identifies a cardiac progenitor population that proliferates prior to differentiation and contributes a majority of cells to the heart. *Dev. Cell* **5:** 877–89

Cecconi F, Proetzel G, Alvarez-Bolado G, Jay D & Gruss P (1997) Expression ofMeis2, aKnotted-related murine homeobox gene, indicates a role in the differentiation of the forebrain and the somitic mesoderm. *Dev. Dyn.* **210:** 184–190

Cerrone M, Noorman M, Lin X, Chkourko H, Liang F-X, van der Nagel R, Hund T, Birchmeier W, Mohler P, van Veen TA, van Rijen H V. & Delmar M (2012a) Sodium current deficit and

arrhythmogenesis in a murine model of plakophilin-2 haploinsufficiency. *Cardiovasc. Res.* **95:** 460–468

Cerrone M, Noorman M, Lin X, Chkourko H, Liang F-X, van der Nagel R, Hund T, Birchmeier W, Mohler P, van Veen TA, van Rijen H V. & Delmar M (2012b) Sodium current deficit and arrhythmogenesis in a murine model of plakophilin-2 haploinsufficiency. *Cardiovasc. Res.* **95:** 460–468

Challice CE & Virágh S (1980) Origin and early differentiation of the sinus node in the mouse embryo heart. *Adv. Myocardiol.* **1:** 267–77

Chiamvimonvat N & Song L (2018) LRRC10 (Leucine-Rich Repeat Containing Protein 10) and REEP5 (Receptor Accessory Protein 5) as Novel Regulators of Cardiac Excitation-Contraction Coupling Structure and Function. *J. Am. Heart Assoc.* **7:**

Christoffels VM, Habets PEMH, Franco D, Campione M, de Jong F, Lamers WH, Bao Z-Z, Palmer S, Biben C, Harvey RP & Moorman AFM (2000) Chamber Formation and Morphogenesis in the Developing Mammalian Heart. *Dev. Biol.* **223:** 266–278

Christoffels VM, Mommersteeg MTM, Trowe MO, Prall OWJ, De Gier-De Vries C, Soufan AT, Bussen M, Schuster-Gossler K, Harvey RP, Moorman a. FM & Kispert A (2006) Formation of the venous pole of the heart from an Nkx2-5-negative precursor population requires Tbx18. *Circ. Res.* **98:** 1555–1563

Christoffels VM & Moorman AFM (2009) Development of the cardiac conduction system: why are some regions of the heart more arrhythmogenic than others? *Circ. Arrhythm. Electrophysiol.* **2:** 195–207

Clauss S, Bleyer C, Schüttler D, Tomsits P, Renner S, Klymiuk N, Wakili R, Massberg S, Wolf E & Kääb S (2019) Animal models of arrhythmia: classic electrophysiology to genetically modified large animals. *Nat. Rev. Cardiol.*

Cole-Jeffrey CT, Terada R, Neth MR, Wessels A & Kasahara H (2012) Progressive Anatomical Closure of Foramen Ovale in Normal Neonatal Mouse Hearts. *Anat. Rec. Adv. Integr. Anat. Evol. Biol.* **295:** 764–768

Coppen SR, Severs NJ & Gourdie RG (1999) Connexin45 (?6) expression delineates an extended conduction system in the embryonic and mature rodent heart. *Dev. Genet.* **24:** 82–90

Czyzyk TA, Ning Y, Hsu M-S, Peng B, Mains RE, Eipper BA & Pintar JE (2005) Deletion of peptide

amidation enzymatic activity leads to edema and embryonic lethality in the mouse. *Dev. Biol.* **287:** 301–313

D'Uva G, Aharonov A, Lauriola M, Kain D, Yahalom-Ronen Y, Carvalho S, Weisinger K, Bassat E, Rajchman D, Yifa O, Lysenko M, Konfino T, Hegesh J, Brenner O, Neeman M, Yarden Y, Leor J, Sarig R, Harvey RP & Tzahor E (2015) ERBB2 triggers mammalian heart regeneration by promoting cardiomyocyte dedifferentiation and proliferation. *Nat. Cell Biol.* **17:** 627–38

Danik SB, Liu F, Zhang J, Suk HJ, Morley GE, Fishman GI & Gutstein DE (2004) Modulation of Cardiac Gap Junction Expression and Arrhythmic Susceptibility. *Circ. Res.* **95:** 1035–1041

Davis LM, Kanter HL, Beyer EC & Saffitz JE (1994) Distinct gap junction protein phenotypes in cardiac tissues with disparate conduction properties. *J. Am. Coll. Cardiol.* **24:** 1124–32

Desai AD, Yaw TS, Yamazaki T, Kaykha A, Chun S & Froelicher VF (2006) Prognostic Significance of Quantitative QRS Duration. *Am. J. Med.* **119:** 600–606

Dhar Malhotra J, Chen C, Rivolta I, Abriel H, Malhotra R, Mattei LN, Brosius FC, Kass RS & Isom LL (2001) Characterization of sodium channel alpha- and beta-subunits in rat and mouse cardiac myocytes. *Circulation* **103:** 1303–10

Domes K, Ding J, Lemke T, Blaich A, Rg J, Wegener W, Brandmayr J, Moosmang S & Hofmann F (2011) Truncation of Murine Ca v 1.2 at Asp-1904 Results in Heart Failure after Birth * □ S The carboxyl-terminal intracellular tail of the L-type Ca 2 channel Ca V 1.2 modulates various aspects of channel activity. For example, deletion of the carboxyl-terminal sequence at Ser-1905 increased Ca V 1.2 currents in an expression model Downloaded from. *NUMBER 39 J. Biol. Chem.* **286:** 33863–33871

van Eif VWW, Devalla HD, Boink GJJ & Christoffels VM (2018) Transcriptional regulation of the cardiac conduction system. *Nat. Rev. Cardiol.* **15:** 617–630

Eipper BA, May V & Braas KM (1988) Membrane-associated peptidylglycine alpha-amidating monooxygenase in the heart. *J. Biol. Chem.* **263:** 8371–9

Elhendy A, Hammill SC, Mahoney DW & Pellikka PA (2005) Relation of QRS Duration on the Surface 12-Lead Electrocardiogram With Mortality in Patients With Known or Suspected Coronary Artery Disease. *Am. J. Cardiol.* **96:** 1082–1088

Engel FB, Schebesta M, Duong MT, Lu G, Ren S, Madwed JB, Jiang H, Wang Y & Keating MT (2005) p38 MAP kinase inhibition enables proliferation of adult mammalian cardiomyocytes.

Genes Dev. **19:** 1175–87

Estigoy CB, Pontén F, Odeberg J, Herbert B, Guilhaus M, Charleston M, Ho JWK, Cameron D & dos Remedios CG (2009) Intercalated discs: multiple proteins perform multiple functions in non-failing and failing human hearts. *Biophys. Rev.* **1:** 43–49

Evans SM, Yelon D, Conlon FL & Kirby ML (2010) Myocardial Lineage Development. *Circ. Res.* **107:** 1428–1444

Fahed AC, Gelb BD, Seidman JG & Seidman CE (2013) Genetics of Congenital Heart Disease. *Circ. Res.* **112:** 707–720

Fearnley CJ, Llewelyn Roderick H & Bootman MD (2011) Calcium signaling in cardiac myocytes. *Cold Spring Harb. Perspect. Biol.* **3:**

Fye WB (1994) A history of the origin, evolution, and impact of electrocardiography. *Am. J. Cardiol.* **73:** 937–49

Gabisonia K, Prosdocimo G, Aquaro GD, Carlucci L, Zentilin L, Secco I, Ali H, Braga L, Gorgodze N, Bernini F, Burchielli S, Collesi C, Zandonà L, Sinagra G, Piacenti M, Zacchigna S, Bussani R, Recchia FA & Giacca M (2019) MicroRNA therapy stimulates uncontrolled cardiac repair after myocardial infarction in pigs. *Nature* **569:** 418–422

Gard JJ, Yamada K, Green KG, Eloff BC, Rosenbaum DS, Wang X, Robbins J, Schuessler RB, Yamada KA & Saffitz JE (2005) Remodeling of gap junctions and slow conduction in a mouse model of desmin-related cardiomyopathy. *Cardiovasc. Res.* **67:** 539–47

Giliberti A, Currò A, Papa FT, Frullanti E, Ariani F, Coriolani G, Grosso S, Renieri A & Mari F (2019) MEIS2 gene is responsible for intellectual disability, cardiac defects and a distinct facial phenotype. *Eur. J. Med. Genet.*

von Gise A, Lin Z, Schlegelmilch K, Honor LB, Pan GM, Buck JN, Ma Q, Ishiwata T, Zhou B, Camargo FD & Pu WT (2012) YAP1, the nuclear target of Hippo signaling, stimulates heart growth through cardiomyocyte proliferation but not hypertrophy. *Proc. Natl. Acad. Sci.* **109:** 2394–2399

Goldbarg AN, Hellerstein HK, Bruell JH & Daroczy AF (1968) Electrocardiogram of the Normal Mouse, Mus Musculus: General Considerations and Genetic Aspects. *Cardiovasc. Res.* **2:** 93–99

González-Lázaro M, Roselló-Díez A, Delgado I, Carramolino L, Sanguino MA, Giovinazzo G & Torres M (2014) Two new targeted alleles for the comprehensive analysis of M

eis1 functions in the mouse. *Genesis* **52:** 967–975

Gordan R, Gwathmey JK & Xie L-H (2015) Autonomic and endocrine control of cardiovascular function. *World J. Cardiol.* **7:** 204–14

Gutstein DE, Morley GE, Tamaddon H, Vaidya D, Schneider MD, Chen J, Chien KR, Stuhlmann H & Fishman GI (2001) Conduction slowing and sudden arrhythmic death in mice with cardiac-restricted inactivation of connexin43. *Circ. Res.* **88:** 333–9

Heallen T, Zhang M, Wang J, Bonilla-Claudio M, Klysik E, Johnson RL & Martin JF (2011) Hippo Pathway Inhibits Wnt Signaling to Restrain Cardiomyocyte Proliferation and Heart Size. *Science (80-.).* **332:** 458–461

Hisa T, Spence SE, Rachel R a, Fujita M, Nakamura T, Ward JM, Devor-Henneman DE, Saiki Y, Kutsuna H, Tessarollo L, Jenkins N a & Copeland NG (2004) Hematopoietic, angiogenic and eye defects in Meis1 mutant animals. *EMBO J.* **23:** 450–459

Ivanovitch K, Temiño S & Torres M (2017) Live imaging of heart tube development in mouse reveals alternating phases of cardiac differentiation and morphogenesis. *Elife* **6:**

Jansen JA, van Veen TAB, de Bakker JMT & van Rijen HVM (2010) Cardiac connexins and impulse propagation. *J. Mol. Cell. Cardiol.* **48:** 76–82

Jiang X, Rowitch DH, Soriano P, McMahon AP & Sucov HM (2000) Fate of the mammalian cardiac neural crest. *Development* **127:** 1607–16

Kelly RG (2012) The Second Heart Field. In *Current topics in developmental biology* pp 33–65.

Kelly RG, Brown NA & Buckingham ME (2001) The arterial pole of the mouse heart forms from Fgf10-expressing cells in pharyngeal mesoderm. *Dev. Cell* **1:** 435–40

Kelly RG, Buckingham ME & Moorman AF (2014) Heart Fields and Cardiac Morphogenesis. *Cold Spring Harb. Perspect. Med.* **4:** a015750–a015750

Keyte AL, Alonzo-Johnsen M & Hutson MR (2014) Evolutionary and developmental origins of the cardiac neural crest: Building a divided outflow tract. *Birth Defects Res. Part C Embryo Today Rev.* **102:** 309–323

Kimura W, Muralidhar S, Canseco DC, Puente B, Zhang CC, Xiao F, Abderrahman YH & Sadek HA (2014) Redox Signaling in Cardiac Renewal. *Antioxid. Redox Signal.* **21:** 1660–1673

Koitabashi N, Bedja D, Zaiman AL, Pinto YM, Zhang M, Gabrielson KL, Takimoto E & Kass DA (2009) Avoidance of Transient Cardiomyopathy in Cardiomyocyte-Targeted Tamoxifen-

Induced MerCreMer Gene Deletion Models. *Circ. Res.* **105:** 12–15

Krainock M, Toubat O, Danopoulos S, Beckham A, Warburton D & Kim R (2016) Epicardial Epithelial-to-Mesenchymal Transition in Heart Development and Disease. *J. Clin. Med.* **5:**

Kreuzberg MM, Liebermann M, Segschneider S, Dobrowolski R, Dobrzynski H, Kaba R, Rowlinson G, Dupont E, Severs NJ & Willecke K (2009) Human connexin31.9, unlike its orthologous protein connexin30.2 in the mouse, is not detectable in the human cardiac conduction system. *J. Mol. Cell. Cardiol.* **46:** 553–559

Kreuzberg MM, Söhl G, Kim J-S, Verselis VK, Willecke K & Bukauskas FF (2005) Functional Properties of Mouse Connexin30.2 Expressed in the Conduction System of the Heart. *Circ. Res.* **96:** 1169–1177

Lambiase PD & Tinker A (2015) Connexins in the heart. *Cell Tissue Res.* **360:** 675–684

Lawson KA, Meneses JJ & Pedersen RA (1991) Clonal analysis of epiblast fate during germ layer formation in the mouse embryo. *Development* **113:** 891–911

Lee K-F, Simon H, Chen H, Bates B, Hung M-C & Hauser C (1995) Requirement for neuregulin receptor erbB2 in neural and cardiac development. *Nature* **378:** 394–398

Lerner DL, Yamada KA, Schuessler RB & Saffitz JE (2000) Accelerated onset and increased incidence of ventricular arrhythmias induced by ischemia in Cx43-deficient mice. *Circulation* **101:** 547–52

Li F, Wang X, Capasso JM & Gerdes AM (1996) Rapid Transition of Cardiac Myocytes from Hyperplasia to Hypertrophy During Postnatal Development. *J. Mol. Cell. Cardiol.* **28:** 1737–1746

Longobardi E, Penkov D, Mateos D, De Florian G, Torres M & Blasi F (2014a) Biochemistry of the tale transcription factors PREP, MEIS, and PBX in vertebrates. *Dev. Dyn.* **243:** 59–75

Longobardi E, Penkov D, Mateos D, De Florian G, Torres M & Blasi F (2014b) Biochemistry of the tale transcription factors PREP, MEIS, and PBX in vertebrates. *Dev. Dyn.* **243:** 59–75

Louw JJ, Corveleyn A, Jia Y, Hens G, Gewillig M & Devriendt K (2015) MEIS2 involvement in cardiac development, cleft palate, and intellectual disability. *Am. J. Med. Genet. Part A* **167:** 1142–1146

Machon O, Masek J, Machonova O, Krauss S & Kozmik Z (2015) Meis2 is essential for cranial and cardiac neural crest development. *BMC Dev. Biol.* **15:** 40

Madisen L, Zwingman TA, Sunkin SM, Oh SW, Zariwala HA, Gu H, Ng LL, Palmiter RD, Hawrylycz MJ, Jones AR, Lein ES & Zeng H (2010) A robust and high-throughput Cre reporting and characterization system for the whole mouse brain. *Nat. Neurosci.* **13:** 133–140

Mahmoud AI, Canseco D, Xiao F & Sadek H a. (2014) Cardiomyocyte cell cycle: Meis-ing something? *Cell Cycle* **13:** 1057–1058

Mahmoud AI, Kocabas F, Muralidhar S a, Kimura W, Koura AS, Thet S, Porrello ER & Sadek H a (2013) Meis1 regulates postnatal cardiomyocyte cell cycle arrest. *Nature* **497:** 249–53

Mann RS & Affolter M (1998) Hox proteins meet more partners. *Curr. Opin. Genet. Dev.* **8:** 423–9

Mannava S, Grachtchouk V, Wheeler LJ, Im M, Zhuang D, Slavina EG, Mathews CK, Shewach DS & Nikiforov MA (2008) Direct role of nucleotide metabolism in C-MYC-dependent proliferation of melanoma cells. *Cell Cycle* **7:** 2392–2400

Martin-Puig S, Wang Z & Chien KR (2008) Lives of a heart cell: tracing the origins of cardiac progenitors. *Cell Stem Cell* **2:** 320–31

Mercader N (2005) Proximodistal identity during vertebrate limb regeneration is regulated by Meis homeodomain proteins. *Development* **132:** 4131–4142

Mercader N, Leonardo E, Azpiazu N, Serrano a, Morata G, Martínez C & Torres M (1999) Conserved regulation of proximodistal limb axis development by Meis1/Hth. *Nature* **402:** 425–429

Miquerol L, Beyer S & Kelly RG (2011) Establishment of the mouse ventricular conduction system. *Cardiovasc. Res.* **91:** 232–42

Miquerol L, Moreno-Rascon N, Beyer S, Dupays L, Meilhac SM, Buckingham ME, Franco D & Kelly RG (2010) Biphasic Development of the Mammalian Ventricular Conduction System. *Circ. Res.* **107:** 153–161

Mitchell GF, Jeron A & Koren G (1998) Measurement of heart rate and Q-T interval in the conscious mouse. *Am. J. Physiol.* **274:** H747-51

Mjaatvedt CH, Nakaoka T, Moreno-Rodriguez R, Norris RA, Kern MJ, Eisenberg CA, Turner D & Markwald RR (2001) The outflow tract of the heart is recruited from a novel heart-forming field. *Dev. Biol.* **238:** 97–109

Mohan R, Boukens BJ, Christoffels VM, Mohan R, Boukens BJ & Christoffels VM (2017) Lineages of the Cardiac Conduction System. *J. Cardiovasc. Dev. Dis.* **4:** 5

Mollova M, Bersell K, Walsh S, Savla J, Das LT, Park S-Y, Silberstein LE, dos Remedios CG, Graham D, Colan S & Kühn B (2013) Cardiomyocyte proliferation contributes to heart growth in young humans. *Proc. Natl. Acad. Sci.* **110:** 1446–1451

Mommersteeg MTM, Hoogaars WMH & Prall OWJ Molecular Pathway for the Localized Formation of the Sinoatrial Node.

Moncayo-Arlandi J & Brugada R (2017) Unmasking the molecular link between arrhythmogenic cardiomyopathy and Brugada syndrome. *Nat. Rev. Cardiol.* **14:** 744–756

Moskow JJ, Bullrich F, Huebner K, Daar IO & Buchberg AM (1995) Meis1, a PBX1-related homeobox gene involved in myeloid leukemia in BXH-2 mice. *Mol. Cell. Biol.* **15:** 5434–43

Munshi N V (2012) Gene regulatory networks in cardiac conduction system development. *Circ. Res.* **110:** 1525–37

Munshi N V, McAnally J, Bezprozvannaya S, Berry JM, Richardson JA, Hill JA & Olson EN (2009) Cx30.2 enhancer analysis identifies Gata4 as a novel regulator of atrioventricular delay. *Development* **136:** 2665–74

Myers DC & Fishman GI (2003) Molecular and functional maturation of the murine cardiac conduction system. *Trends Cardiovasc. Med.* **13:** 289–95

Nakamura M & Sadoshima J (2018) Mechanisms of physiological and pathological cardiac hypertrophy. *Nat. Rev. Cardiol.* **15:** 387–407

Nakamura T, Colbert MC & Robbins J (2006) Neural Crest Cells Retain Multipotential Characteristics in the Developing Valves and Label the Cardiac Conduction System. *Circ. Res.* **98:** 1547–1554

Nakamura T, Jenkins NA & Copeland NG (1996) Identification of a new family of Pbx-related homeobox genes. *Oncogene* **13:** 2235–42

Nerbonne JM & Kass RS (2005) Molecular Physiology of Cardiac Repolarization. *Physiol. Rev.* **85:** 1205–1253

Nielsen MS, Axelsen LN, Sorgen PL, Verma V, Delmar M & Holstein-Rathlou N-H (2012) Gap junctions. *Compr. Physiol.* **2:** 1981–2035

Obame FN, Plin-Mercier C, Assaly R, Zini R, Dubois-Randé JL, Berdeaux A & Morin D (2008)

Cardioprotective effect of morphine and a blocker of glycogen synthase kinase 3 beta, SB216763 [3-(2,4-dichlorophenyl)-4(1-methyl-1H-indol-3-yl)-1H-pyrrole-2,5-dione], via inhibition of the mitochondrial permeability transition pore. *J. Pharmacol. Exp. Ther.* **326:** 252–8

Okamoto R, Li Y, Noma K, Hiroi Y, Liu P-Y, Taniguchi M, Ito M & Liao JK (2013) FHL2 prevents cardiac hypertrophy in mice with cardiac-specific deletion of ROCK2. *FASEB J.* **27:** 1439–1449

Ollion J, Cochennec J, Loll F, Escudé C & Boudier T (2013) TANGO: a generic tool for high-throughput 3D image analysis for studying nuclear organization. *Bioinformatics* **29:** 1840–1841

Oulad-Abdelghani M, Chazaud C, Bouillet P, Sapin V, Chambon P & Dollé P (1997) Meis2, a novel mouse Pbx-related homeobox gene induced by retinoic acid during differentiation of P19 embryonal carcinoma cells. *Dev. Dyn.* **210:** 173–83

Parker SE, Mai CT, Canfield MA, Rickard R, Wang Y, Meyer RE, Anderson P, Mason CA, Collins JS, Kirby RS, Correa A & National Birth Defects Prevention Network (2010) Updated national birth prevalence estimates for selected birth defects in the United States, 2004-2006. *Birth Defects Res. Part A Clin. Mol. Teratol.* **88:** 1008–1016

Pfeufer A, van Noord C, Marciante KD, Arking DE, Larson MG, Smith AV, Tarasov K V, Müller M, Sotoodehnia N, Sinner MF, Verwoert GC, Li M, Kao WHL, Köttgen A, Coresh J, Bis JC, Psaty BM, Rice K, Rotter JI, Rivadeneira F, et al (2010) Genome-wide association study of PR interval. *Nat. Genet.* **42:** 153–159

Ponnalagu D, Rao SG, Farber J, Xin W, Hussain AT, Shah K, Tanda S, Berryman MA, Edwards JC & Singh H (2016) Data supporting characterization of CLIC1, CLIC4, CLIC5 and DmCLIC antibodies and localization of CLICs in endoplasmic reticulum of cardiomyocytes. *Data Br.* **7:** 1038–1044

Porrello ER, Mahmoud AI, Simpson E, Hill J a, Richardson J a, Olson EN & Sadek H a (2011) Transient regenerative potential of the neonatal mouse heart. *Science* **331:** 1078–1080

Puente BN, Kimura W, Muralidhar SA, Moon J, Amatruda JF, Phelps KL, Grinsfelder D, Rothermel BA, Chen R, Garcia JA, Santos CX, Thet S, Mori E, Kinter MT, Rindler PM, Zacchigna S, Mukherjee S, Chen DJ, Mahmoud AI, Giacca M, et al (2014) The Oxygen-Rich Postnatal Environment Induces Cardiomyocyte Cell-Cycle Arrest through DNA Damage Response.

Cell **157:** 565–579

Quaife-Ryan GA, Sim CB, Ziemann M, Kaspi A, Rafehi H, Ramialison M, El-Osta A, Hudson JE & Porrello ER (2017) Multicellular Transcriptional Analysis of Mammalian Heart Regeneration. *Circulation* **136:** 1123–1139

van Rijen HVM, Eckardt D, Degen J, Theis M, Ott T, Willecke K, Jongsma HJ, Opthof T & de Bakker JMT (2004) Slow conduction and enhanced anisotropy increase the propensity for ventricular tachyarrhythmias in adult mice with induced deletion of connexin43. *Circulation* **109:** 1048–55

Ryoo HD, Marty T, Casares F, Affolter M & Mann RS (1999) Regulation of Hox target genes by a DNA bound Homothorax/Hox/Extradenticle complex. *Development* **126:** 5137–48

Saga Y, Kitajima S & Miyagawa-Tomita S (2000) Mesp1 expression is the earliest sign of cardiovascular development. *Trends Cardiovasc. Med.* **10:** 345–52

Saga Y, Miyagawa-Tomita S, Takagi A, Kitajima S, Miyazaki J i & Inoue T (1999) MesP1 is expressed in the heart precursor cells and required for the formation of a single heart tube. *Development* **126:** 3437–47

Sedmera D, Pexieder T, Vuillemin M, Thompson RP & Anderson RH (2000) Developmental patterning of the myocardium. *Anat. Rec.* **258:** 319–37

Sedmera D, Reckova M, DeAlmeida A, Coppen SR, Kubalak SW, Gourdie RG & Thompson RP (2003) Spatiotemporal pattern of commitment to slowed proliferation in the embryonic mouse heart indicates progressive differentiation of the cardiac conduction system. *Anat. Rec.* **274A:** 773–777

Severs NJ, Dupont E, Coppen SR, Halliday D, Inett E, Baylis D & Rothery S (2004) Remodelling of gap junctions and connexin expression in heart disease. *Biochim. Biophys. Acta - Biomembr.* **1662:** 138–148

SHANNON TR & BERS DM (2004) Integrated Ca $^{2+}$ Management in Cardiac Myocytes. *Ann. N. Y. Acad. Sci.* **1015:** 28–38

Shen Y, Yue F, McCleary DF, Ye Z, Edsall L, Kuan S, Wagner U, Dixon J, Lee L, Lobanenkov V V. & Ren B (2012) A map of the cis-regulatory sequences in the mouse genome. *Nature* **488:** 116–120

Simsek T, Kocabas F, Zheng J, Deberardinis RJ, Ahmed I, Olson EN, Schneider JW, Zhang CC & Hesham A (2014) Reflects Their Location in a Hypoxic Niche. **7:** 380–390

Singh R, Hoogaars WM, Barnett P, Grieskamp T, Rana MS, Buermans H, Farin HF, Petry M, Heallen T, Martin JF, Moorman AFM, 't Hoen PAC, Kispert A & Christoffels VM (2012) Tbx2 and Tbx3 induce atrioventricular myocardial development and endocardial cushion formation. *Cell. Mol. Life Sci.* **69:** 1377–89

Smith JG, Magnani JW, Palmer C, Meng Y a., Soliman EZ, Musani SK, Kerr KF, Schnabel RB, Lubitz S a., Sotoodehnia N, Redline S, Pfeufer A, Müller M, Evans DS, Nalls M a., Liu Y, Newman AB, Zonderman AB, Evans MK, Deo R, et al (2011a) Genome-wide association studies of the PR interval in African Americans. *PLoS Genet.* **7:**

Smith JG, Magnani JW, Palmer C, Meng YA, Soliman EZ, Musani SK, Kerr KF, Schnabel RB, Lubitz SA, Sotoodehnia N, Redline S, Pfeufer A, Müller M, Evans DS, Nalls MA, Liu Y, Newman AB, Zonderman AB, Evans MK, Deo R, et al (2011b) Genome-Wide Association Studies of the PR Interval in African Americans. *PLoS Genet.* **7:** e1001304

Sohal DS, Nghiem M, Crackower MA, Witt SA, Kimball TR, Tymitz KM, Penninger JM & Molkentin JD (2001) Temporally regulated and tissue-specific gene manipulations in the adult and embryonic heart using a tamoxifen-inducible Cre protein. *Circ. Res.* **89:** 20–5

Soonpaa MH, Kim KK, Pajak L, Franklin M & Field LJ (1996) Cardiomyocyte DNA synthesis and binucleation during murine development. *Am. J. Physiol. Circ. Physiol.* **271:** H2183–H2189

Später D, Abramczuk MK, Buac K, Zangi L, Stachel MW, Clarke J, Sahara M, Ludwig A & Chien KR (2013) A HCN4+ cardiomyogenic progenitor derived from the first heart field and human pluripotent stem cells. *Nat. Cell Biol.* **15:** 1098–106

Spieler D, Kaffe M, Knauf F, Bessa J, Tena JJ, Giesert F, Schormair B, Tilch E, Lee H, Horsch M, Czamara D, Karbalai N, Toerne C Von, Waldenberger M, Gieger C, Lichtner P, Claussnitzer M, Naumann R, Müller-Myhsok B, Torres M, et al (2014) Restless Legs Syndrome-Associated intronic common variant in Meis1 alters enhancer function in the developing telencephalon. *Genome Res.* **24:** 592–603

Stankunas K, Shang C, Twu KY, Kao SC, Jenkins N a., Copeland NG, Sanyal M, Selleri L, Cleary ML & Chang CP (2008) Pbx/Meis deficiencies demonstrate multigenetic origins of congenital heart disease. *Circ. Res.* **103:** 702–709

Staudt DW, Liu J, Thorn KS, Stuurman N, Liebling M & Stainier DYR (2014) High-resolution imaging of cardiomyocyte behavior reveals two distinct steps in ventricular trabeculation. *Development* **141:** 585–593

Susaki EA, Tainaka K, Perrin D, Yukinaga H, Kuno A & Ueda HR (2015) Advanced CUBIC protocols for whole-brain and whole-body clearing and imaging. *Nat. Protoc.* **10:** 1709–1727

Tam PP & Behringer RR (1997) Mouse gastrulation: the formation of a mammalian body plan. *Mech. Dev.* **68:** 3–25

Tzahor E & Poss KD (2017) Cardiac regeneration strategies: Staying young at heart. *Science* **356:** 1035–1039

Unnisa Z, Clark JP, Roychoudhury J, Thomas E, Tessarollo L, Copeland NG, Jenkins NA, Grimes HL & Kumar AR (2012) Meis1 preserves hematopoietic stem cells in mice by limiting oxidative stress. *Blood* **120:** 4973–4981

Vakhitova I V, Antipina EI, Yamidanov RS, Khisamutdinova RI, Zarudiĭ FS, Baschenko NZ, Dokichev VA, Tomilov I V & Nefedov OM [Animal in vivo model of arrhythmia for genes target identification for 5-amino-exo-3-azatricyclo[5.2.1.0(2,6)]decan-4-one]. *Bioorg. Khim.* **37:** 821–9

van Veen TAB, Stein M, Royer A, Le Quang K, Charpentier F, Colledge WH, Huang CL-H, Wilders R, Grace AA, Escande D, de Bakker JMT & van Rijen HVM (2005) Impaired Impulse Propagation in *Scn5a* -Knockout Mice. *Circulation* **112:** 1927–1935

Verheije R, Kupchik GS, Isidor B, Kroes HY, Lynch SA, Hawkes L, Hempel M, Gelb BD, Ghoumid J, D'Amours G, Chandler K, Dubourg C, Loddo S, Tümer Z, Shaw-Smith C, Nizon M, Shevell M, Van Hoof E, Anyane-Yeboa K, Cerbone G, et al (2019) Heterozygous loss-of-function variants of MEIS2 cause a triad of palatal defects, congenital heart defects, and intellectual disability. *Eur. J. Hum. Genet.* **27:** 278–290

Vincent SD & Buckingham ME (2010) How to Make a Heart. In pp 1–41.

Virágh S CC (1977) The development of the conduction system in the mouse embryo heart. II. Histogenesis of the atrioventricular node and bundle. - PubMed - NCBI. *Dev Biol***:** 397–411 Available at: https://www.ncbi.nlm.nih.gov/pubmed/849806 [Accessed May 21, 2019]

Viragh S & Challice CE (1981) The origin of the epicardium and the embryonic myocardial circulation in the mouse. *Anat. Rec.* **201:** 157–168

Waldo KL, Kumiski DH, Wallis KT, Stadt HA, Hutson MR, Platt DH & Kirby ML (2001) Conotruncal myocardium arises from a secondary heart field. *Development* **128:** 3179–88

Walsh S, Pontén A, Fleischmann BK & Jovinge S (2010) Cardiomyocyte cell cycle control and growth estimation in vivo—an analysis based on cardiomyocyte nuclei. *Cardiovasc. Res.* **86:**

365–373

Watanabe Y & Buckingham M (2010) The formation of the embryonic mouse heart. *Ann. N. Y. Acad. Sci.* **1188:** 15–24

Van Weerd JH & Christoffels VM (2016) The formation and function of the cardiac conduction system.

Wessels A & Pérez-Pomares JM (2004) The epicardium and epicardially derived cells (EPDCs) as cardiac stem cells. *Anat. Rec. Part A Discov. Mol. Cell. Evol. Biol.* **276A:** 43–57

Wessels A & Sedmera D (2003) Developmental anatomy of the heart: a tale of mice and man. *Physiol. Genomics* **15:** 165–176

Wiegerinck RF, Verkerk AO, Belterman CN, van Veen TAB, Baartscheer A, Opthof T, Wilders R, de Bakker JMT & Coronel R (2006) Larger Cell Size in Rabbits With Heart Failure Increases Myocardial Conduction Velocity and QRS Duration. *Circulation* **113:** 806–813

Wiese C, Grieskamp T, Airik R, Mommersteeg MTM, Gardiwal A, de Gier-de Vries C, Schuster-Gossler K, Moorman AFM, Kispert A & Christoffels VM (2009) Formation of the Sinus Node Head and Differentiation of Sinus Node Myocardium Are Independently Regulated by Tbx18 and Tbx3. *Circ. Res.* **104:** 388–397

Wong P, Iwasaki M, Somervaille TCP, So CWE & Cleary ML (2007) Meis1 is an essential and rate-limiting regulator of MLL leukemia stem cell potential. *Genes Dev.* **21:** 2762–2774

Wu M, Smith CL, Hall JA, Lee I, Luby-Phelps K & Tallquist MD (2010) Epicardial spindle orientation controls cell entry into the myocardium. *Dev. Cell* **19:** 114

You J, Wu J, Zhang Q, Ye Y, Wang S, Huang J, Liu H, Wang X, Zhang W, Bu L, Li J, Lin L, Ge J & Zou Y (2017) Differential cardiac hypertrophy and signaling pathways in pressure versus volume overload. *Am. J. Physiol. Circ. Physiol.***:** ajpheart.00212.

Zaffran S, Kelly RG, Meilhac SM, Buckingham ME & Brown NA (2004) Right ventricular myocardium derives from the anterior heart field. *Circ. Res.* **95:** 261–8

Zha Y, Xia Y, Ding J, Choi J-H, Yang L, Dong Z, Yan C, Huang S & Ding H-F (2014) MEIS2 is essential for neuroblastoma cell survival and proliferation by transcriptional control of M-phase progression. *Cell Death Dis.* **5:** e1417

Zhao G, Qiu Y, Zhang HM & Yang D (2019) Intercalated discs: cellular adhesion and signaling in heart health and diseases. *Heart Fail. Rev.* **24:** 115–132

Zoni-Berisso M, Lercari F, Carazza T & Domenicucci S (2014) Epidemiology of atrial fibrillation: European perspective. *Clin. Epidemiol.* **6:** 213

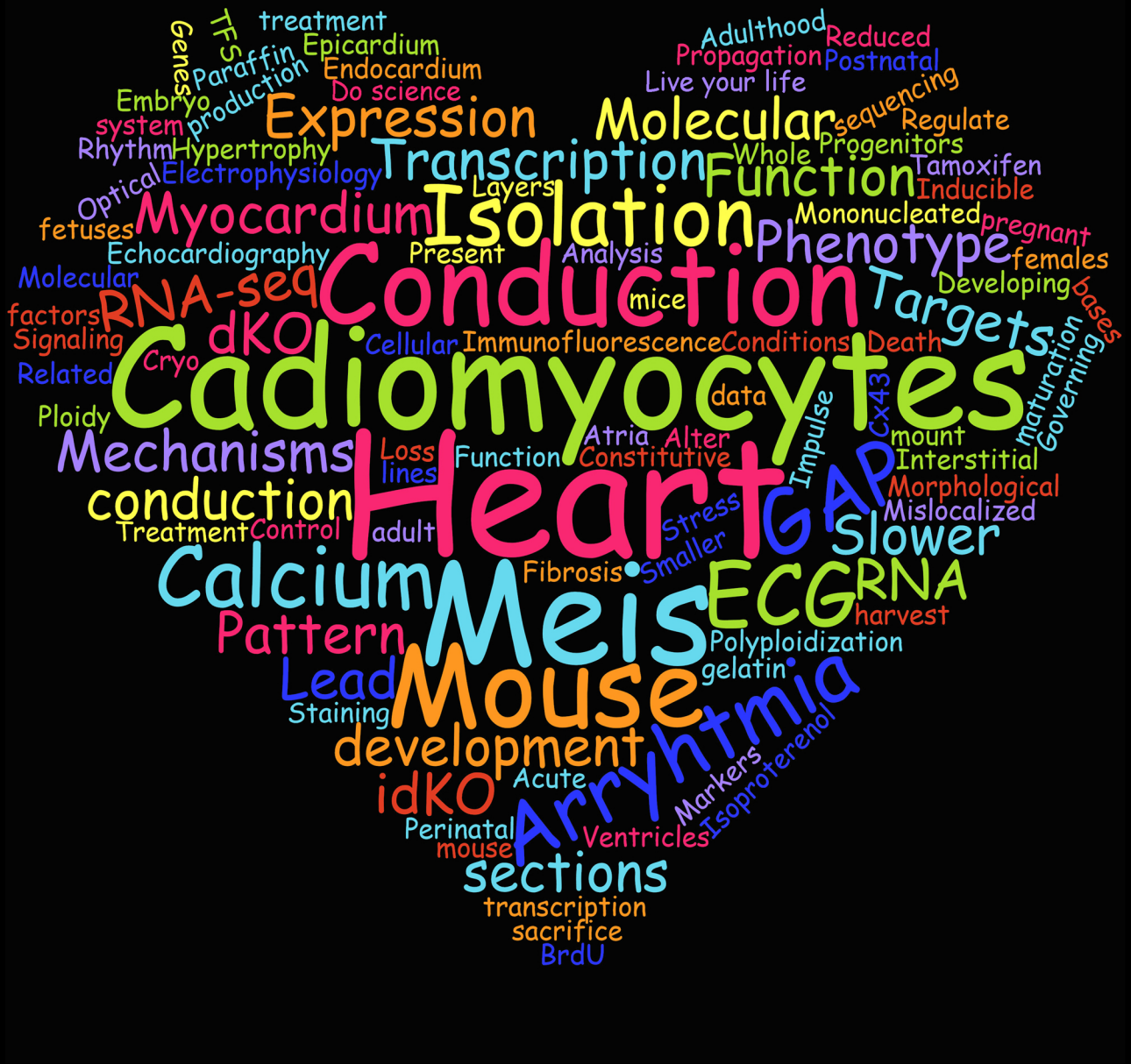

UAM

Universidad Autónoma
de Madrid